DOE/ID/13292

Miniaturized Environmental Monitoring Instrumentation

Final Report

C. B. Freidhoff

September 1997

Work Performed Under Contract No. DE-FC07-94ID13292

For
U.S. Department of Energy
Assistant Secretary for
Environmental Management
Washington, DC

By
Northrop Grumman Corporation
Baltimore, MD

DISCLAIMER

DOE/ID/13292

MINIATURIZED ENVIRONMENTAL MONITORING INSTRUMENTATION

FINAL REPORT

C. B. Freidhoff

September 1997

Work Performed Under Contract No. DE-FC07-94ID13292

Prepared for the
U.S. Department of Energy
Assistant Secretary for
Environmental Management
Washington, DC

Prepared by
Northrop Grumman Corporation
Baltimore, MD

Miniaturized Environmental Monitoring Instrumentation

Final Report

Presented To:

Department of Energy

Idaho Operations Office

Office of Program Execution

Under:

Cooperative Agreement

No. DE-FC07-94ID13292

TABLE OF CONTENTS

LIST OF FIGURES iii
LIST OF TABLES vi
1 EXECUTIVE SUMMARY 1
1.1 Background 1
1.2 Accomplishments 2
1.3 Patents 3
1.4 Commercialization 3
1.5 Program Objectives 4
1.6 Program Development History 7
1.6.1 MSOC work leading up to the TRP 7
1.6.1.1 The Mass Spectrograph on a Chip: Introduction 7
1.6.1.2 Solid State Ionizer 9
1.6.1.3 Mass Filter 10
1.6.1.4 Ion Detector Array 11
1.6.1.5 Conclusions 13
1.6.2 The TRP 13
1.6.3 Portable unit progress and deletion of the hand held unit 14
2 MASS SPECTROGRAPH ON A CHIP 15
2.1 Overview 15
2.2 Performance Goals 15
2.3 MSOC Operations 16
2.4 MSOC Design 21
2.4.1 Ionizer 21
2.4.1.1 Cold cathode: Reverse bias p-n junction 22
2.4.1.2 Radioactive particles 23
2.4.1.3 Electrical discharges 23
2.4.1.4 Cold cathode: point emitters 24
2.4.1.5 Hot cathodes: thermionic emitters 25
2.4.1.6 Details of p-n junction design incorporated in MSOC 25
2.4.2 Mass Filter 26
2.4.3 Detector 33
2.4.4 Integrated Gas Sensor 36
2.5 Component Development 39
2.5.1 Ionizer 39
2.5.2 Mass Filter Component 43

2.5.3 Detector Array and Interface Fabrication 48
2.6 Integration Of Components Into Gas Sensor 52
2.7 Test 56
2.7.1 Ionizer 56
2.7.2 Mass Filter 64
2.7.3 Detector 66
2.7.4 Integrated Gas Sensor 69
2.8 Conclusions 73
2.9 References For Section 2 73
3 PORTABLE UNIT VACUUM PUMP 75
3.1 Overview 75
3.2 Performance Goals 76
3.3 Vacuum Pump Operations 79
3.4 Design 79
3.5 Balzers PUMP 83
3.6 References Section 3 83
4 PORTABLE UNIT: GAS CHROMATOGRAPH/MASS SPECTROMETER 84
4.1 Overview 84
4.2 Performance Goals 84
4.3 Gas Chromatograph/Mass Spectrometer Operations 85
4.4 Design 87
4.5 Development 89
4.6 References For Section 4 90
5 PORTABLE UNIT 91
5.1 Mechanical 91
5.1.1 Overview 91
5.1.2 MSOC Manifold 91
5.1.3 Portable Instrument 93
5.2 Electrical 94
5.2.1. Overview 94
5.2.2. Functional Block Diagram 94
5.2.3. Vacuum Pump 95
5.2.4. Gas Chromatograph 95
5.2.5. MSOC Chip 96
5.2.6 Power Distribution 96
5.2.7. Analog Functions 97

5.2.8. Digital Functions 98
5.2.9. Operator Interface 98
5.2.10. Embedded PC 99
5.2.11. Power 99
5.2.12. System Cabling 100
6 CONCLUSIONS 101

LIST OF FIGURES

Figure 1-1. A block diagram of the operation of a chemical sensor is illustrated with the signal generated by a system utilizing a mass spectrometer as the detector. 4

Figure 1-2. A briefcase sized GC/MS was composed of technologies from a number of team members, so that a chemical sensing unit that was orders of magnitude smaller and easier to use than state of the art units would be demonstrated. 5

Figure 1-3 The Mass-Spec-on-a-Chip program will result in the demonstration of a hand held chemical gas sensor which is orders of magnitude smaller than a bench top unit but with equivalent or improved performance. 7

Figure 1-4 Assembly of the major components of the MSOC are shown in this cross-sectional drawing. The length of the MSOC is approximately two centimeters and the thickness is one millimeter, excluding the bias magnet. 8

Figure 1-5 The MSOC development approach involves the demonstration of the individual components and their integration into the demonstration hand held unit for the DARPA ETO program. 8

Figure 1-6. The MSOC development programs will take an initial concept demonstration in 1991 to military and commercial availability in 1997+. 9

Figure 1-7. Solid state ionizers with a circular emitter geometry achieves the desired current. a) Cross-section of shallow reverse biased p-n emitter. b) Measurements on devices with circular emitters show minutes operation. ..10

Figure 1-8 The mass spectrum obtained using a one centimeter long magnet of 0.6 T and electrostatic field plates inserted into the magnet gap. 10

Figure 1-9 One half of the mass filter component is shown here with the first attempt to fabricate the ionizer array in the well of the chip. 11

Figure 1-10 The flip-chip mass filter test component is shown above that contained a seven segment electrostatic field plate. 11

Figure 1-11 The twenty element array test component shown has the integral shift registers (lower block) and charge to current amplifier 12

Figure 1-12 The development of a photoresist application and exposure technique was crucial to be able to produce a low cost device with large changes in topography 12

Figure 1-13 The interface card and detector chip were placed in a vacuum and subjected to a low energy ion beam.13

Figure 2.3-1. The coordinate system of the mass filter is such that the magnetic field is directed along the y-axis, the electrostatic field along the x-axis and the initial ion velocity vector is directed along the z-axis. 19

Figure 2.4-1 The reverse bias p-n junction is a solid-state device that can inject low energy electrons into the vacuum above the junction surface 22

Figure 2.4-2 A point emitter, such as those produced by Spindt and co-workers,[2-7] emit electrons due to the high fields generated at the sharp tips of metal deposits 24

Figure 2.4-3 The ions must be formed so that the rest of the device presents attractive potentials to it so that the highest efficiency can be obtained in transporting them to the detector array. 26

Figure 2.4-4 The permanent, yoke magnets have high, smoothly varying magnetic fields that are highly uniform in the transverse or mass selection direction, as seen in the right-hand plot....27

Figure 2.4-5 The electrostatic field configuration for the mass filter cavity are illustrated above for the (top) cavity having electrically grounded plates, such as in the bare magnet case, (middle) the use of segmented metal plates with a stepped voltage drop, and (bottom) a resistive film with a smoothly varying potential with position. 29

Figure 2.4-6 The modeled electrostatic field variance for a seven segment field plane shows electrostatic field variations of 4.1% across the beam width, yielding a resolution of 1 amu at ~20 amu....30

Figure 2.4-7 The modeled electrostatic field for a twenty-nine segment field plane shows electrostatic field variations of 0.58% across the beam width, yielding a resolution of 1 amu at ~100 amu....31

Figure 2.4-8 The estimate of the number of evenly spaced metal grid plates is shown with both the linear fit results and logarithmic fit results plotted. 32

Figure 2.4-9 The resistivity of the resistor bridge film under a segmented metal film is shown here for the number of segments with 1 mA current in the resistor bridge for a 30 volts potential drop. 32

Figure 2.4-10 The "faraday" cage is shown with one potential embodiment of the readout circuit for both an external and integrated magnet design. 34

Figure 2.4-11. The integrated gas sensor is shown here with the three silicon chips 37

Figure 2.4-12 The interior detail of both halves of the tri-lithic mass spec structure showing the physical location of key components and functions....38

Figure 2.5-1. Top view and cross section of the reverse bias emitter structure being utilized as an electron source for the ionization of neutral gases in the miniature mass spectrograph....39

Figure 2.5-2 Die layout for linear designs of developmental emitter test structures. 41

Figure 2.5-3 Electron emission characteristics for a circular and striped emitter structure. 42

Figure 2.5-4 Measurements of xenon with the silicon mass filter showing the singly and doubly ionized isotopes.44

Figure 2.5-5 Expanded scale view of singly charged xenon isotope mass region with simulated isotope abundance pattern. 45

Figure 2.5-6 Schematic cross-sectional view of detector ion collector pad illustrating self-aligned deposition of collector and ground plane metal....46

Figure 2.5-7 SEM photograph of ion collection pads on wall of mass filter. 47

Figure 2.5-8 SEM photograph of ion optics region of mass filter. 48

Figure 2.5-9 Response of 20 element detector test circuit to verify design parameters. 50

Figure 2.5-10 Photograph of 64-element array on 22 μm pitch. 51

Figure 2.5-11 Response of 64 element detector array to ion beam. 52

Figure 2.6.-1 Photograph of assembled gas sensor chip showing the three component chips from which it is comprised....52

Figure 2.6-2 SEM photograph of ion collection pads patterned in photoresist. 53

Figure 2.6-3 SEM photograph of ion collection pads used in gas sensor. 54

Figure 2.6-4 SEM of ionizer region of gas sensor component. 54

Figure 2.6-5 Photograph of integrated gas sensor in test housing with electronic control board. 55

Figure 2.7-1 This circular emitter is very typical of the data acquired for such devices. 61

Figure 2.7-2 This device is a three striped emission area that was controlled to maintain the emitted current as constant. 61

Figure 2.7-4 Cold-cathode point emitters of the Spindt design and fabrication were tested using constant voltage control through a ballast resistor.....64

Figure 2.7-5 The seven segment, mass filter separates xenon with the expected resolution of about 1 amu at 50 amu.65

Figure 2.7-6 Mass spectrum obtained from the polysilicon, mass filter component and 3 element ion optics. 66

Figure 2.7-7 The isotope pattern for xenon has been resolved at the resolution of 1 amu at 130 amu using a polysilicon mass filter component test piece and 9 element laboratory ion optics. 66

Figure 2.7-8 The response of the twenty element MOS switch linear detector array to an ion beam in a vacuum system shows that the detector and amplifier perform to the design performance. 67

Figure 2.7-9 The new interface electronics for the detector array divides the analog and digital portions of the board in the horizontal direction to reduce noise of the overall section. 67

Figure 2.7-10 The sixty-four element detector test component is wire bonded in a dual inline header for testing.....68

Figure 2.7-12 The sixty-four element test component showed both the sensitivity and lower noise levels than required by the program, allowing the sensitivity of the detector to be 10 ppm rather than 100 ppm. 69

Figure 2.7-13. The process to define a metal line on a dielectric through lift-off resist technique is illustrated. 70

Figure 2.7-14. The deposition of metal on a "self-aligned" geometry is illustrated. 71

Figure 2.7-15. A scanning electron microphotograph of the detector array end of the integrated gas sensor during a test fabrication over the integrated gas sensor well geometry. 71

Figure 2.7-16. An assembled integrated gas sensor is shown with a set of individual chips that are being hybridized to form the integrated gas sensor. 72

Figure 2.7-17 The integrated gas sensor is pictured with its external permanent magnet and detector electronics. ...73

Figure 3.2-1 The schematic of the pumping system for the mass spectrograph on a chip is illustrated above with the size, throughputs (Q) and conductances (C) of the passages. 76

Figure 3.3-1 The multistage, rotary vane pump is connected to the MSOC though a manifold and the compressed gas from each stage is part of the load of the next pumping stage, so that gas flows from chamber 1 to 2, etc. before being discharged back into the atmosphere by the roughing pump. 79

Figure 3.4-1 The electrical control circuit for the Bechdon rotary vane pump shows the photoelectric pickup for the valve control and the valve delay timing adjustment circuit. 80

Figure 3.4-2 The details and overall layout is shown in these design drawings. 81

Figure 3.4-3 The complete disassembly of the Bechdon vacuum pump is shown. 82

Figure 3.4-4 The assembled Bechdon vacuum pump with a six inch (fifteen centimeter) ruler is shown. 82

Figure 3.4-5 The measured and expected pump down curves are shown. 82

Figure 3.5-1 A small commercially available pump from Balzers has the pumping speed and size for the portable unit. 83

Figure 3.5-2 The backing diaphragm pump for the Balzers drag pump is the smallest commercially available at the time of the program that could maintain the foreline pressure required of the drag pump. 83

Figure 4.3-1 During the elution of a GC peak, the mass spectrum obtained can be very different due to the changing concentration of the chemical species during the scan. 86

Figure 4.4-1 The pre-column and analytical column are clearly shown in the schematic of the MTI back flush GC.88

Figure 4.4-2 The fabrication of the back flush valve system used the same processes as the valve/injector system already in use and permitted the integration of the two functions into one die. 89

Figure 4.5-1 The pre-column back flush GC performed as expected and eliminated the necessity of waiting for the elution of the heavy organics prior to the injection of a new sample onto the GC. 90

Figure 5.1-1 Mass spectrograph interfaces 91

Figure 5.1-2 The MSOC Manifold 92

Figure 5.1-3 MSOC and substrate 92

Figure 5.1-4 Drawing of mounted MSOC in sensor housing 92

Figure 5.1-5 Substrate, Magnet and Bottom Manifold 92

Figure 5.1-6 Buildup Including Upper Magnet 92

Figure 5.2-1 The functional blocks are schematically shown so that the discussion in the following subsections can be organized. 95

Figure 5.2-2 The system cabling does the power and signal routing in a simple and noise free way. 100

LIST OF TABLES

Table 1-1. The program goals for the GC/MS unit to incorporate the mass spectrograph chip as the detector to a commercially available gas chromatograph column 5

Table 1-2 Portable GC/MS Instrument Specification Goals 13

Table 1-3 Hand Held MSOC Instrument with MEMS Preconcentrator Specification Goals 14

Table 2.3-1. Cross section coefficients for organic molecules to determine total ionization cross section, if ionization cross section by electron impact has not been measured. 18

Table 2.4-1 The electrostatic field for a mass filter needs to have a uniformity of 0.25% or better 28

Table 2.4-2 Summary of processes for MSOC fabrication 39

Table 2.5-1 Summary of process variables investigated which affect performance of the reverse bias junctions as electron emitters 40

Table 2.7-1 The variations in emitter performance was tested using closed loop control on the junction current and determining the peak emitted electron current. 57

Table 2.7-2 The variations in emitter performance was tested using closed loop control on the junction current and determining the peak emitted electron current. 58

Table 2.7-3 The variations in emitter performance was tested using closed loop control on the emitted electron current and was used to determine the best device design to provide the lifetime of the integrated gas sensor 59

Table 2.7-4. Summary of process variables investigated and tolerances found for desired performance of the reverse bias junctions as electron emitters. 63

Table 3.2-1 The vacuum pump is required to meet these goals in order to fabricate a miniature GC/MS that is less than 10 kg in mass and 28 liters in volume 77

Table 3.2-2 The multi-stage, rotary vane pump design parameters are summarized for a four stage pump that is roughed by a diaphragm pump to 455 Torr. 78

Table 4.2-1. The program goals for the GC/MS unit to incorporate the mass spectrograph chip as the detector to a commercially available gas chromatograph column 84

1 EXECUTIVE SUMMARY

1.1 Background

Compact, affordable and versatile chemical sensing instruments are needed for environmental, commercial, defense and medical applications. Monitoring of chemicals has a number of benefits for the users whether they are chemical releasers or geographic areas affected by chemical users. The key items that have prevented the widespread use of chemical sensing instrumentation are the cost and the level of expertise to operate and interpret the data from the instrument. With the advent of high performance computation, search-able information databases of mass spectra, and the development of MEMS devices, the ability to affordably produce and field a general purpose, high sensitivity chemical sensing instrument is near at hand.

Over the past decades, the understanding of the interpretation of mass spectra has lead to the realization that different instruments tend to produce nearly identical spectra under the same ionization conditions. In addition, probability-based algorithms have been formulated that make library searches fast and accurate. This reduces the interpretation expertise required by the user and eliminates the need to develop a new database for each new instrument. The computational power available in modern personal computers is phenomenal and allows the data acquisition and control of instruments to be performed with low power, compact board-based units. These computers are powerful enough to also provide the analysis due to the speed with which they operate.

Microelectromechanical systems (MEMS) has developed to the point since the 1960's that subsystems and systems based on the batch fabrication process used by the semiconductor industry can produce high performance sensors at low cost. A prime example is the airbag sensor in cars today is a MEMS silicon accelerometer that costs under $10 for a quantity of one, due to the high volume that is produced for the automotive industry.

The vacuum industry has also been responding to the need for more compact systems that utilize pumps with minimal organic lubrication. Hybrid designs have been built with energy efficient concepts that reduce the friction and maintain high throughputs.

Taken together, the time has come when a compact portable chemical sensing instrument is possible. With this capability, costs of cleanup of waste sites can be reduced by allowing screening of a site and cleanup work to continue without having to wait for the results from an analysis laboratory that can take weeks to obtain. Chemical users and producers can self monitor and detect leaks more efficiently, reducing emissions and also improving yield and quality. DOD will be able to monitor wider areas and provide chemical information for more missions with units that are smaller and lighter than currently available. The programmability of the instrument described in the report eliminates the need to have specialized detectors for a small number of targets and allow new targets to be detected by units already in the field with a minimal change. The integration of the these ideas will allow the analytical laboratory to be taken to the field.

1.2 Accomplishments

The TRP program consisted of a team from three companies: Northrop Grumman, formerly Westinghouse Electric; Microsensors Technology, Inc. (MTI); and Bechdon, Inc. Each company had responsibility for a particular part of the portable gas chromatograph/mass spectrometer (GC/MS) unit. Northrop Grumman had responsibility for the optimization and fabrication of the mass spectrograph on a chip (MSOC) detector; initial design of the multi-stage, rotary vane vacuum pump; integration of the vacuum pump, gas chromatograph, and MSOC into the portable GC/MS; and program management. MTI had responsibility for delivering modules of their gas chromatography units and developing a back flush valve system as an improvement to the present gas chromatograph. Bechdon had responsibility for the manufacturing of the multi-stage rotary vane vacuum pump, based on the initial design generated by Northrop Grumman.

Every member of the program contributed significantly. MTI developed and delivered the back flush gas chromatograph. This back flush allowed the column to be flushed of slowly eluting compounds that were of no interest to the analysis. The timing of the back flush is programmable and allows a new sample to be introduced sooner to the gas chromatography column.

Northrop Grumman made a number of improvements to the components of the MSOC and integrated these components into an all silicon sensor. This integration included the ceramic substrate design that combined the vacuum and electrical manifold into a single piece. This ceramic also provided the alignment to the external magnet and mechanical stability of the sensor unit. The electronics was designed form commercial off the shelf items in a compact and energy efficient form. The software control was implemented in C-based code and interfaced successfully to the gas chromatograph and chemical library software. A number of accomplishments were made on the MSOC to take the components and optimize them for a commercial application. A summary of the accomplishments for the MSOC are:

- Solid-state emitter with lifetime to achieve 12 month continuous sensor operation. Lifetime achieved under vacuum conditions and gases. Integrated emitters operating and short term data is similar to test components. Array of emitters provides device lifetime. Achieved on March 31, 1996.
- MOS detector array and interface electronics with high gain and low noise meeting specifications. Array fabricated and tested with low energy ions. Achieved on September 30, 1994.
- Silicon mass filter demonstrating 1 amu at 150 amu resolution with single-channel detector. Demonstrated April 1996 with 0.9 amu at 135 amu.
- Integrated gas sensor fabrication and functional testing to show operation at specifications. Earlier hybridization was found to have premature dielectric stack voltage breakdown. This has been improved and a new set of chips were hybridized.

Bechdon fabricated a multi-stage rotary vane vacuum pump that did operate and produce a significant vacuum level. The pump did not show that long term operation due to design details in the vane seals that lead to friction and leakage paths. This pump did show the feasibility of a dry lubricated, rotary vane vacuum pump with

the appropriate ultimate pressures and capacity for a number of applications. During this program, Pfeiffer Corporation developed and commercialized a molecular drag/diaphragm pump combination that met the program requirements. Further development of the multi-stage rotary pump was discontinued due to this alternative pump source.

1.3 Patents

A total of six patent applications on the mass spectrograph technology related to the TRP were filed with the United States Patent Office, all of which were granted patent status. The issued patents are listed below:

- 1 US Patent Number 5,386,115, C.B. Freidhoff and R.M. Young, "Universal Gas Detection (UGD) Sensor," granted on January 31, 1995.

- 2 US Patent Number 5,481,110, S.V. Krishnaswamy and C.B. Freidhoff, "Thin Film Preconcentrator Array," granted on January 2, 1996.

- 3 US Patent Number 5,492,867, J.C. Kotvas, T.T. Braggins, R.M. Young and C.B. Freidhoff, "Manufacturing Methods for the Production of a Miniature Mass Spectrograph," granted on February 20, 1996.

- 4 US Patent Number 5,530,244, S. Sriram and C.B. Freidhoff, "Solid-state Detector for Sensing Low Energy Charge Particles," granted on June 25, 1996.

- 5 US Patent Number 5,536,939, R.M. Young and C.B. Freidhoff, "Miniature Mass Spectrograph Separation Embodiments," granted on July 16, 1996.

- 6 US Patent Number 5,747,815, R.M. Young, C.B. Freidhoff, T.T. Braggins, T.V. Congedo, "Micro-miniature ionizer for gas sensor applications and method of making micro-miniature ionizer," granted on May 5, 1998.

1.4 Commercialization

Northrop Grumman has taken an active role in determining the best route to market for the portable GC/MS. From the beginning of the TRP program, a commercial partner was recognized as being required to productize the DOD developed technology and generate the unit volume required to lower the overall cost of the unit for both commercial and DOD applications. To this end, a market survey was conducted for Nothrop Grumman by Sullivan and Foster, a well known market surveying company in chemical sensing instrumentation. In addition, the companies in the industry of analytical instrument manufacturing and process control instruments were briefed under confidentiality agreements as to the technology under development. The companies contacted include

both small and big businesses. These conversations have continued and a set of partners will be signed within the next year.

Defense Advanced Research Projects Agency

1.5 Program Objectives

this project

The goal of ~~the DARPA TRP~~ was to produce a prototype of a small chemical analyzer with sensitivity in the part per billion range, using the silicon mass spectrograph chip that was being developed under a (DARPA) program from the Electronics Technology Office along with vacuum pumps and sample conditioners. ~~The operation of the prototype system is illustrated in Figure 1-1.~~ ~~This~~ The prototype of a chemical sensor would revolutionize the method of performing environmental monitoring for both commercial and government applications. The portable unit mutually decided upon by Northrop Grumman and the Government agencies (~~DOE~~ Department of Energy and DARPA/DSO) was the miniaturized gas chromatograph with a mass spectrometer detector, referred to as a GC/MS in the analytical marketplace. ~~The desired performance goals of the GC/MS are shown in Table 1-1. The prototype and the sources of its technology envisioned for this program are illustrated in Figure 1-2.~~

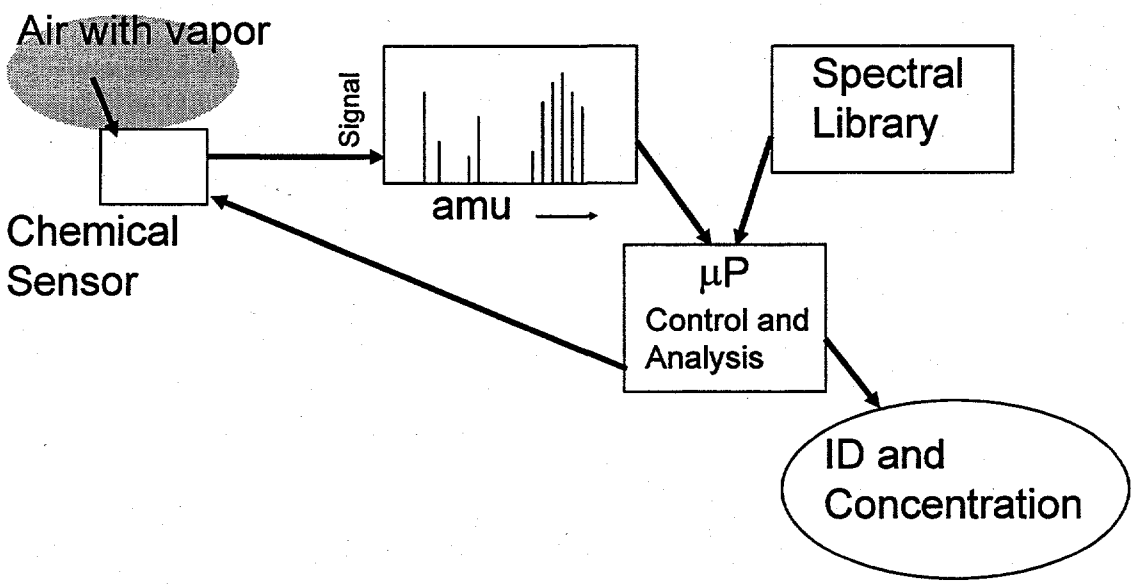

Figure 1-1. A block diagram of the operation of a chemical sensor is illustrated with the signal generated by a system utilizing a mass spectrometer as the detector.

A gas chromatograph elution time plot could also be used with the appropriate spectral library, as well as any other detection system.

The major development work to be done on this program was the optimization of the mass spectrograph chip performance to take the developments of the DARPA/ETO program and bring the device operation to a level where commercial devices would be producible at marketable prices. This effort included the optimization of the ionizer for lifetime and low power operation, increased speed and sensitivity of the detector array, and mating of the

mass spectrograph chip to the electronics and vacuum pump. This also included the mechanical and electrical engineering to take the laboratory device and integrate the mass spectrograph chip with a gas chromatograph in a field-able package. The vacuum pump miniaturization was also an engineering task with moderate risk. The gas chromatograph had some commercially available units in the size and power range desired at the start of the program and therefore, low risk, but enhancements of this product will make the prototype even more versatile and faster.

Mass Range:	1 to 400 amu
Mass Resolution:	1 amu at 150 amu
Sensitivity:	100 ppb in 4 minutes
Power:	100 Watts or less
Size:	< 19,000 cm^3
Weight:	< 10 kilograms

Table 1-1. The program goals for the GC/MS unit to incorporate the mass spectrograph chip as the detector to a commercially available gas chromatograph column.

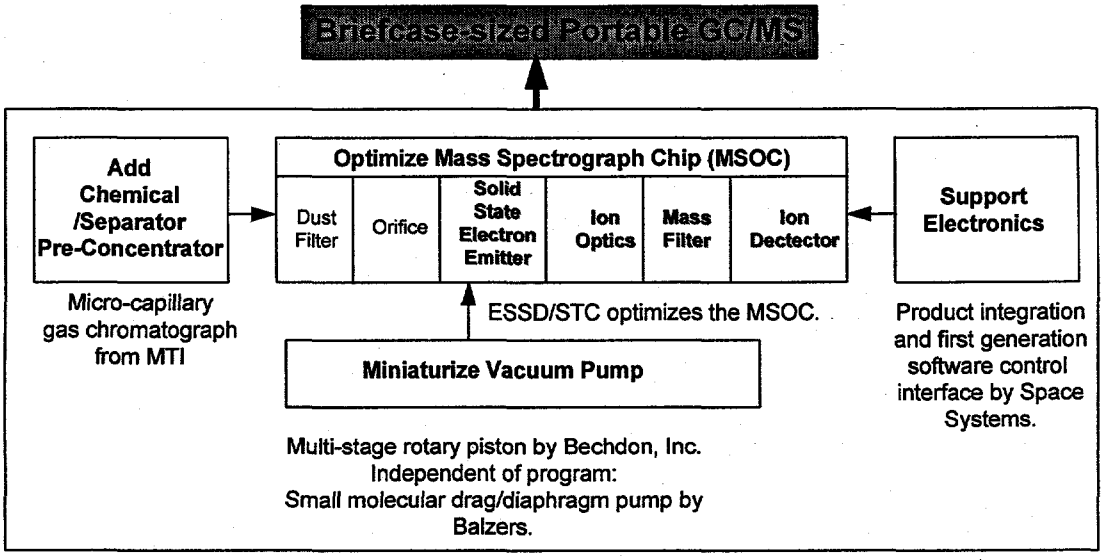

Figure 1-2. A briefcase sized GC/MS was composed of technologies from a number of team members, so that a chemical sensing unit that was orders of magnitude smaller and easier to use than state of the art units would be demonstrated.

The objective of this program, the prototype of the GC/MS unit, was closely coupled to the team's ability to deliver their hardware responsibility for the program. To reduce the risk on the program for the miniature

vacuum pump, a survey of commercial vendors was done for the requirements of the vacuum pump. Balzers, now Pfeiffer Vacuum Corporation, was interested in developing a miniature vacuum pump combination that could potentially meet our needs with minor modifications to our pumping manifold. This pump was based on a molecular drag pump backed by a multistage diaphragm pump. This pump was developed solely with their funds. Bechdon was given the task of manufacturing prototypes of the multi-stage rotary vane pump backed by a single stage diaphragm pump. The prototype base design was made by Northrop Grumman STC and is discussed in Section 3.2.

The sample conditioner of the portable unit was chosen to be a gas chromatography (GC) column. Prior to the program being awarded, Microsensor Technology, Inc. was chosen as the supplier of the GC and associated parts. This company was chosen for its leadership in providing small GC units that were faster (ten times faster) and less power hungry than other commercially available units. In addition, a back flush system was to be developed under this program and be incorporated into the portable unit for evaluation. This is further discussed in Section 4.

The mass spectrograph on a chip (MSOC), or the detector of the portable unit, was to be optimized for lifetime and durability from where the DARPA/ETO program had shown the feasibility of the device to something that was field-able for evaluation purposes. The optimization effort would be performed by Northrop Grumman STC and the detector units would be provided to the program for integration into the portable unit. As shown in Figure 1-2, the components of the MSOC are the inlet filter, orifices, ionizer, ion optics, mass filter and detector array. The inlet filter is replaced by the GC and its inlet system, the orifices and associated differential pumping chambers are left as the DARPA/ETO program developed them. The other components: the ionizer, ion optics, mass filter and detector array; required optimization to meet the requirements of field-able applications. The overall sensitivity of the system was desired to the increased as well as the scan speed to be shortened. The results of this effort are discussed in Section 2.

The electrical and mechanical engineering for the prototype unit was performed by a team of engineers at Space Systems of the Northrop Grumman Electronic Sensors and Systems Division. This effort included the first generation software control, the power supply design and fabrication, the mechanical design and assembly, and the laboratory verification testing of the unit. Documentation of the unit would be done and provided upon field testing of the unit. This effort is discussed in Section 5.

1.6 Program Development History

1.6.1 MSOC work leading up to the TRP

1.6.1.1 The Mass Spectrograph on a Chip: Introduction

The objective of the Mass Spectrograph on a Chip (MSOC) program is the development of a miniature, multi-species gas sensor fabricated using silicon micromachining technology, Figure 1-3, which will be orders of magnitude smaller and lower power consumption than a conventional mass spectrometer.

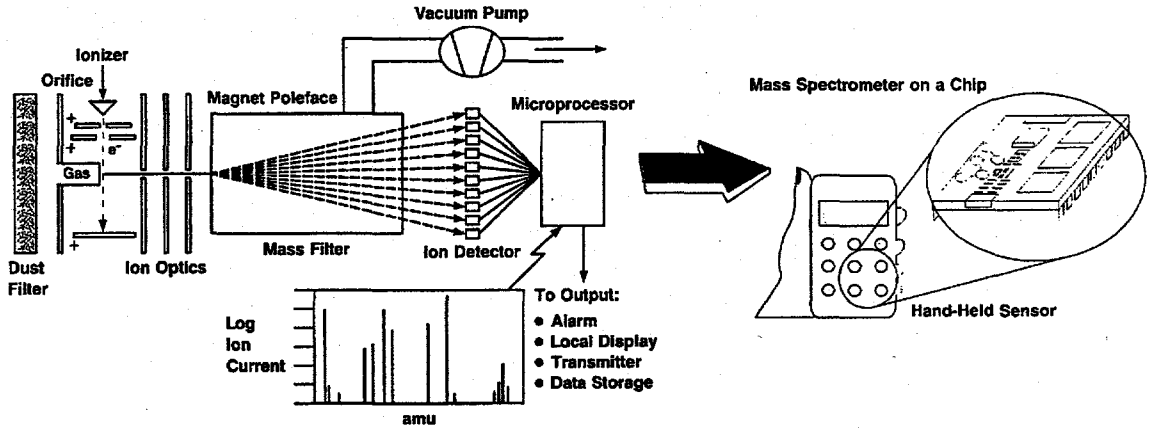

Figure 1-3 The Mass-Spec-on-a-Chip program will result in the demonstration of a hand held chemical gas sensor which is orders of magnitude smaller than a bench top unit but with equivalent or improved performance.

The sensing and discrimination of this gas sensor are based on an ionic mass spectrograph, using magnetic and/or electrostatic fields. The fields cause a spatial separation of the ions according to their respective mass to charge ratio. The fabrication of this device involves the combination of microelectronics with micromechanically built sensors and ultimately, vacuum pumps. cross-sectional view of the silicon MSOC gas sensor is shown in Figure 1-4. Note that the vertical scale is greatly exaggerated and that the mass filter region is shortened. The one Tesla magnetic bias field is supplied by a rare earth cobalt magnet in an iron yoke. Since the approximately eight cm^3 volume of the magnet can be accommodated within our size and weight objective no attempt has be made to improve our initial design.

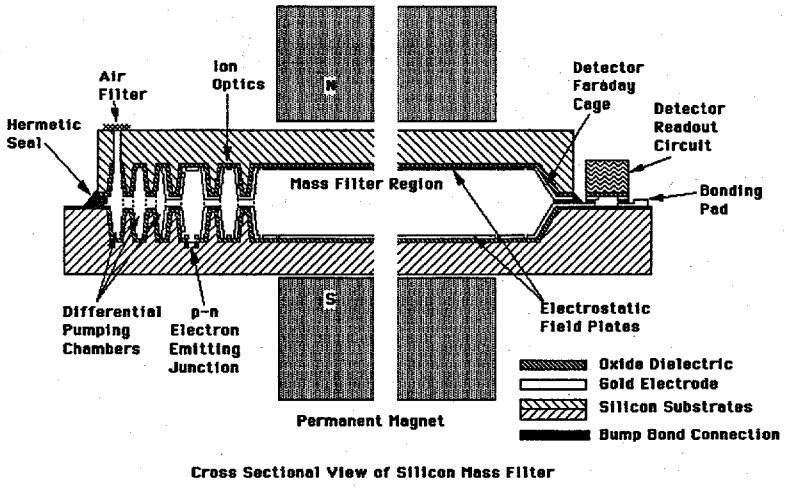

Figure 1-4 Assembly of the major components of the MSOC are shown in this cross-sectional drawing. The length of the MSOC is approximately two centimeters and the thickness is one millimeter, excluding the bias magnet.

The development of the gas sensor can be divided into three parts as shown in Figure 1-5. The first part involves the improvement of essential components comprising the gas sensor: the ionizer, mass filter and detector array. The second part is the integration of these components into the gas sensor that can act as the detector for a small bore, gas chromatography column or as a direct air sampler. The third part is the development of a miniature vacuum pump and its integration with the gas sensor.

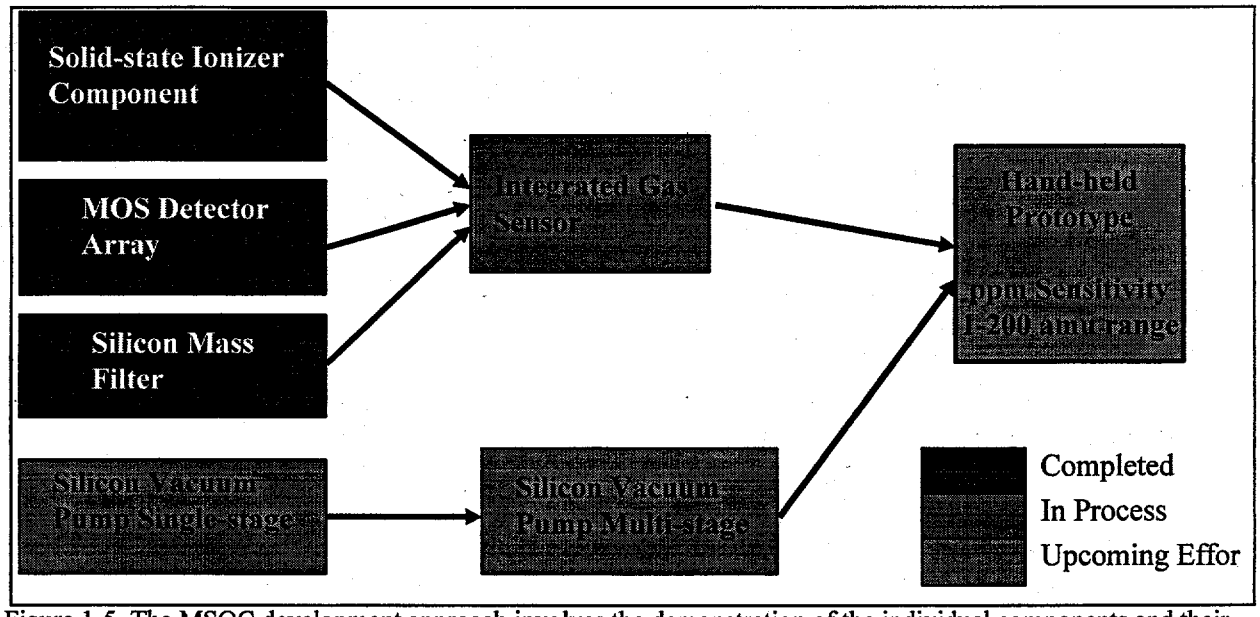

Figure 1-5 The MSOC development approach involves the demonstration of the individual components and their integration into the demonstration hand held unit for the DARPA ETO program.

The mass -spec on a chip program development time line is shown in Figure 1-6. Initial feasibility demonstrations of the critical components were performed under IR&D in 1991 and the development is now supported by two synergistic DARPA programs. One sponsored by the DARPA Electronics Technology Office for

the hand-held device with MEMS vacuum pumps, whose program approach is shown in Figure 1-5. The second DARPA program is sponsored by the Defense Sciences Office under the Technology Reinvestment Program and is the subject of this report.

The performance goals of the MSOC gas sensor , to be demonstrated on the DARPA ETO program by March 1997 are:

Mass Range:	1 to 200 amu
Mass Resolution:	1 amu at 200 amu
Sensitivity:	100 ppm in 10 seconds
	1 ppm in 4 minutes.
Power :	<0.5 watts
Size:	<170 cm^3
Weight:	<300 grams

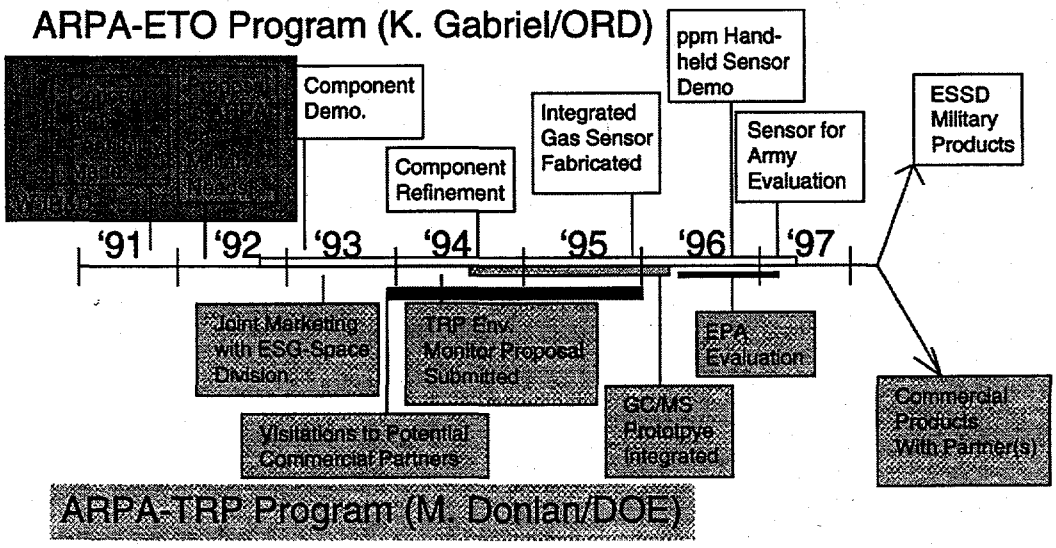

Figure 1-6. The MSOC development programs will take an initial concept demonstration in 1991 to military and commercial availability in 1997+.

1.6.1.2 Solid State Ionizer

The gas molecules, to be analyzed, are ionized by impact with 100 eV electrons produced by a solid state emitter comprising a shallow reversed biased p-n junction in avalanche breakdown as shown in Figure 1-7a. Initial results demonstrated that the required 750 nA electron emission could be achieved, but with device lifetimes of only a few minutes. The performance of the initial emitters is shown in Figure 1-7b, where the 750 nA current was achieved for times on the order of minutes. Emitters were tested in vacuum and in gases.

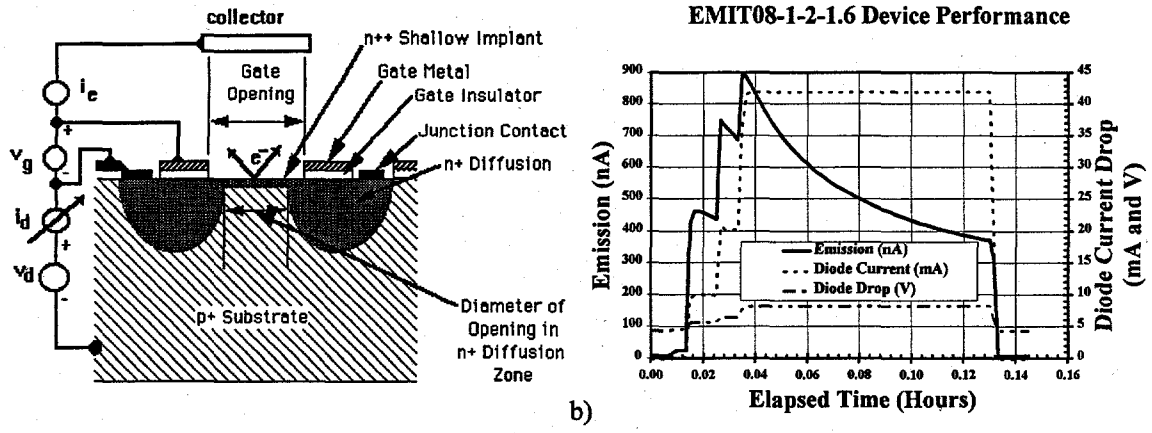

Figure 1-7. Solid state ionizers with a circular emitter geometry achieves the desired current. a) Cross-section of shallow reverse biased p-n emitter. b) Measurements on devices with circular emitters show minutes operation.

1.6.1.3 Mass Filter

Early in the MSOC ETO program, a demonstration of the mass separation of a low energy ion beam was performed. The resolution achieved was about one amu at 30 amu and is shown in Figure 1-8. A non uniform electrostatic field, resulting from the interaction between the grounded magnet poles of the Wien filter and the fields generated by the electrostatic field plates, caused the low resolution. This problem was eliminated in our later designs by the use of segmented electrodes on the upper and lower surfaces of the mass filter chamber. These segmented electrodes are fed from a voltage divider circuit and assure that the correct electrostatic boundary conditions are provided. The silicon chip for the mass filter tests with the segmented field plate are shown in Figure 1-9. Two of these chips were flip-chip bonded to allow testing of the mass filter component of the MSOC. Measurements of Xe ions in a mass filter with 7 electrode segments are shown in Figure 1-10 and compared with a calculation based on a normal isotope abundance. These measurements, performed using a laboratory ion source and a point detector demonstrate a resolution of one amu at 70 amu.

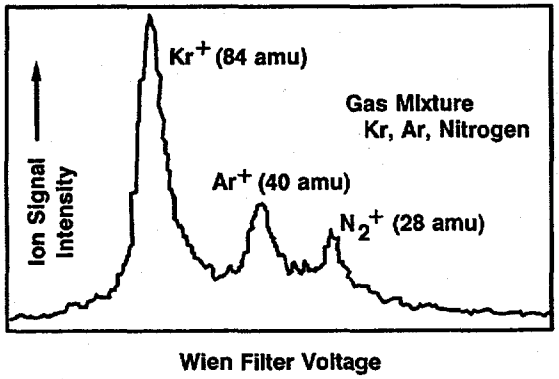

Figure 1-8 The mass spectrum obtained using a one centimeter long magnet of 0.6 T and electrostatic field plates inserted into the magnet gap.

The gas mixture used was 50% krypton, 25% argon and 25% nitrogen. The resolution obtained was expected due to the non-uniform electrostatic field produced in the test configuration.

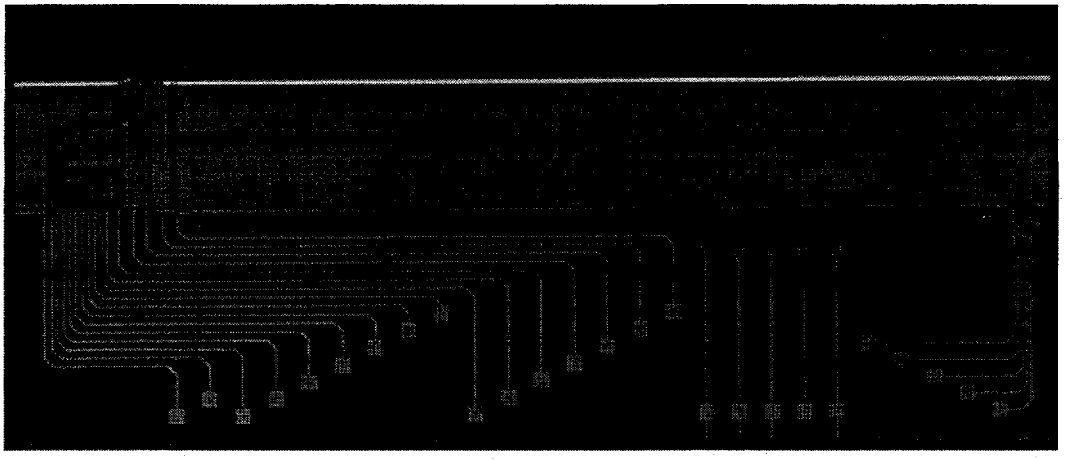

Figure 1-9 One half of the mass filter component is shown here with the first attempt to fabricate the ionizer array in the well of the chip.

The number of electrical connections were large at this stage due to the thin film resistor bridge having been built separately at this stage. It was later incorporated, reducing the number of connections by nearly 60%.

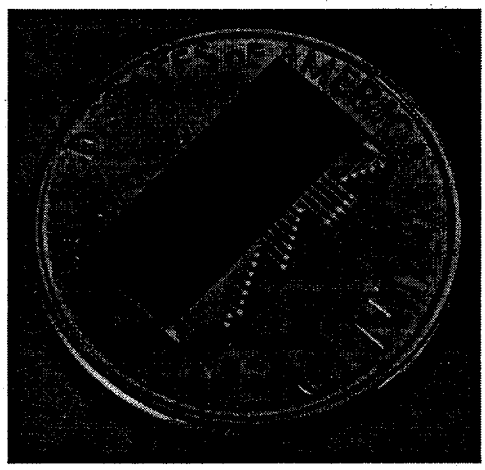

Figure 1-10 The flip-chip mass filter test component is shown above that contained a seven segment electrostatic field plate.

The bonding pads seen the side of the chip allowed electrical connections to the elements inside of the cavity. This unit was inserted into a flange with a magnet around and placed in a vacuum system with a laboratory ionizer for testing.

1.6.1.4 Ion Detector Array

Following their passage through the Wien filter, the spatially separated ions are collected by the array of electrodes shown in Figure 1-11. To prove out the design of the ion detector based on a CMOS switch and common charge to current electrometer, a 20 element array was fabricated with a number of options, dealing with the location of the shift registers, ground plane configurations and the charge to current amplifier. A picture of the 20 element array that contained the shift registers and charge to current amplifier is shown in Figure 1-11. In addition, the detectors were to be fabricated along a etched wall. In order to determine the feasibility of the fabrication, photolithography was developed to define structures over the wall and the etch profiles for the well was

investigated. Figure 1-12 shows the successful definition of a metal over an acid etched wall. With this information, the feasibility of producing a 22 μm pitch for the detector array was established.

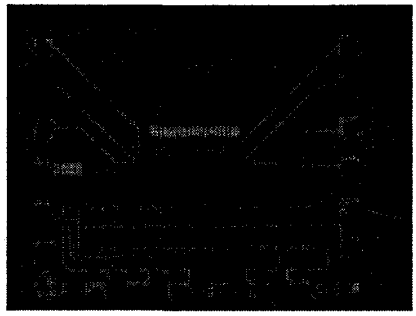

Figure 1-11 The twenty element array test component shown has the integral shift registers (lower block) and charge to current amplifier.

This test device lead to the design of the 64 element array incorporated in the MSOC.

These devices were subjected to a low energy ion beam in a vacuum system. The interface electronics were designed and tested under these conditions. The results of the tests are shown in Figure 1-13. The detector array worked, but the output voltage was low to be easily read by a standard data acquisition system.

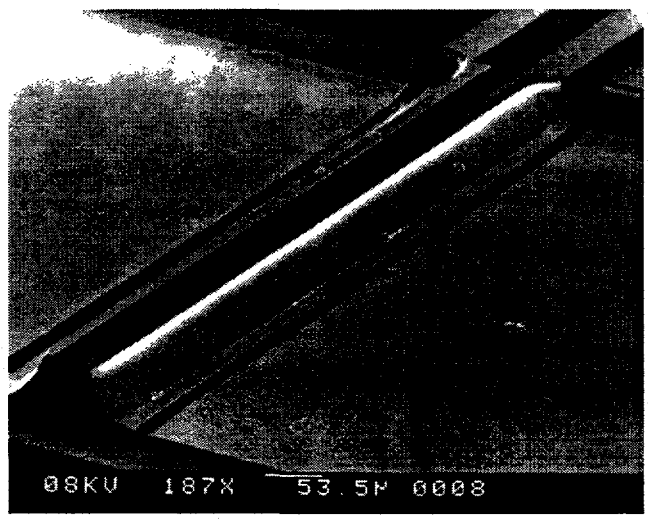

Figure 1-12 The development of a photoresist application and exposure technique was crucial to be able to produce a low cost device with large changes in topography.

Here is a metalization deposited on an acid etched structure in silicon. The photolithography is optical and performed in one step.

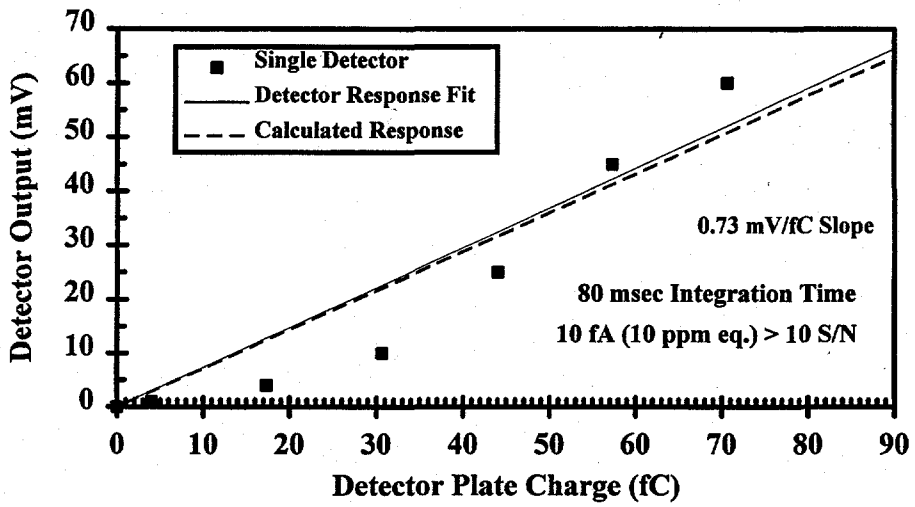

Figure 1-13 The interface card and detector chip were placed in a vacuum and subjected to a low energy ion beam. *The response of the system was determined to be the designed response, but a higher gain and better linearity would be needed for the final device.*

1.6.1.5 Conclusions

The DARPA ETO program showed the feasibility of the fabrication of a MEMS silicon mass spectrograph. The limitations determined at the time of the TRP proposal were engineering and process refinement and held the promise to bring a paradigm shift in the instrumentation marketplace.

1.6.2 The TRP

The objective of the TRP was to optimize the MSOC for performance and integrate it with an external gas chromatograph and vacuum pump to produce a portable GC/MS instrument. In addition, in the original proposal, a hand held instrument using a MEMS preconcentrator and MEMS silicon vacuum pump was proposed. The hand held unit was mutually agreed upon to not be exercised. This decision is discussed further in Section 1.6.3.

For the portable unit, the specifications are shown in Table 1-2.

Table 1-2 Portable GC/MS Instrument Specification Goals

Parameter	Program Goal
Mass Range	1 to 400 amu
Mass Resolution	1 amu @ 150 amu
Sensitivity	10 to 100 ppb
Volume and Weight	19,000 cm^3 and <10 kg

The hand held instrument had the goals outlined in Table 1-3.

Table 1-3 Hand Held MSOC Instrument with MEMS Preconcentrator Specification Goals

Parameter	Program Goal
Mass Range	1-400 amu
Mass Resolution	1 amu @ 150 amu
Sensitivity	10 to 100 ppb
Volume and Weight	3,250 cm^3 and <2.5 kg

1.6.3 Portable unit progress and deletion of the hand held unit

The portable GC/MS instrument has been mechanically and electrically designed and fabricated. The GC column has been installed along with the Pfeiffer vacuum pump. Tests have been performed on the software control using a MTI thermocouple detector. These tests checked the control signals to the GC and the change of the detector status from a steady-state check of the carrier gas to a scanning mode when a peak was detected coming out of the column. The library search routine code was obtained from Palisades Corporation, NY and check against simulated spectra. An earlier problem with identifying and quantifying low molecular weight chemicals (those between 20 and 60 amu) was corrected by Palisades. The portable unit is awaiting a tested and calibrated MSOC, so that final performance data can be obtained. The MSOC is in assembly of the second lot.

During the optimization of the MSOC, the ionizer component was noted to be insufficient to have operating lifetime required for a field-able unit. The effort to optimize this component was significant and shared with the DARPA ETO program. Even so, the additional effort was substantial. In addition, the Bechdon pump fabrication required extra effort due to the complexity of the cavities needed in fabricating the pump. A number of redesigns of the vanes and channels were required to fabricated the pump that was tested. Valving was added between the pumps to reduce the back flow that was found to occur during the pumping cycle. Due to this added effort for the portable unit, the Government and program team mutually decided to reduce the scope of the program to only the portable GC/MS instrument, since this could possibly be completed within the budgeted funds.

The electrical and mechanical engineering for the prototype unit was performed by a team of engineers at Space Systems of Northrop Grumman Electronic Sensors and Systems Division. This effort included the first generation software control, the power supply design and fabrication, the mechanical design and assembly, and the laboratory verification testing of the unit. Documentation of the unit would be done and provided with the unit on field testing. This effort is discussed in Section 5.

2 MASS SPECTROGRAPH ON A CHIP

2.1 Overview

The mass spectrograph on a chip is the development and optimization of a miniature, multi-species gas sensor fabricated using silicon micromachining technology. The sensing and discrimination of this gas sensor are based on an ionic mass spectrograph, using magnetic and/or electrostatic fields. The fields cause a spatial separation of the ions according to their respective mass to charge ratio. The fabrication of this device involves the combination of micromechanically built sensors with solid-state microelectronics to provide a high performance, miniature chemical detector.

The development of the gas sensor can be divided into two parts. The first part involves the improvement of essential components comprising the gas sensor: the ionizer, mass filter and detector array. The second part is the integration of these components into the gas sensor that can act as the detector for a small bore, gas chromatography column or as a direct air sampler. This section of the report will summarize the progress made on the components for the gas sensor and the integration of the components into a detector for a gas chromatography column.

The discussion on each of the components will include the downselection process that lead to the choice of the preferred component and its particular design. For the ionizer, electron impact was chosen as the energetic particle, due to the simplicity of electron sources. In addition, energetic particles from radioactive sources were also included in the selection process. The types of electron sources considered were cold cathode sources: reverse bias p-n junctions, and electrostatic point emitters; thermionic emitters and radioactive sources. For the ion optics, electrostatic lenses were considered of the three and nine element varieties. The mass filter was chosen to be a combination of an electrostatic and magnetic fields. Finally, the detector array was chosen from between a CMOS based and charge-coupled detector (CCD) design. The details of the designs of the components can be found in Section 2.4.

2.2 Performance Goals

The performance goals of the mass spectrograph on a chip detector to be demonstrated are:

Mass Range:	1 to 400 amu
Mass Resolution:	1 amu at 150 amu
Single Scan Sensitivity:	100 ppm in 5 seconds
Multi-Scan Sensitivity:	1 ppm in 4 minutes

2.3 MSOC Operations

The identification of chemicals by mass spectroscopy is performed by ionizing the electrically neutral vapor molecules by an energetic process that either removes or adds an electron to the molecule to from an ion. Some of the energy from an ionization process can be deposited into the molecule itself. This can lead to fragmentation and fragment ions. The degree and probability of fragmentation is a function of the type of ionization method. Electron impact is a common form of ionization used in mass spectrometers and leads to a moderate amount of fragmentation. This fragmentation is influenced by the structure of the molecule and therefore, if sufficient, leads to a fingerprint pattern that is uniquely identifiable with a particular chemical species.

For a GC/MS, the carrier will be used as the calibrant for both mass range and concentration. If the MSOC unit is operating by sampling air directly, then argon in the atmosphere would be used as the calibrant. In both cases the following discussion holds. The first calculation will deal with the ion signal determination. For any vapor species, the neutral gas must be ionized. There are many methods of accomplishing this. For the MSOC, electron-impact at between 70 and 100 eV ionizes the vapor species. At this electron energy and under reduced collision conditions, the vapor species not only ionizes, but also fragments, due to the excess energy imparted to the vapor species molecules. Some of these fragments are also ions. Due to the molecular bonding, the fragments are related to the structure of the vapor molecule from which they are formed. Libraries of the fragment ions and there relative intensities can be utilized to identify the vapor species. Even the atomic gases, such as helium, neon and argon, exhibit ions at different masses with varying intensities. Some of this variation is due to isotope abundance and some is due to the formation of multiply charged ions, since the electron impact energy is higher that the thresholds for the ejection of multiple electrons and the atomic gas species can not fragment to dissipate the excess energy imparted by the electron impact.

The quantity of ions produced is a vapor species dependent quantity that also depends on the electron energy, density of vapor species and electron current density. The quantity that refers to the probability of an ion being produced from a neutral gas molecule is called the ionization cross section and is usually given the symbol σ. In this discussion, a subscript on σ will denote the gas species. The cross-sections referred to in this discussion will pertain to electron-impact ionization at 100 electron volts energy. The ionization cross-section of helium, σ_{He}, by electron impact is very well known and represents the worse case for signal considerations, since its' cross-section is the smallest for noble gases. The cross-section has an electron kinetic energy dependency, with a 10-30 eV threshold and climbing very steeply (3-4 orders of magnitude or more) beyond the threshold to a maximum near 100 eV electron kinetic energy. The cross-section gently falls off at higher electron kinetic energies. Most molecules follow this basic form of the ionization cross-section. The number of ions, I_b, passing through the mass filter and impinging upon the detector can be determined using the equation for fixed electron energy:

[2.3.1] $I_b = N_a * N_b * \sigma_b * y * T_{eff}$, where

N_a = current of electrons passing through extractable ionization region, (electrons/s)

N_b = gas molecule density of species b, (molecules/μm^3)

σ_b = electron impact ionization cross-section of species b, [ions-cm^2/(electron-molecule)]

y = distance that N_a travels across the extraction aperture, (μm)

T_{eff} = ion transmission efficiency to the detector. ( )

N_{total} = gas molecule density of all species. (From ideal gas law, P/(RT) = n/V.)

$N_b = N_{total} * c/10^6$, where c is the concentration in parts per million, ppm.

For helium, with 100 eV electron beam and 1 μA of electrons and a 26 micrometer extraction aperture, 100 milliTorr of helium would produce 290 pA of extractable helium ions. (For Xenon, under the same conditions, approximately 4,300 pA are generated.) This is 1.8×10^9 ions per second. In traversing the mass filter and the ion optics sections, one out of hundred ions are estimated to reach the detector array from the ion source, resulting in a total beam current of 1.8×10^7 ions per second. With a nominal single scan integration time of 100 milliseconds, this translates to 1,800 charges for a 100 ppm helium gas concentration. (For Xenon, under the same conditions, approximately 8,000 are generated for one of xenon's major isotopes with a concentration of 100 ppm.)

The ionization cross-section can be referred to as a total ionization cross-section (sum of all ion currents produced from a gas species) or a partial ionization cross section which pertains to a particular fragment ion's signal. For the calculation of concentrations, the partial ionization cross-section will be used. The total ionization cross-section for organic molecules has been found to follow a simple algorithm.[2-2] The best correlation was found by simply taking the atoms and assigning them coefficients and then summing the coefficients for a particular molecular formula.

The following table gives the coefficients. All values are to be multiplied by 10^{-16} cm^2. The partial ionization cross section is simply determined by determining the fraction of the total ion fingerprint a particular ion is and multiplying it by the total ionization cross section.

Atom	Cross Section Coefficient
C	1.43
H	0.73
O	1.10
Cl	3.98
Br	5.19
I	6.62
F	0.61
N	1.20

Table 2.3-1. Cross section coefficients for organic molecules to determine total ionization cross section, if ionization cross section by electron impact has not been measured.

These should yield values good to about 5%.

In order to take into account the differences in transmission efficiency between units and over time, equation 2.3.1 can utilize a constant, κ.

[2.3.2] $$\kappa = N_{total} * y * T_{eff}.$$

This makes equation 2.3.1 become

[2.3.3] $$I_b = N_a * c_b * \sigma_b * \kappa.$$

Therefore, if the calibrant is run, then κ for the system can be used to quantify an unknown. The calibrant determines κ by

[2.3.4] $$\kappa = \frac{I_b}{N_a * s_b * c_b}.$$

To determine mass, the magnetic field for the present design is fixed in the system. The magnetic field will become an input value to be maintained in memory, since there will be some variations in the field produced by the magnets used. Figure 2.3-1 provides the coordinate system to be utilized in the following discussion. In the discussion, vectors are given boldface names, whereas the vector components are subscripted with the unit vector direction in normal text. Since the discussion is taking place in the Cartesian coordinate system, the subscripts are x, y and z.

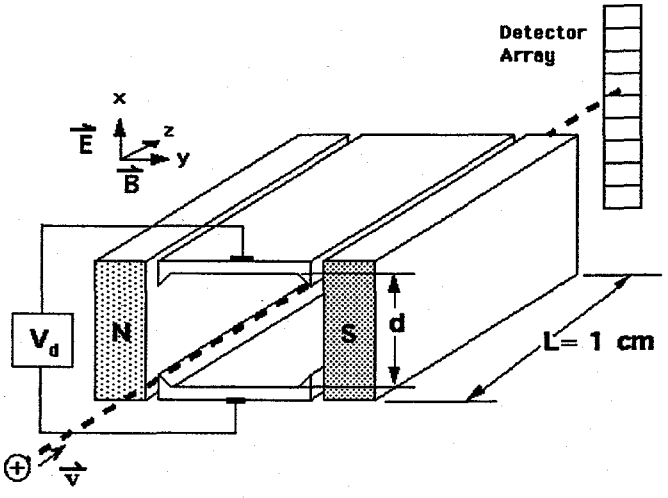

Figure 2.3-1. The coordinate system of the mass filter is such that the magnetic field is directed along the y-axis, the electrostatic field along the x-axis and the initial ion velocity vector is directed along the z-axis.

The simple dispersion of a mass filter is determined by the following equation:

[2.3.5] $$D = x + p * (\frac{v_x}{v_z}), \text{ where}$$

D = distance from the center of array in μm,

x = distance ion is from center due to Lorentz force at the magnetic field section end,

p = distance from end of magnetic field (mass filter) and detector array (1mm in design),

v_x = velocity in the x-direction (mass dispersion) when the ion exits the mass filter,

v_z = velocity in the z-direction (perpendicular to entrance and exit plane of mass filter).

This equation assumes that the ion is in a field-free region after the mass filter.

In order to calculate the x, v_x, and v_z values, the trajectory of the ion in the mass filter must be determined. The mass filter operates by taking a monoenergetic ion beam and velocity filtering the ions. This is due to the fact that a crossed electrostatic/magnetic field in the form here acts as a momentum or velocity filter. Since the beam is monoenergetic and no fragmentation of the ions occurs while the ion is in the mass filter, the separation of velocities also effects a mass separation. For the mass filter in this discussion, the ion is accelerated in the +z direction, the magnetic field is in the +y direction and the electrostatic field is in the +x direction. The forces experienced by the ion are described by the Lorentz equation:

[2.3.6] $$\mathbf{F} = q * [\mathbf{E} + (\mathbf{v} \times \mathbf{B})], \text{ where}$$

F is the net force vector experienced by an ion with velocity vector, **v**, in an electrostatic field vector, **E**, and magnetic field vector, **B**. The velocity vector, **v**, can be determined from

[2.3.7] $$KE_a = \frac{1}{2} * m_a * v^2, \text{ or, } v = \sqrt{\frac{2 * KE_a}{m_a}}$$

where KE_a is the kinetic energy of the ion dropping through a potential difference from the source to the point in question, m_a is the mass of the ion a, and **v** is the resulting velocity vector. With the initial velocity vector, **v**; magnetic field, **B**; and electrostatic field, **E**, being mutually perpendicular to one another, the accelerations can be written as

[2.3.8] $$\frac{\partial v_x}{\partial t} = \frac{q*(E - v_z*B)}{m},$$

[2.3.9] $$\frac{\partial v_z}{\partial t} = \frac{q*v_x*B}{m}, \text{ and}$$

[2.3.10] $$\frac{\partial v_y}{\partial t} = 0.$$

Solving for v_x, v_z and x gives

[2.3.11] $$v_x = v_{x0}*\cos\left(\frac{q*B*t}{m}\right) + \left(\frac{E}{B} - v_{z0}\right)*\sin\left(\frac{q*B*t}{m}\right),$$

[2.3.12] $$v_z = v_{x0}*\sin\left(\frac{q*B*t}{m}\right) - \left(\frac{E}{B} - v_{z0}\right)*\cos\left(\frac{q*B*t}{m}\right) + \frac{E}{B}, \text{ and}$$

[2.3.13] $$x = x_0 + \left(\frac{m}{q*B}\right)*\left(\frac{E}{B} - v_{z0}\right)*\left[1 - \cos\left(\frac{q*B*t}{m}\right)\right] + v_{x0}*\sin\left(\frac{q*B*t}{m}\right).$$

Assuming $x_0 = 0$ m, $v_{x0} = 0$ m-s^{-1}, and $v_{z0} = (2*Ke_a*m^{-1/2}$, then time, t, for the flight of the ion through the mass filter, can be approximated as

[2.3.14] $$\mathbf{t} = \frac{l*\mathbf{B}}{\mathbf{E}}.$$

l is the length of the mass filter (10,000 μm in the present design). The equations that described the ion trajectory while inside of the mass filter simplify to the following with the above assumptions:

[2.3.15] $$v_x = \left(\frac{E}{B} - v_{z0}\right)*\sin\left(\frac{q*B*t}{m}\right),$$

[2.3.16] $$v_z = \left(v_{z0} - \frac{E}{B}\right)*\cos\left(\frac{q*B*T}{m}\right) + \frac{E}{B}, \text{ and}$$

[2.3.17] $$x = \left(\frac{m}{q*B}\right)*\left(\frac{E}{B} - v_{z0}\right)*\left[1 - \cos\left(\frac{q*B*t}{m}\right)\right].$$

The filter is geometrically set up, so that the masses are linearly distributed across the array. In addition, the position, x, of the ion upon exiting the filter is nearly the same as on the detector array. This is due to $v_z >> v_x$. Therefore, the detector array position to mass conversion is approximated by

[2.3.18] $x \cong 22\mu m * (D\#-32)$, and

[2.3.19] $$m = \frac{2 * q * KE_a * B^2}{\left[E - \left(\frac{4 * q * KE_a * x}{q * l^2}\right)\right] * 1.675 * 10^{-27} \frac{kg}{amu}}.$$

Now to calibrate **E**, use the calibrants mass and set an appropriate field and determine the array position for the peak. The applied electrostatic field, $\mathbf{E}_{app}$, would be simply

[2.3.20] $$\mathbf{E}_{app} = \frac{\Delta V_{WF}}{0.014m}.$$

whereas the field experienced by the ion in the mass filter cavity is different from $\mathbf{E}_{app}$ due to a number of phenomena commonly lumped under the term, contact potential. Contact potentials have contributions from junctions of wires having a potential drop to the potential drop going across the solid metal to gas interface. This can also change from metal grain to metal grain. One of the reasons for the use of gold metallizations in the MSOC is that gold has a low contact potential and this contact potential does not vary widely due to changing atmospheres above its surface. Therefore the true electrostatic field is

[2.3.21] $$\mathbf{E} = \frac{(V - CP)}{d},$$

where **E** is the electric field, V is the potential difference measured between the plates forming the electrostatic field, CP is the contact potential, and d is the distance between the plates. This contact potential will lead to a correction factor for the mass assignment of the ion. This value should remain constant over long periods of time and will be monitored by the system.

This know allows the detector array data to be converted to a mass spectrum with both the amu assignment and intensity. This mass spectrum will be compared against a spectral library and the quantity and identification of the chemical species can be made.

2.4 MSOC Design

2.4.1 Ionizer

Ionization in commonly used mass spectrometers is accomplished through the impact of energetic electrons with neutral gas molecules. Here, we will discuss the types of devices that were considered for the mass

spectrograph on a chip implementation and then give more details on solid-state, p-n junction that has been successfully incorporated into the integrated gas sensor.

2.4.1.1 Cold cathode: Reverse bias p-n junction

It has been known for decades that reversed bias p-n junction semiconductor diodes can emit electrons into the vacuum. Indeed, some of the earliest work was done at Westinghouse R&D Center.[2-3] A good review of the history and state of the art in back-biased junction cold cathodes has been written by van Gorkom and Hoeberechts.[2-1] A schematic of such a device, reproduced from reference 2-1, is shown in Fig. 2.4-1. The p-n junction is found at the center of this device, where a shallow, 10 nm layer of implanted n-type semiconductor meets the p-type. Reverse biasing of this diode causes a small fraction of the electron in the circuit to emit to the vacuum.

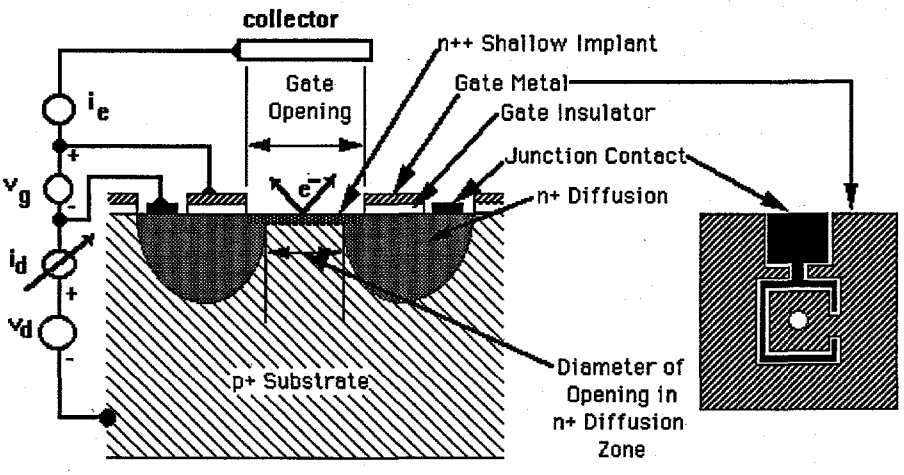

Figure 2.4-1 The reverse bias p-n junction is a solid-state device that can inject low energy electrons into the vacuum above the junction surface.

In the past, many investigators have been concerned with increasing the current emitted per junction area of the electron source for use in CRT, flat panel displays. Exotic methods, such as adding a monolayer coating of low work function cesium on the exterior surface have been used. However, for the MSOC gas sensor application, this current density requirement is relaxed by approximately 5 orders of magnitude. The electron gun current needed for operation of the MSOC is only 750 nanoAmp.

Cold cathode p-n junction electron emitters were demonstrate as early as 1971 as the electron source in a conventional mass spectrometer.[2-4] At present, Northrop Grumman is pursuing p-n junction electron emitters as the primary embodiment of the ionizer for the MSOC. Other feasible embodiments are list below.

For enhancement of the emission efficiency of p-n junctions and to provide durability for the emitting surface in oxidizing atmospheres, thin coatings of cesium or halides of the alkaline metals. The surface energies for

some of these materials are lower than that for silicon, but need to be thin to allow the energetic electrons to penetrate the bulk with sufficient energy to be released into the region above the junction. The coating will also act as a barrier to oxidizing neutral gases and ions from reaching the surface and altering the junction's characteristics.

2.4.1.2 Radioactive particles

Through radioactive decay processes, radioisotopes emit subatomic particles which upon impact with a gas molecule, can ionize these molecules. Thus to their advantage such ionizers require no electrical power; to their disadvantage they are not amenable to switching on and off like an electrically powered ionizer. They are different in energies and particle types emitted compared to the other emitters discussed here.

Regulatory limits and licensing requirements also place obstacles to the use of radioisotopes in sensors. Here another novel advantage to the miniaturization of gas sensors in general, and the MSOC in general, comes forward: the amounts of radioisotope required is tiny, often near or below the exemption limit. This then places a great commercial advantage to the use of radioisotope ionizers in micro- sensors, as it potentially obviates the need for licensing, tracking, and disposal.

The MSOC, in its current embodiment, requires generation of about 1 million ions per second for operation. Any number of radioisotopes may be used to create this quantity. Some of the examples currently under study are ^{45}Ca, ^{241}Am, ^{63}Ni, ^{90}Sr, ^{210}Po, and tritium, the last element being held in a palladium host.

2.4.1.3 Electrical discharges

Electrical discharges operated across a gaseous conducting medium. The electrical current flowing through the discharge volume may be direct current or alternating current, from frequencies of a few Hertz up through radio-frequencies in the kiloHertz and megaHertz and beyond into the microwave at gigaHertz. Such discharges have already been reduced down to the 100 micron dimension for use in flat panel displays, where the electrons accelerated in the discharge field, collide with gas molecules (e.g. neon) and create photon (light) emission. A review of small alternating current discharge technology for use in TV and computer flat panel displays is given by Criscimagna and Pleshko.[2-5] DC discharges are also possible.[2-6]

Structurally, such discharges are very simple, basically consisting of two flat plate conductors facing each other across a gap (typically a few hundred microns). These plates may be covered with a dielectric layer (typically an oxide chosen for its secondary electron emission characteristics) which insures that the ac discharge operates in the capacitive mode. Electrons are created both by other electrons impacting gas molecules, and by secondary emission when electrons collide with the ionization chamber's electrode walls. Operating voltages are typically 100-150 Volts.

Since this means of ion production has already been reduced to the miniature, this is an attractive potential component for MSOC gas sensor. However, the ions created in an ac discharge on these dimensions has a kinetic energy of about 1-2 eV. The range of ion energies produced in a gaseous discharge limits the resolution of the

MSOC device, because it increases the ion beam size through the mass filter and its projection onto the detector pads. Thus a gas discharge ionizer is a workable, though not necessarily preferred, embodiment for our MSOC use.

2.4.1.4 Cold cathode: point emitters

Point emitters consists of small, sharpened points, which create high electric fields at their tips, emitting electrons. These emitters are sometimes referred to as "Spindt" cathodes.[2-7] They operate at or close to room temperature, and are thus a type of cold cathode. A schematic of such a point emitter, reproduced from reference 2-7, is shown in Figure 2.4-2. The points may take various forms, with cones being most popular, but pyramids and wedges have also been used. Materials used for the field emitter points are metals and semiconductors.

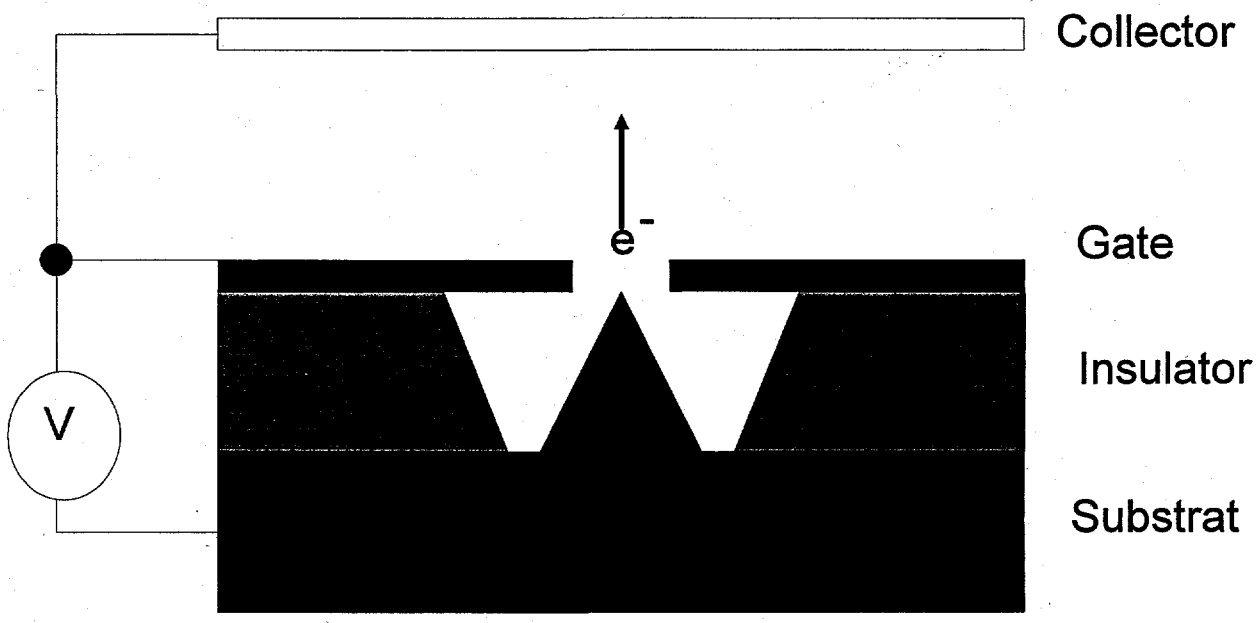

Figure 2.4-2 A point emitter, such as those produced by Spindt and co-workers,[2-7] emit electrons due to the high fields generated at the sharp tips of metal deposits.

Arrays of such emitters were used as the electron source for the ionizer section of a (macroscopic) mass spectrometer built for space exploration.[2-8] Typically, peak emission currents for individual tips ranges from 1-100 microAmps. Thus, to produce enough electron current for a macroscopic mass spectrometer, arrays of multiple emitter tips are required. The novelty invented here is that for the MSOC gas sensor, only one tip, operating at very low current, might be required.

Point emitters are subject to fouling; they usually operate in vacuums far below 10^{-5} Torr.[2-7] Oxygen is usually the destructive agent. Since a primary market for MSOC gas sensors will be atmospheric sampling, and since the ionizer section of the MSOC is expected to operate at a vacuum pressure of 100 milliTorr, protection of the tip is necessary. Recently, work has begun on the use of gold coatings to protect these cold cathodes.[2-9] Other

air resistant emission materials have been used in point emitters, such as diamond coatings.[2-10] Protection of the emitter tip can help emission current, and prolong lifetime.

2.4.1.5 Hot cathodes: thermionic emitters

Thermionic electron emitters differ from the other cathodes mentioned above by operating at very high temperatures, often 2000°K or more. They are the most common electron gun source used in today's bench top size mass spectrometers. Such instruments use an ohmically heated refractory metal wire, usually tungsten, coated with a low-work function substance. Barium or lanthanum oxides are a common choice, as this combines a moderately low work function with a degree of oxidation resistance.

Small and microscopic incandescent elements for microlamp displays have been fabricated since the 1970's.[2-11,12,13] Thermionic electron emission has been demonstrated from metal microbridges fabricated by integrated circuit lithography, with currents up to 10 nanoAmps.[2-14] Lifetimes were only in the minute range.

Still, with the proper choice of materials, a thermionic electron emitter can be used as the ionizer source in the MSOC. Again, due to the miniscule electron current required for the MSOC's electron gun, miniaturization of a thermionic electron source for gas bombardment and ionization is quite viable.

2.4.1.6 Details of p-n junction design incorporated in MSOC

Figure 2.4-1 shows the cross-section and a top view of the reverse-bias p-n junction. The emission of electrons from the device is primarily due to the high fields generated at the edge of the junction, rather than from the edge of the junction. In addition, the thin junction acts as a resistor for the current flowing through it, heating the device. As with most semiconductor devices, temperature will reduce the effectiveness of the device electrically. The temperature will also affect the surface of the junction and therefore, its work function. Therefore, a device geometry that optimizes the edge length is the most desirable to obtain the highest efficiency with respect to current and power. This is accomplished through the use of long thin stripes.

Electrically, the ions must be formed at a well defined potential to obtain the highest resolution for the mass spectrum. The electrical potential is illustrated in Figure 2.4-3. The ions are formed at between 5 and 10 volts above earth ground, so that ground is an attractive potential for positive ions. This means that the gate voltage, V_g of Figure 2.4-1, is set at this potential. This potential is nominally the kinetic energy of the ions. In order for the electrons to have 100 volts of energy at this point, the emitter surface must be maintained at between 90 and 95 volts below earth ground. This places some constraints on the design.

One specification is that the gate insulator must be able to isolate 100 volts of potential difference for long periods of time. Fabrication processes that can affect this are the dielectric deposition condition, the gate metallization, and junction implantation.

In order to control the potential in the region where the ions are formed, the penetration of the emitter junction potential must be shielded from this region. Effective shields should have openings that are no wider than

the distance between them and the point under consideration. To be conservative, we have defined the distance as from the emitter surface to the bottom of the region to be shielded. The well depth will be about 40 micrometers deep and the orifice will extend about 10 micrometer down, so the shield opening should be no wider than 30 micrometers (40 minus 10). The gate has been designed to go between the emission region and is only 15 to 20 micrometers wide.

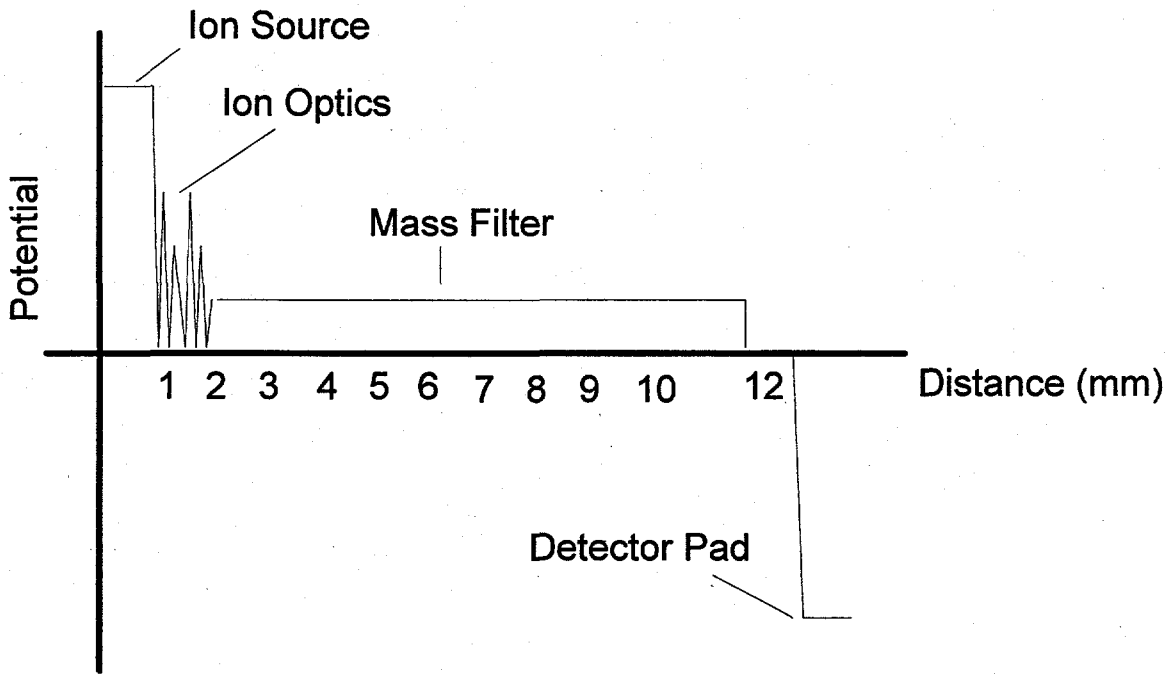

Figure 2.4-3 The ions must be formed so that the rest of the device presents attractive potentials to it so that the highest efficiency can be obtained in transporting them to the detector array.

2.4.2 Mass Filter

The mass filter that is used for the mass selection process has been discussed in detail in section 2.3 as to the operation of the device. In this subsection, the details on the design that affect the performance of the device will be discussed.

In the previous discussion, the assumption was made that both the magnetic and electrostatic fields were uniform. This can be made to be practically true for macroscopic systems, but needs more attention in the microscopic level. One of the reasons for the use of silicon to fabricate the mass spectrograph on a chip was to take advantage of the oxide of silicon for an insulating dielectric. Since the magnet is an external, permanent one, the field will generally vary slowly with respect to position and an average of the field over the mass selection region can be used to determine the final position of the ions. The longitudinal and transverse magnetic fields of one of the magnet yokes fabricated are shown in Figure 2.4-4.

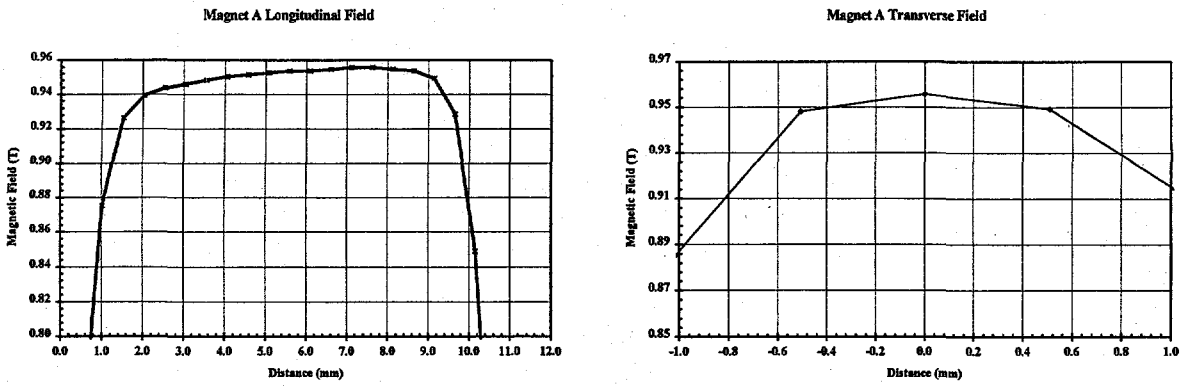

Figure 2.4-4 The permanent, yoke magnets have high, smoothly varying magnetic fields that are highly uniform in the transverse or mass selection direction, as seen in the right-hand plot.

The mass selection region extends from ±0.75 mm of the center.

The resolution of a mass filter with uniform fields follows the equation:

[2.4.1] $\Delta m/m = 2 * V_a * w / (E * L^2)$, where

$\Delta m/m$ = resolution of filter at ion with a mass to charge ratio of m,

w = the slit width of the input or exit aperture, nominally 22 micrometers,

Va = the kinetic energy of ion with mass m passing undiverted,

E = the electrostatic field whose ratio with B passes mass m undiverted, and

L = the length of the filter, typically 10 mm for the present MSOC.

With a magnetic field strength of 0.8 Tesla and an with a mass, m, of 200, the theoretical resolution of the filter is approximately 0.3 amu at 200 amu. If the fields are non-uniform, then what is the limiting resolution that one can obtain? In order to resolve two adjacent masses, the electrostatic field, **E**, can not have variations greater than the difference in **E** required to balance each mass. At balance, let

[2.4.2] $v_m * B = E_m$ and

[2.4.3] $v_{m+1} * B = E_{m+1}$,

where v_m is the velocity of ion with mass m, E_m is the electrostatic field to balance the magnetic field B, so that the ion with mass m can traverse the mass filter without being deflected. The fractional difference between E_m and E_{m+1} is

$$[2.4.4] \quad \frac{E_m - E_{m+1}}{E_m} = \frac{v_m * B - v_{m+1} * B}{v_m * B} = 1 - \frac{v_{m+1}}{v_m}.$$

The kinetic energy of the ions is the same, so

$$[2.4.5] \quad v_m = \sqrt{\frac{2 * q * V_a}{m}},$$

where q is the charge on the ion. Substituting equation 2.4.5 into 2.4.4 gives

$$[2.4.6] \quad \frac{\Delta E_{m,m+1}}{E_m} = 1 - \frac{\sqrt{\frac{2 * q * V_a}{m+1}}}{\sqrt{\frac{2 * q * V_a}{m}}} = 1 - \sqrt{\frac{m}{m+1}}.$$

The uniformity of the electrostatic field can then be determined for a number of resolving powers and is given in Table 2.4-1.

Resolving Power (Δm/m at m)	$\frac{\Delta E_{m,m+1}}{E_m}$
20	2.4%
50	1%
100	0.5%
200	0.25%

Table 2.4-1 The electrostatic field for a mass filter needs to have a uniformity of 0.25% or better.

The aspect ratio of the desired filter is that the cavity is roughly 100 micrometers high and 1500 micrometers wide. The magnetic field is oriented so that its field lines are traversing the 100 micrometer dimension. This places the electrostatic field plates roughly 1500 micrometers apart. Depending on the state of the plate between the electrostatic field plates, this geometry can produce a very non-uniform field. The types of fields that can be produced are shown in Figure 2.4-5. The silicon allows the modification of the surfaces perpendicular to the magnetic field due to the ease that an insulator can be grown or deposited upon it. This allows one to avoid the topmost illustration in Figure 2.4-5 where the magnet poles are electrically grounded. In larger scale systems, the

electrostatic field is made more uniform by reducing the aspect ratio, or the insertion of shims with electrically varying potentials. This is the approach of the middle illustration. The ideal situation is to use a resistive film.

SIMION[2-15] was used to model the generated electrostatic field for the segmented and resistive film cases. Numerous factors were involved in the choice of the design. These included the ability to lithographically define any feature, whether it be a gap between metallizations or the metallization line itself; the ability to dissipate charges that did land on the surface; the uniformity

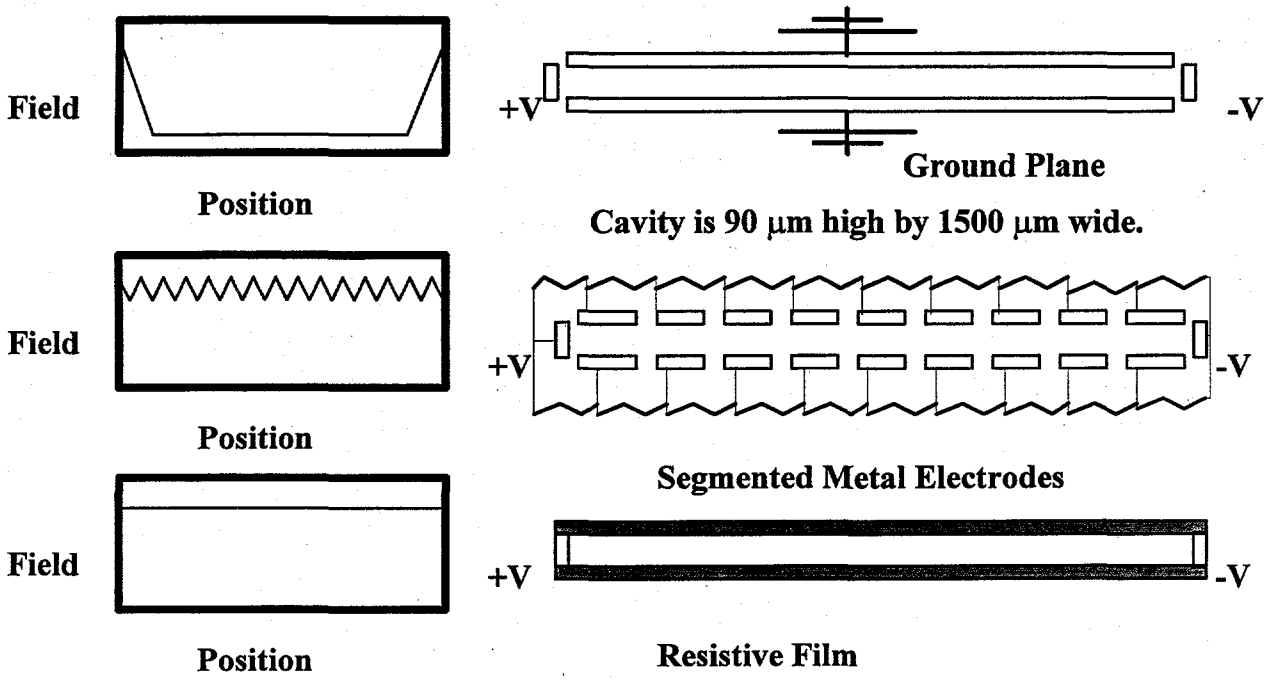

Figure 2.4-5 The electrostatic field configuration for the mass filter cavity are illustrated above for the (top) cavity having electrically grounded plates, such as in the bare magnet case, (middle) the use of segmented metal plates with a stepped voltage drop, and (bottom) a resistive film with a smoothly varying potential with position.

of the electrostatic field generated and the power dissipated when the electrostatic field was at its maximum (30 volts potential difference).

The uniformity of the electrostatic field also depended on how the segmented field plates were connected to the thin film resistor bridge. Three designs were considered for this. The first was to bring the electrical connections to each segment out the detector end of the mass filter cavity to a thin film circuit that was fabricated on a dielectric film. The second was to do the same idea, but at the ion source end of the mass filter cavity. The third was to define the metallized segments on a thin film resistor deposited in the cavity. The second design was actually implemented in early testing and the third was a backup for the thin film resistor approach. The first and second design were adequate when the number of segments was small, such as seven and allowed the evaluation of thin film resistor design. For higher numbers of segments, the third design, where the resistor bridge is fabricated below the segments, was the easiest to fabricate. The third design also has the advantage that the field is well-defined at

The SIMION results for a 7 and 29 segmented field are shown in Figures 2.4-6 and 2.4-7. The fields have the form of the middle part of Figure 2.4-5. The electrostatic field has a large DC component with an oscillating component on top of DC field that is varying according to spatial position. The amplitude of the oscillations from peak to peak determines the anticipated resolution of the system. The beam width is estimated to be about 12 micrometers in width due to the collimation in the mass selection direction in the ion optics section. Non-uniform fields will tend to widen the beam width due to the differing values of the electrostatic field across the ion beam. (The magnetic field variations would also do the same, but since it is monotonically changing very little, the discussion will focus on the electrostatic field effects.) As can be seen in comparing Figures 2.4-6 and 2.4-7, the field has less variance over the beam width for planes that contain higher numbers of segments. The modeling indicates that between 48 and 64 segments are required to obtain a resolution of 1 amu at 200 amu.

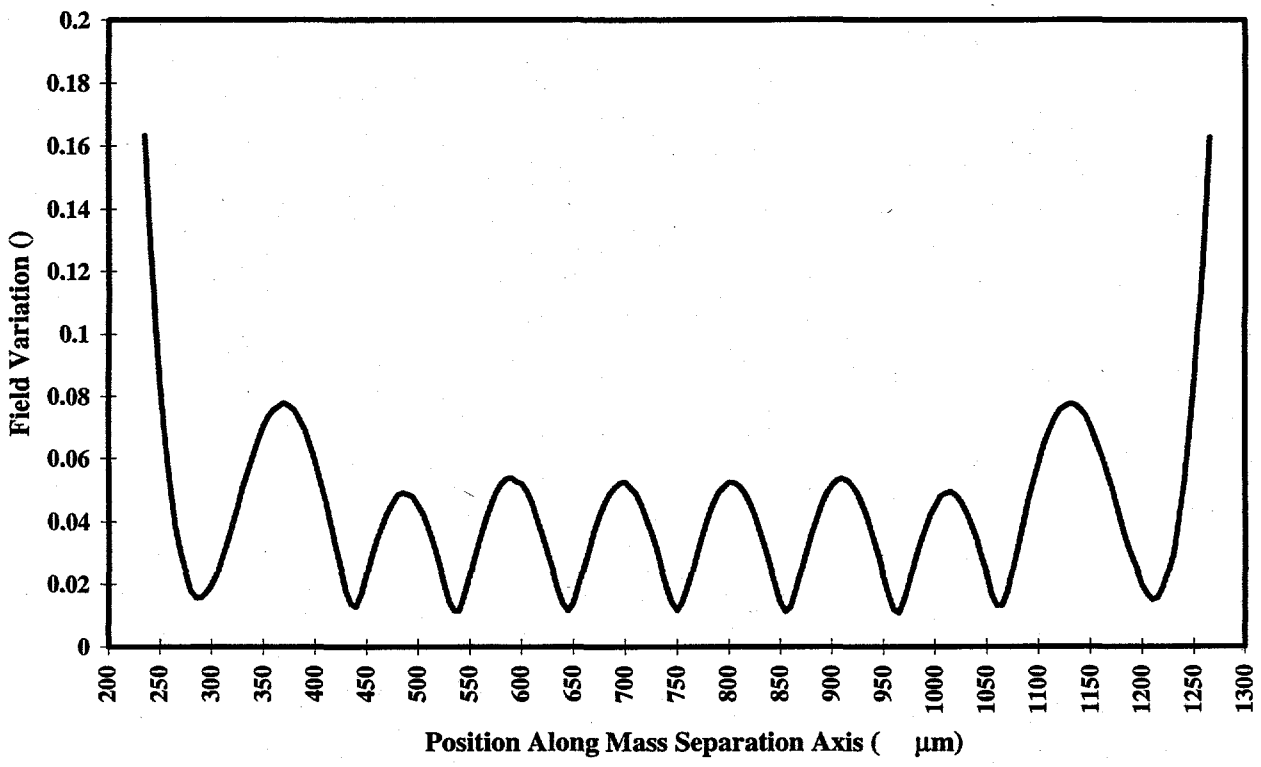

Figure 2.4-6 The modeled electrostatic field variance for a seven segment field plane shows electrostatic field variations of 4.1% across the beam width, yielding a resolution of 1 amu at ~20 amu.

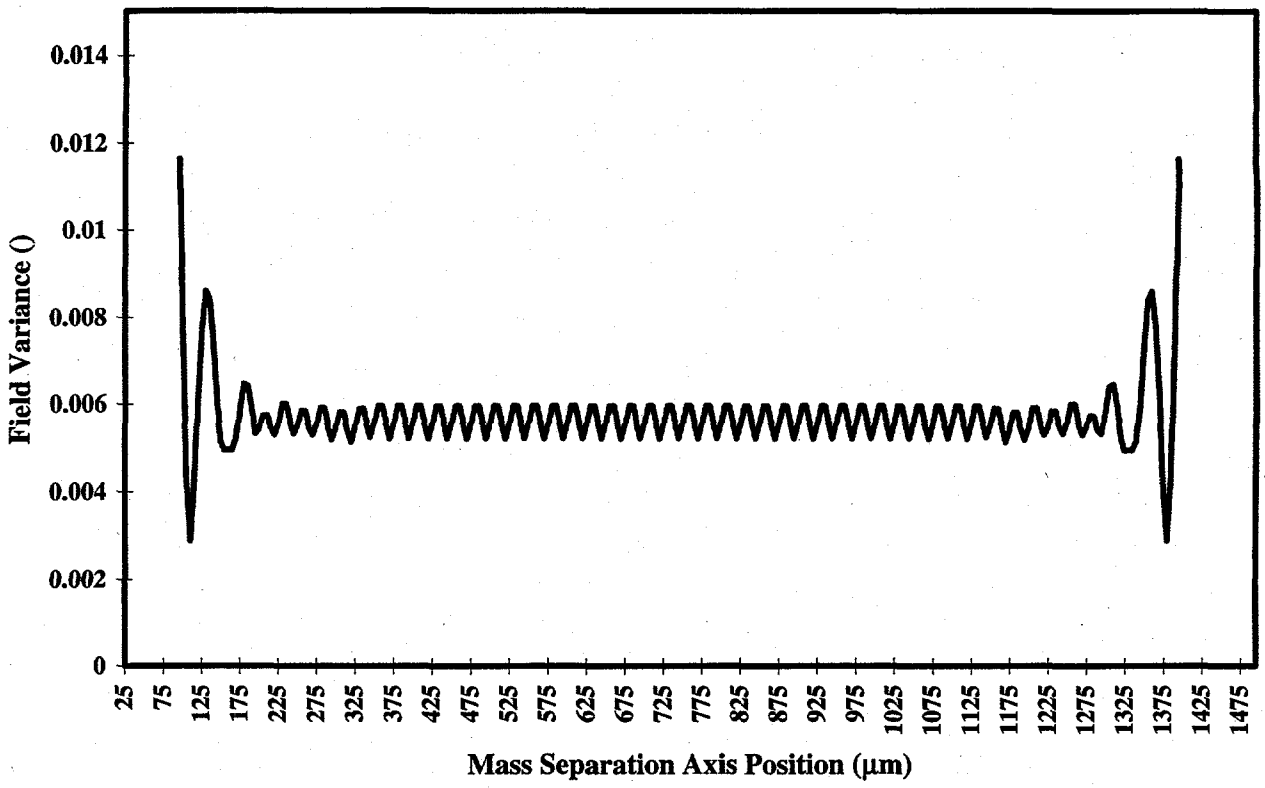

Figure 2.4-7 The modeled electrostatic field for a twenty-nine segment field plane shows electrostatic field variations of 0.58% across the beam width, yielding a resolution of 1 amu at ~100 amu.

With the number of shims becoming large to obtain the electrostatic field uniformity, the desire is to have the resistor bridge film being placed under the shims, rather than run leads to the individual shims to a resistor network located elsewhere on the chip. Linear and exponential fits of the simulations for 13, 22 and 29 segments were made to determine the number of segments to achieve the desired uniformity. The data is shown in Figure 2.4-8. The point for the seven segment design is far off the line of the other simulations. This is believed to be due to the width of the seven segments being wide compared to the chamber height. (100 micrometers width to 90-100 micrometers height)

The greater the number of shims, the narrower the metal and gap spaces are. The line widths would be between 11 and 15 micrometers for the 48 to 64 segment design. For these thin lines, the lithography would need to be excellent to define the gaps and shims to good tolerances over a one centimeter length line. These would be very narrow for contact lithography in the deep wells and are avoided in other areas of the design, such as the ion optics where the narrow lines are defined only in the critical regions (<500 μm in length). With these considerations, the use of a resistive film was the desired approach to obtain a uniform electrostatic field. The next consideration is for the power dissipation.

The power dissipation for the mass filter was desired to be low, so the current flowing through the resistor circuit was desired to be a few microAmperes. This current is orders of magnitude higher that the tens of nanoAmperes that the ion beam might contain. Even if the current is 100 microAmperes at 30 volts, the power of

this component will only be 3 mW. This is negligible when compared to the ionizer (100 to 1000 mW) or the detector (50 mW) for the silicon chip components. The film resistivity was calculated to determine films that could be potential candidates. The results of the calculation are shown in Figure 2.4-9.

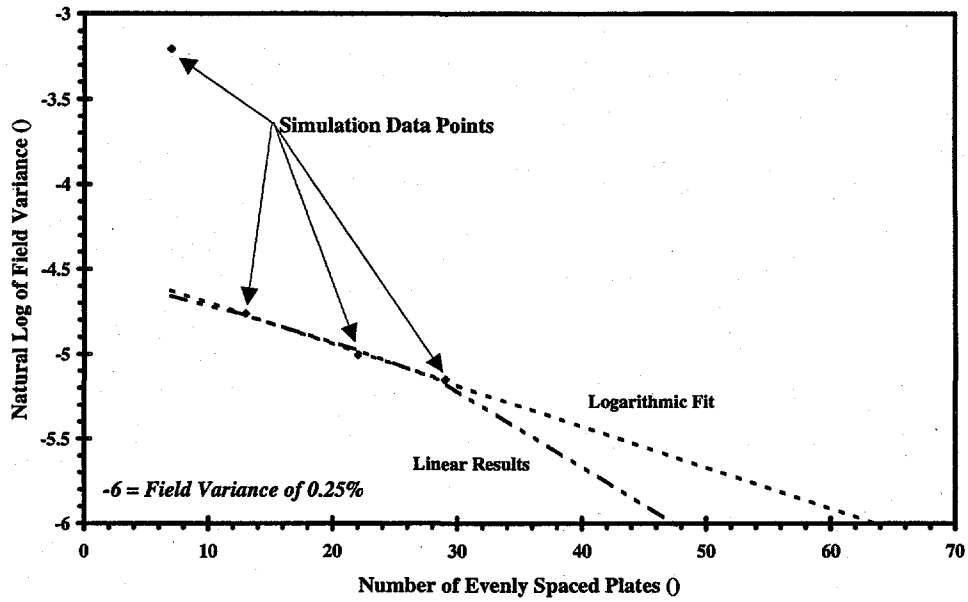

Figure 2.4-8 The estimate of the number of evenly spaced metal grid plates is shown with both the linear fit results and logarithmic fit results plotted.

The number of plates requires strict lithography to maintain line quality over a 1 cm distance and so a resistive film approach is more attractive to meet resolution goals and cost effective fabrication.

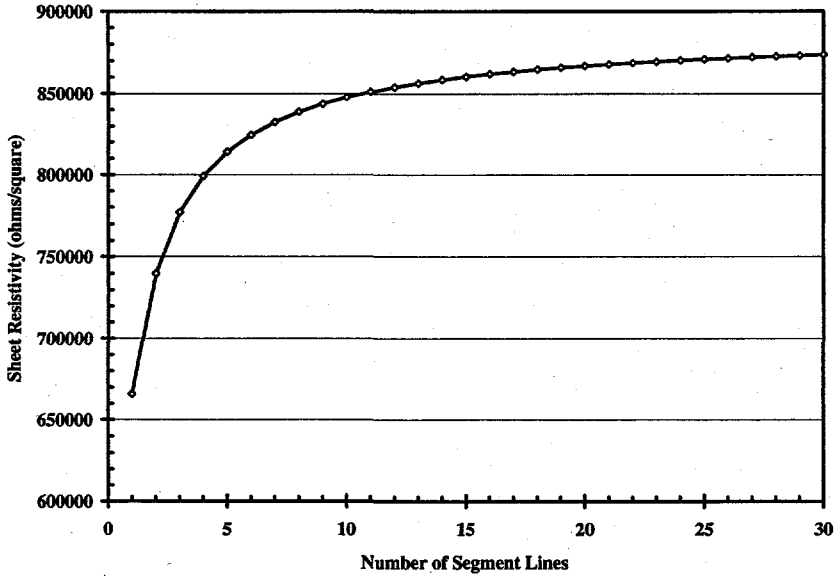

Figure 2.4-9 The resistivity of the resistor bridge film under a segmented metal film is shown here for the number of segments with 1 mA current in the resistor bridge for a 30 volts potential drop.

Equal width of the segment and gap was assumed in this calculation.

This also gave an estimate for the thin film resistor resistivity of between 600,000 and 60,000,000 ohms per square. Undoped polysilicon in our laboratory fits this resistivity requirement for films between 200 and 500 nm in thickness. Measurements have shown that these films have a resistivity of 15,000,000 ohms per square (1500 ohm-cm resistivity for a 0.2 micrometer thick film). This will be used in testing and the final design if charging of the surface is found to be negligible. The native oxide on polysilicon is not expected to be a problem due to its very small thickness of 0.6 to 1.0 nm.

2.4.3 Detector

In any ionic mass spectrometer or charge sensing device, there must be some means to collect the charge and determine its magnitude. For high performance devices, sensitivity of 10's of charges at speeds of 10's of kilocycles is required. An additional resolution constraint is mandated for mass spectrographs : the detector pitch must be smaller than the ion beam while insuring that the ion beam is not missed due to inter-detector spacing of non-contiguous detector elements. As detector pitch is reduced, smaller displacements (i.e. better mass resolution in a miniaturized package) can more readily be discerned.

In the present state of the art, charge multiplication devices and high gain current sensors have been utilized. Charge multiplication devices require high voltages (>1000 volts) in order to operate. This is difficult to implement on a silicon chip where voltages are generally less than 100 volts. High gain current amplifiers, often referred to as electrometers, operate at low voltages and can be used to measure total charge. Electrometers typically found in laboratory instruments are useful for currents on the order of 1E-14 amperes. However, this sensitivity is at the expense of speed, with response time approaching several seconds for these low current values.

Another charge sensor which is typically used for the detection of light and high energy particles is the charge-coupled device (CCD). Photoelectrons generated at a capacitor or charge injection from a high energy particle onto a capacitor are moved by the CCD to a charge sensitive amplifier and converted to a voltage signal which can be sensed. CCD's are capable of sensing low amounts of charge (some as low as 10's of charges per read cycle) with read rates in the 10's of kilocycles, but require a passivating dielectric over the conductive capacitor to protect the active CCD semiconductor layers from environmental degradation. This dielectric precludes sensing of low energy molecular and atomic ions.

High speed and low charge sensing devices capable of accurately detecting low energy molecular and atomic ions are required to effectively miniaturize ionic gas sensors. This disclosure addresses a novel approach which overcomes the limitations of the state of the art charge particle detectors.

Scaling down to the micron level will need low charge sensing, thus we plan to use MOS (Metal-Oxide Semiconductor) switches or CCDs with novel charge injection scheme. MOS switch arrays and CCD's are solid

state devices which are both fast and very sensitive. For linear arrays, MOS switches are easier to fabricate and are comparable to CCD's in performance and therefore, are the preferred embodiment.

State of the art MOS switches and CCD arrays are encapsulated in a passivating dielectric to protect the active device from environmental deterioration. This dielectric is too thick for low energy molecular and atomic ions to penetrate and reach the collecting capacitor. Therefore, these devices will not sense low energy particles.

In the novel MOS implementation discussed in this disclosure, the charge collecting electrode of the capacitor is a bare metal, preferably gold, which is exposed in the mass separation region. Gold is preferred due to its low chemical activity at ambient conditions (i.e. it does not oxidize or react at room temperature). Charges directed onto the metal electrode deposit their charge, become neutral gas species and are removed from the mass filter section via pumps. In the MSOC, the collecting electrode can be formed into a "V" to enhance the collection efficiency by forming a 2-dimensional "faraday " cage. In this "cage", the ions can potentially collide with the collection electrode surface a number of times, increasing the probability of the charge becoming collected. This configuration is illustrated in Figure 2.4-10. Charge is then conducted along an isolated metal line to the CMOS switch circuit, located external to the mass filter section, which controls the readout and resetting of each collection capacitor. The readout and signal processing are performed using double correlated sampling.

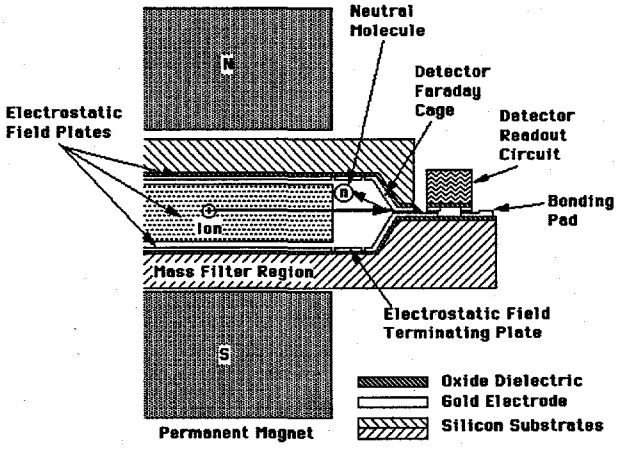

Figure 2.4-10 The "faraday" cage is shown with one potential embodiment of the readout circuit for both an external and integrated magnet design.

The size of the capacitor is bounded by a number of factors which determine sensitivity performance. These factors include : noise induced by the capacitor, the leakage of the capacitor and the space charge limit on the ion current which can be generated and transported through the ion optics.

The detector circuit due to its semiconductor nature possesses a number of noise sources which must be considered in order to determine the correct size of the detector pad. These noise factors come from the collection

capacitor itself, and shot noises from the current flowing as a leakage through the capacitor dielectric and MOS switch. Our present embodiment has reduced the leakage current to below 10 fA and utilizes double correlated sampling to minimize the shot noises. Therefore, the dominant noise factor is the root mean square noise from the capacitor itself. Uncertainty in the detected charge follows the equation :

[2.4.7] $$\text{rms noise} = \sqrt{\frac{k * T * C}{q}},$$

where k is the Boltzmann constant, T is the temperature in degrees Kelvin, C is the capacitance of the charge collecting electrode and q is the value of an elemental charge (1.6E-19 charges per coulomb). The design capacitance for the collecting electrode is 200 fF, and the rms noise is 183 charges at 300 Kelvin. Use of 1 micrometer of silicon oxide as the capacitor dielectric, the size of the collection electrode for 200 fF is roughly 15 micrometers x 250 micrometers. A capacitance between 100 and 1,000 fF can be used with this device to maintain reasonable signal to noise ratios. Larger capacitances require either wider or longer pads.

The ion beam is designed to have a width of approximately 12 to 20 micrometers at resolutions which give less than 1 amu resolution on the detector array. A ten micrometer wide aperture is magnified by the ion optic system by a factor of between 1.2 and 2. Therefore, to maintain adequate resolution in desired areas of the mass range and to match design rules for cost-effective silicon foundries, a pitch of 22 micrometers was chosen for the detector array. For a mass filter width of 1500 micrometers, 64 array elements will be fabricated at the end of the mass filter. Larger capacitors would require long lines or higher dielectric constant insulators in the present design.

At the small end of the detector size scale, the voltage developed on the capacitor during charging, and the photolithographic design rules for the collection pads over the mass filter regions' well wall and the definition of the readout circuitry dominate. The electrical scheme of the detector array is such that the reset voltage of the collection electrodes is between 6 and 12 volts below system ground. The ion energy is set at between 5 and 10 volts above system ground, so the collection capacitors potential will not come up to a value which will electrostatically repel the incoming ions. If the potential change of the collection capacitor is significant, then the efficiency of the ion collection would be affected.

An ion from a gas with 100% concentration would deposit 26,870,000 charges onto a single collection capacitor. This would charge the 200 fF collection capacitor to about 50 mV above its original voltage. This is only a fraction of the 11 to 17 volts difference with which the collection electrodes will be relative to the ion energies. Ideally designed collection electrodes would keep the charging voltage to less than 1V to maintain the same efficiency in collecting the charges for low and high intensity ion beams. The smallest capacitor by this criteria is 20 fF, which would be only about 2 micrometers wide for the collection pad. This pitch would require sub-micron design rules to fabricate the readout circuitry connected to the collection capacitor. The performance does not require this for present applications, but can be used in the future.

With an ionization electron current of 0.75 microAmps in a 10 micrometer diameter beam and a gas pressure of 100 mTorr, a 10 x 26 micrometer opening will draw approximately 4300 pA of positive ion current. Approximately 1% of the extracted ion beam is anticipated to reach the detector array with most of the losses occurring at the ion optic apertures. This results in approximately 43 pA traversing the mass filter region. The calculated space charge limit for this region is 3400 pA for nitrogen at 5 eV, so the current is many orders of magnitude below the space charge limit. Capacitors in the range of 100 fF to 1,000 fF are preferred to accommodate low sensitivity (ppm) and high dynamic range (3 orders of magnitude). This capacitance consists primarily of the Faraday cage, and to a lesser extent, the metal interconnect between the cage and external MOS switch. This novel approach enables the bulk of the capacitor to remain a bare metal surface and therefore sensitive to low energy molecular and atomic ions, since environmental issues are not a major concern in the evacuated mass filter cavity.

For an ion with concentration of 100 ppm, the amount of charge which would be detected by the detector array in a 100 millisecond integration time is 2600 charges. This gives a signal to noise ratio of greater than 14 for the low current signal from a gas with a concentration of 100 ppm.

Charge-coupled devices(CCD) used in the capacitor mode will require a lead connecting the charge collecting well with the metal collecting electrode, which is a novel design. The fabrication of the CCD linear array is much more complicated than for the MOS switch linear array, and therefore is the second preferred embodiment.

The CMOS circuitry can be incorporated into the same substrate as one set of the collection electrodes or it can be hybridized by placing the collection electrodes on the two substrates comprising the gas sensor and then flip-chip bond on the CMOS circuits onto one of the substrates which have leads from the collection electrodes extending out into the flip-chip area.

2.4.4 Integrated Gas Sensor

The key components of a mass spectrograph on a chip (MSOC) have been successfully miniaturized and fabricated in silicon through the combination of microelectronic device technology and micromachining. Here the integration of the key components: input orifice, ionizer, ion optics, mass filter, ion detector array; is described. Further details on the ionizer, mass filter and detector are given in Sections 2.4.1, 2.4.2 and 2.4.3. Our current emphasis is towards tri-lithic integration (components are fabricated on three separate silicon wafers which are bonded together to form the complete device). The tri-lithic integrated gas sensor is illustrated in Figure 2.4-11. The tri-lithic approach was taken due to the different substrate requirements for the p-n junction electron emitter and the detector CMOS circuits. The p-n junction requires a heavily doped, p-type silicon substrate (gas sensor upper half), whereas the CMOS circuit requires a low doped, n-type silicon substrate (detector CMOS substrate). The gas sensor lower half does not have any substrate requirements at this time. The lower half could have contained the detector CMOS circuits, but the CMOS process is susceptible to damage by KOH etching which is the preferred

method of fabricating the wells and orifices. The bumpbonding process allows us to maintain yield of the integrated gas sensor.

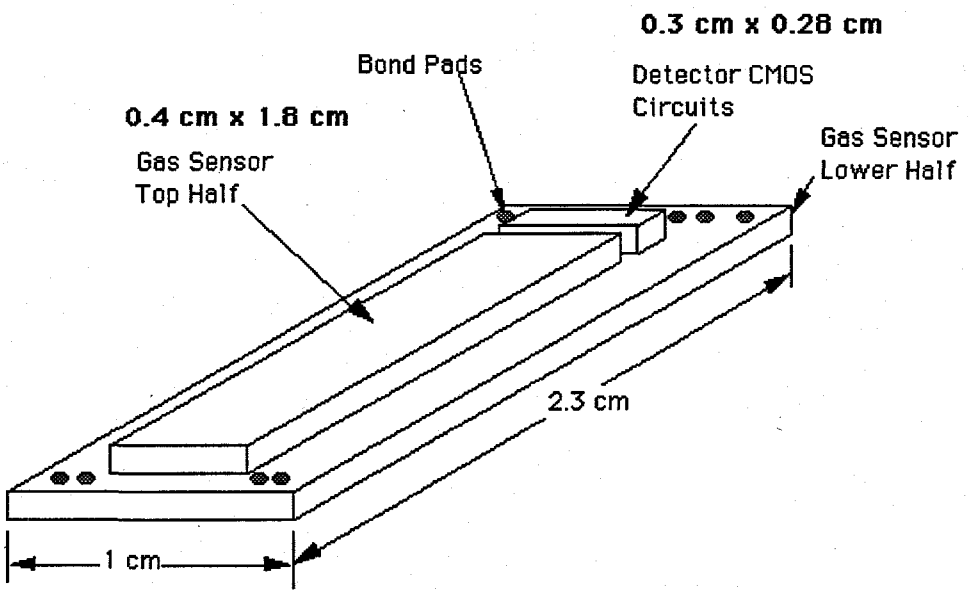

Figure 2.4-11. The integrated gas sensor is shown here with the three silicon chips

The essential semiconductor components are the electron emitter for the ionizer (gas sensor upper half), and the ion detector array (detector CMOS circuits). The other components utilize thin film insulators and conductor electrode patterns which can be formed on other materials as well as silicon. The electron emitter comprises a shallow p-n junction which emits electrons from its surface during breakdown in reverse bias. The emitted electrons are accelerated away from the silicon surface by a suitably biased gate, mounted on the diode structure, and a collector electrode on bottom half of the ionizer chamber. The detector array consists of CMOS capacitors which are read by a MOS switch array. The detector array is connected to an array of Faraday cups which collect the ion charge.

The interior of the miniature mass spec showing the tri-lithic fabrication is shown in Figure 2.4-12. Here the three dimensional geometry of the various parts of the mass spec device are shown together with the location of the ionizer and detector array. The vertical dimension of the drawing has been exaggerated relative to the horizontal dimension. The top and bottom parts of the bi-lithic structure forming the vacuum cavity are bonded together and mounted with a board containing the control and interface electronics and inserted into the permanent bias magnet.

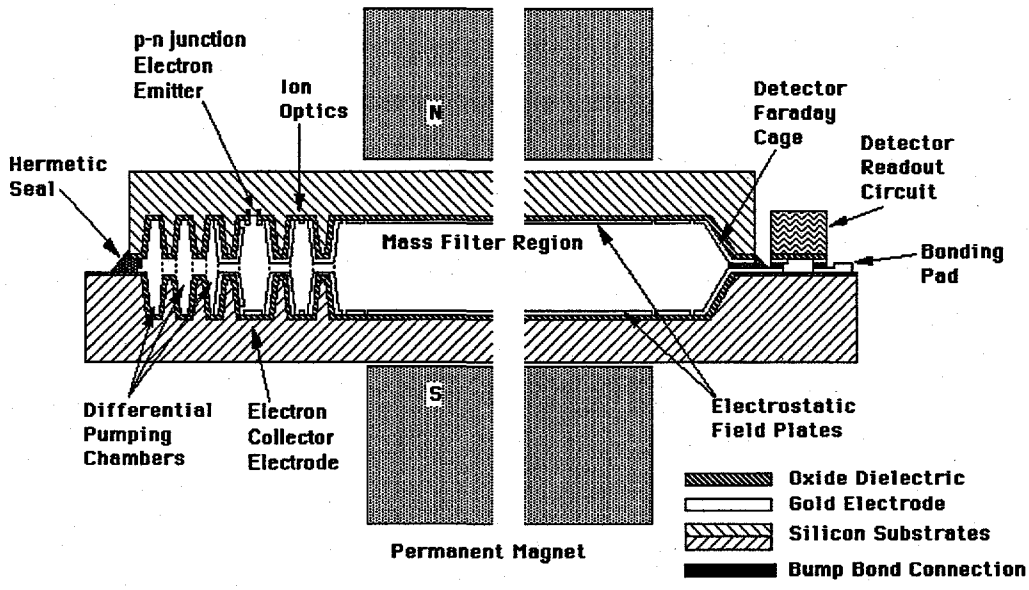

Figure 2.4-12 The interior detail of both halves of the tri-lithic mass spec structure showing the physical location of key components and functions.

The top and bottom silicon pieces are bonded by indium bumps and/or epoxy which is not shown. The main processing steps involved in the fabrication of the all-silicon mass spec are summarized in Table 2.4-2. The processes utilized are found in any microelectronic fabrication facility, except for the spray resist application necessary to uniformly coat the non planar geometry, and the photolithographic techniques used to define electron emitter and electrode structures at the bottom of 40 μm wells. These latter techniques utilize the equipment found in any microelectronic fabrication facility and can be transferred to them.

Table 2.4-2 summarizes the process for the top half silicon piece of the MSOC tri-lith, a similar process is used to form the bottom half silicon piece which contains the electron current collector.

Table 2.4-2 Summary of processes for MSOC fabrication.

	Step	Comment
1.	Etch alignment marks into Si.	Allows alignment of etched geometries with <100> Si.
2.	Etch of 40μm deep wells.	Defines major chambers.
3.	Etch of 10μm deep features.	Defines orifices between chambers.
4.	Oxide growth and etch.	Round sharp edges for metalllization
5.	N+ diffusion.	Defines ionizer.
6.	Grow dielectric stack.	Allows detector collector for the array.
7.	Define dielectric stack.	Forms detector pads and connection to ionizer.
8.	Sb implant.	Defines ionizer emitting junction.
9.	5000 Å Au/ 500 A Cr.	Ionizer, ion optics and interconnect metallization.
10.	Evaporate 5 μm indium.	Defines indium bumps.
11.	100 Å CsI with shadow mask.	Ionizer passivation.

2.5 Component Development

2.5.1 Ionizer

An electron emitter to ionize the incoming gas molecules for a miniature mass spectrometer has been developed based on the avalanche breakdown of a reverse biased p-n junction. A cross section of the device structure is shown in Figure 2.5-1.

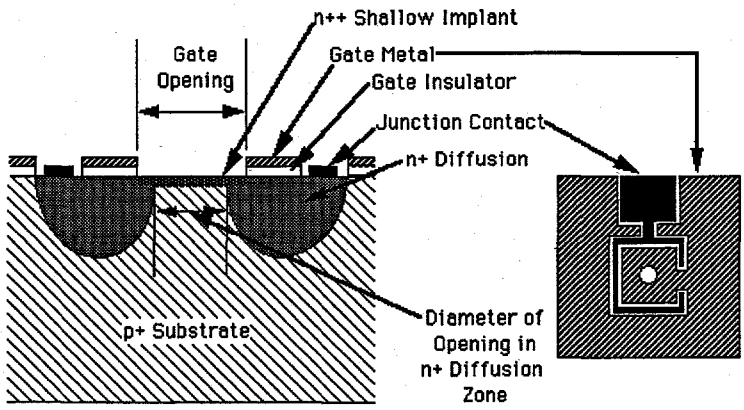

Figure 2.5-1. Top view and cross section of the reverse bias emitter structure being utilized as an electron source for the ionization of neutral gases in the miniature mass spectrograph.

The junction properties are of critical importance to obtain the electron emission current required for the mass spectrometer ionizer. For the abrupt, shallow junctions needed, low energy ion implantation has been used. The junction depth is controlled by the mass and dose of the implanted species, the implant energy, the activation anneal and the substrate resistivity. Additional techniques which affect junction depth are the use of screen oxides and pre-amorphization silicon implants. Both antimony and arsenic implants have been investigated as have screen oxides and pre-amorphization implants. The critical process parameters and the ranges over which they have been investigated are summarized in Table 2.5-1. The ion implantation energy was chosen to be 5 KeV based on the published work conducted at Phillips Laboratories.

PROCESS PARAMETER	INVESTIGATION RANGE
Wafer Resistivity	0.005 to 0.040 Ohm-cm
Implant Ion	Antimony (Sb) and Arsenic (As)
Implant Ion Dose	1.0E14 to 5.0E14 cm^{-2} Sb.
Silicon Pre-amorphization	With and Without Pre-amorphization
Screen Oxide	With and Without 100 Å SiO2
Anneal Temperature Maximum	725 to 800 °C

Table 2.5-1 Summary of process variables investigated which affect performance of the reverse bias junctions as electron emitters.

Considerable effort has been spent to optimize the process for obtaining ionizers meeting the program goal for electron emission of 750 nA. This work is summarized in Section 2.7.1 where the yield for electron emission currents greater than 100, 500, and 1000 nA was a critical performance measure. The desired performance of greater than 750 nA for a period of minutes and high yield was achieved with EMIT 07A which was established as a baseline process for subsequent process optimization. EMIT 08 was a study of ion implantation dose and anneal temperature of both the ion implantation and the metallization. This run indicated that the ion implantation anneal of 725°C and 2E14 cm^{-2} ion implantation dose was the best process to date. In addition, the run indicated that aluminum metallization could be substituted for gold and the pre-amorphization with silicon may not be necessary. EMIT 09 found a contamination in the liner of the rapid thermal annealer (RTA) that poisoned the emitter surface and reduced the electron emission. Subsequent cross-contamination was avoided through the use of a liner dedicated to the MSOC emitters. Runs EMIT 10, 10A, 11 and 11A were fabricated to determine the effect of substrate resistivity on device performance. From these runs, 0.04 ohm-cm resistivity wafers were shown not to be appropriate for our present design and process while a resistivity of approximately 0.01 ohm-cm was encouraging in that the devices exhibited an increase in avalanche breakdown over tunneling breakdown. The emissions were lower due to the fabricated devices being smaller geometrically from the phosphorus diffusing farther under the

same conditions with the 0.01 ohm-cm versus the 0.005 ohm-cm wafers. EMIT 12 was a repeat of the baseline process and exhibited performance similar to that of the baseline.

Up to this point, the improvements to the emitter had been obtained through process optimization. Some data in the literature suggested that a change in geometry also would be beneficial. Indeed, observation of visual light emission under a microscope had shown that the light was observed primarily along the periphery of the device. Thus, devices containing stripes, maximizing the periphery in a given area, were designed. EMIT 14 and EMIT 15 were fabricated with die containing both circular (baseline process geometry) and linear (striped) device geometries. A variety of lengths, widths and number of stripes have been investigated as shown in the device layout in Figure 2.5-2. Multiple striped devices from these runs showed the highest electron emission achieved.

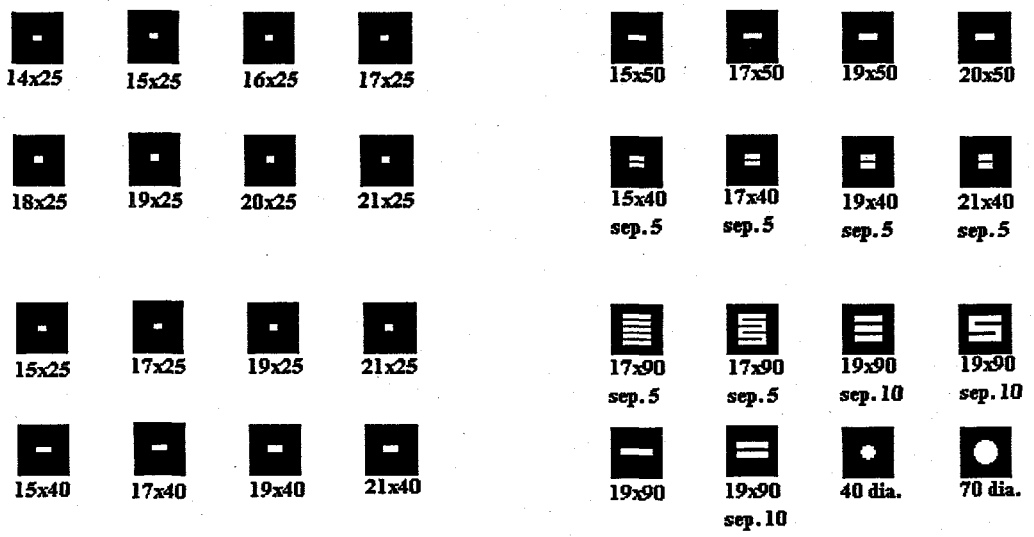

Figure 2.5-2 Die layout for linear designs of developmental emitter test structures.

The multiple stripe elements in the lower right of the figure are devices which have exhibited the best lifetime and emission characteristics.

In addition to the magnitude of electron emission, the lifetime of electron emission is of equal importance. Initial work focused on cylindrically symmetrical emitters of varying diameters and yielded devices that could not maintain emitted currents at the levels required for more than minutes. Figure 2.5-3 shows the emission characteristics as a function of time for both a circular and a striped device.

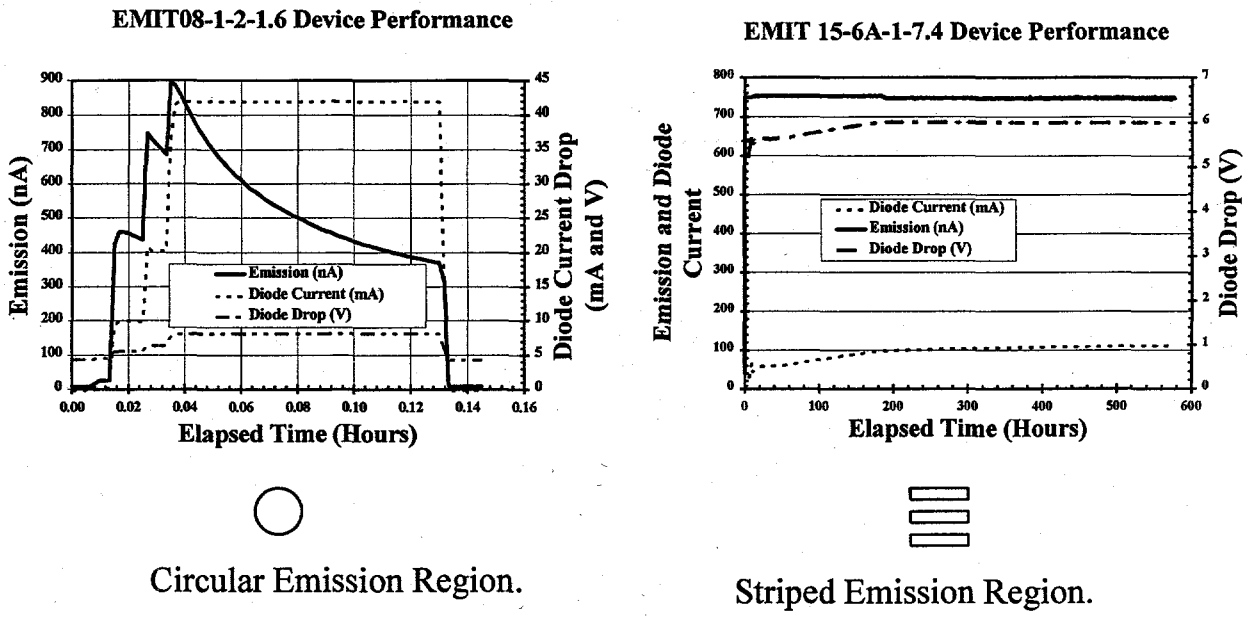

Figure 2.5-3 Electron emission characteristics for a circular and striped emitter structure.

The increase in the lifetime of the striped device is greater than accountable for by only the change of the geometry. There are two possible mechanisms. The first is that the emission brightness is a function of the width of the device. This phenomenon was also noted by workers at Phillips Laboratories.[2-1] A second mechanism is the heating of the emitter surface due to the additional power that these devices are drawing during operation. The power of the larger striped emitters is between 0.5 and 1.0 Watts as compared to 0.1 to 0.15 Watts for the circular emitters. The heated surface may keep the surface free of absorbed gas surface layers that significantly degrade the surface work function.

One interesting note on these devices was the correlation of light and electron emission. Visible light emission was studied under a laboratory microscope in normal atmosphere while power was applied across the device. The visible light emission gave a measurement of the size of the emission area (or periphery). The operation of the reverse bias diode in air did not burn the devices out unless excessive power was applied. After operation in air, emitters annealed at 300°C in forming gas for a half hour were successfully rejuvenated. Alternatively, devices unpowered in vacuum for a period of time (three to four weeks) recovered their emission characteristics. After short periods of time of being off, the electron emission returns to the value prior to shutdown and not the initial emission when the virgin emitter was first operated. These results provide further evidence that the emission changes are due to an instability of the surface work function.

The devices from EMIT 14 and 15 have been tested in both vacuum and at operating pressures with gases. The presence of gases depresses the emission, but the devices still operate for days at the specified currents required. Designs with both the internal and external accelerating gates operated for longer periods of time and with a smaller depression of the electron current. This indicates that the accelerating gate is repelling ions away from the active surface of the emitter and therefore, protecting it from damage.

Long term operation of the device necessitates stabilization of the surface work function. In addition to an increase in emission area, controlling ion bombardment or operating at higher temperatures, the use of surface treatments has been investigated. Cesium oxide and cesium iodide have been applied in thin layers (between 100 and 500 Angstroms) to the surface of the emitters. Those coated with cesium oxide displayed reduced emission characteristics as has been noted with oxides of barium, strontium and calcium. Cesium iodide coated devices, on the otherhand, displayed an enhanced emission (slightly) and better lifetime characteristics. Cesium iodide is the preferred protective coating with bare silicon being second.

Lifetime limitations owing to device fabrication have been found to be due to two areas. The first is the contact line to the phosphorus diffusion. This metal line in the test emitter components must go over a one micrometer dielectric step and thins at this point. During operation at high bias currents, this point opens. The second area is the isolation of the accelerating gate. Some misalignments were encountered during lithography on some of the wafers. Poorly isolated gates lead to poor lifetime performance and conversely, those with good isolation yielded good lifetime. EMIT 15 was fabricated in order to check the lifetime limitations found with EMIT 14 devices. Thicker contact metallizations and better alignment were done with this lot. No failures due to metallization have been found. In fact, no device catastrophically failed in testing.

The ionizer development work described in the above paragraphs was conducted to implement a electron emitter for the integrated gas sensor. This work has showed the importance of both device design and surface condition and the interaction between them. Based on the above work, a substrate resistivity of 0.01 ohm-cm, implanted with $1x10^{14}$ cm^{-2} antimony at 5 KeV and rapid thermally annealed at 725 °C were chosen for the integrated gas sensor. A geometry with multiple stripes which are cesium iodide coated and with an internal gate is preferred.

2.5.2 Mass Filter Component

The mass filter section of the mass spectrometer on a chip is composed of three main elements. These are the mass filter which separates the ion by mass in crossed electric and magnetic fields, the ion optics which focus the ions into the mass filter, and the detector pad inputs on which the ion charge is collected for input to the detector readout.

As discussed previously, several designs of the mass filter have been investigated. Designs which have been fabricated in silicon wells suitable for full integration have included seven segment and nine segment filters, and a continuous polysilicon filter.

A seven segment, electric field plate was fabricated in the silicon mass filter with voltages determined by a fixed, thin film, resistor bridge. The segmented electric field plate was utilized due to the severe aspect ratio of the mass separating cavity. This cavity is 86 micrometers high and 1500 micrometers wide. Both cavity surfaces are parallel to the magnet pole piece (1500 micrometer dimension) and divided into seven gold electrodes defined on top of a thermal oxide dielectric. Upon assembly of the cavity, there are pairs of segments that face each other. One segment is on the upper cavity surface and the other is on the lower. The potential on each member of the electrode pair is nominally the same. Designs were considered that placed a grounded electrode between each powered electrode. Electrostatic modeling shows that a more uniform electrostatic field is generated without interleaving of ground segments between the powered segments. In addition, modeling showed a purely resistive film was determined to provide the ideal electrostatic field. The resistivity of an appropriate film was calculated for the geometry desired and fell in the range of 100 and 10,000 ohm-cm. Undoped polysilicon of between 0.3 and 0.5 micrometers thickness falls in this resistivity range. Films deposited in our facilities have been measured with resistivities of 1500 to 1900 ohm-cm

Testing of the silicon mass filters were performed in a test station using both pure and mixtures of noble gases. The data were collected using an electron multiplier set up for charge particle counting. The field of the permanent magnet used with the silicon mass filter was measured before assembly. The silicon mass filter scan voltage was converted to mass using the magnetic field and ion energy values and plotted as a function of atomic mass units. Data from the mass filter with a seven segment field plate are shown in Figure 2.5-4.

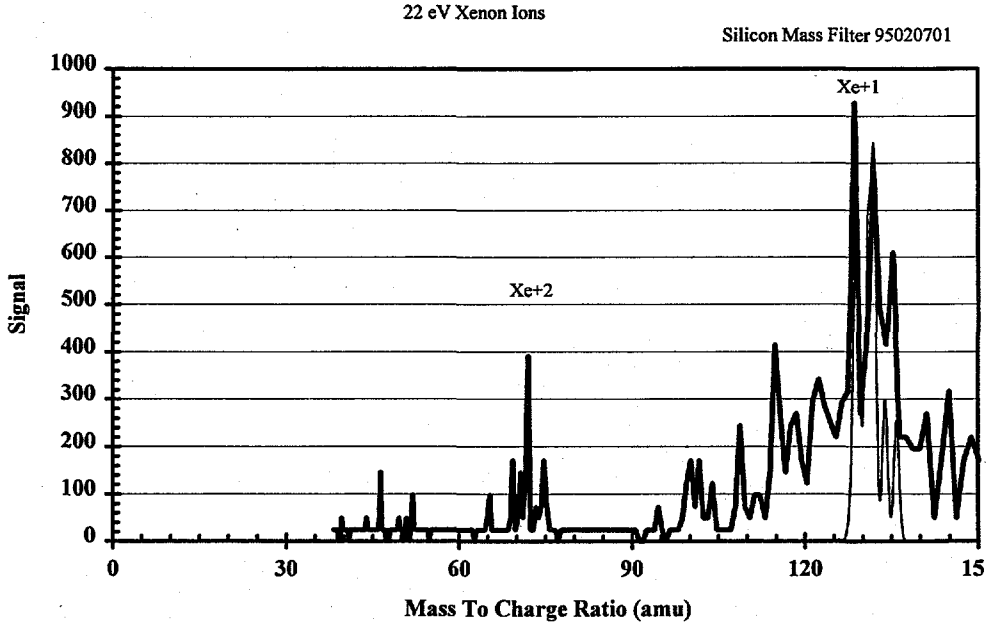

Figure 2.5-4 Measurements of xenon with the silicon mass filter showing the singly and doubly ionized isotopes.

Both xenon singly and doubly charged ions are detected. The signal from the doubly charged xenon ions is higher than that of the singly charged, due to the detector's stronger response to multiply charged ions. The xenon isotopes are separated by the silicon mass filter and analysis of the full width at half maximum (FWHM) indicates that the resolution measured is 1.2 amu at 129 amu. Since a mass filter with a constant magnetic field and ion energy is a non-constant resolution device, this resolution at 129 amu is expected for a system having a resolution of 1 amu at 100 amu.

The test station was improved by replacing the permanent magnet with an electromagnet to aid in passing the ion beam through various silicon mass filters. An ion beam was formed in a laboratory ion source that was constructed with additional electrostatic deflectors. These electrostatic deflectors align the ion beam with the axis of the silicon mass filter. The use of the electromagnet helps in the identification of the peaks detected. Relationships of the peak position with respect to the electrostatic and magnetic field strengths have been confirmed as those expected from our geometry. A mass spectrum was taken of xenon with the electromagnet and a silicon mass filter. An afocal lens and polysilicon resistor film, mass filter prototype have been constructed and evaluated in the improved test station. Both singly and doubly charged ions of xenon are detected as shown in Figure 2.5-4. Figure 2.5-5 shows the mass region around the singly charged xenon on an expanded scale with the nine element ion optics rather than the three element ion optic lens.

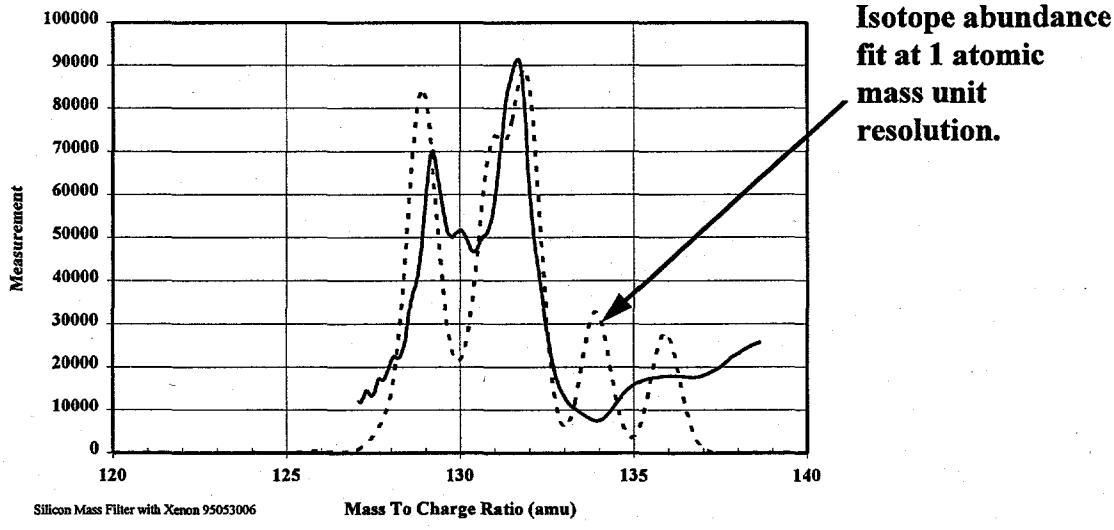

Figure 2.5-5 Expanded scale view of singly charged xenon isotope mass region with simulated isotope abundance pattern.

This data indicates that the resolution of the silicon mass filter here was between 1.3 and 1.5 amu at 129 amu. This corresponds to between 1.0 and 1.3 amu at 100 amu. Figure 2.5-5 shows that the present measurements

are in much better agreement with the natural abundance ratios of xenon. These are simulated on the figure as the narrow line feature with a resolution of 1.0 amu full width at half maximum.

Another major area of development for the mass filter component was the ion collection pads for signal input to the detector multiplexer chip. The collection pads are located at the end of the mass filter charge separation region on the end wall formed from the 40 μm cavity recess Here, sixty-four collection elements are fabricated along the well edge on a twenty-two micrometer pitch to meet the requirements imposed by the integrated gas sensor. A ground plane is desired between the individual collection pads to minimize cross-talk and also to minimize the dielectric exposure that can charge up and deflect ions. Fabrication of the integrated gas sensor utilizes contact lithography, with deep depth of focus requirements, for the thick sprayed resist coating which gives a resist line width of about six micrometers or more. On a twenty-two micrometer pitch, this would leave an unacceptable amount of dielectric exposed.

To overcome the dielectric exposure limitation, a self aligned approach has been developed using a multilayer stack of silicon oxide and silicon nitride. The top nitride is defined using photoresist and etched. The underlying oxide is etched so that the silicon nitride on top of the silicon oxide overhangs the edge of the etched oxide. The photoresist is then removed and the metal film deposited by evaporation. Evaporated films are line of sight deposits with the source located so that the deposition lines are nearly perpendicular to the surface. Side wall coverage is minimal in this technique with the nitride overhang interrupting the metal continuity. The ground plane and collector lines are then isolated vertically instead of horizontally. Figure 2.5-6 schematically illustrates the final stack.

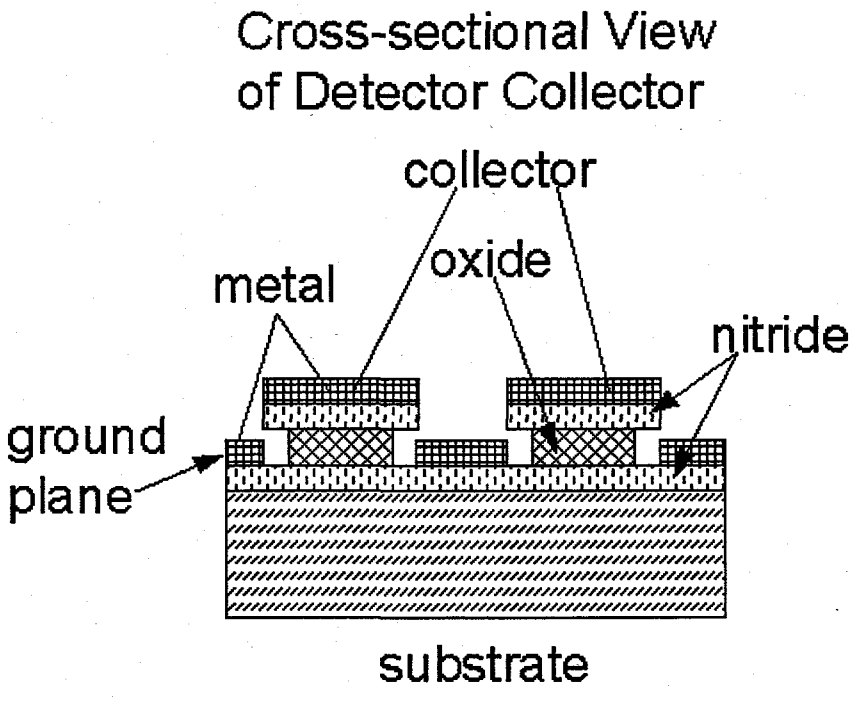

Figure 2.5-6 Schematic cross-sectional view of detector ion collector pad illustrating self-aligned deposition of collector and ground plane metal.

Critical to this process is the silicon oxide thickness which must be controlled so that metal does not bridge the nitride overhang causing shorts to ground. The silicon oxide deposition process for this multilayer stack needs to be conformal so that the oxide thickness does not vary greatly in going from the bottom of the well, up the wall, to the top of the wafer. Three silicon oxide deposition techniques were tested for the integrated gas sensor geometry. These were an atmospheric pressure chemical vapor deposited oxide referred to as silox, magnetron sputtered quartz, and plasma-enhanced chemical vapor deposited (PECVD) oxide. Deposited films of silox are non-conformal with a thickness variation of over a factor of six from the top to bottom of the well wall. Both sputtered quartz and PECVD oxide conformally covered the wall geometry. Sputtered quartz was chosen, since its etching characteristics were slower and thus would give better control for the undercutting geometry. The completed pads are shown in the scanning electron microphotograph of the metallized structures in Figure 2.5-7.

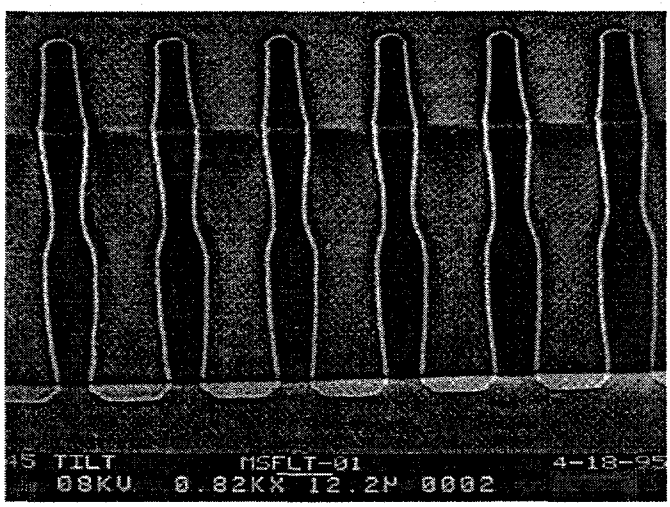

Figure 2.5-7 SEM photograph of ion collection pads on wall of mass filter.
Bright rim shows oxide undercut region which separates metal layers.

The third area of the mass filter component is the ion optics section which focuses the ion beam on the aperture entrance to the mass filter maximizing the ion signal at the detector pads. On a planar wafer where high definition contact lithography would be straightforward, fabricating the metal structure (8 μm gaps between 80 μm segments) would pose little difficulty. However, on the bottom surface of a 40 μm deep well and using sprayed photoresist maintaining constant line width over a 1500 μm length (well width) becomes considerably more challenging. A fabricated ion-optics structure is shown in the microphotograph of Figure 2.5-8. Here, the lithography challenge was eased, after electrostatic modeling, by widening the 8 μm gap in non-critical regions. The fabricated ion optics are near the required dimensions as determined from the modeling effort.

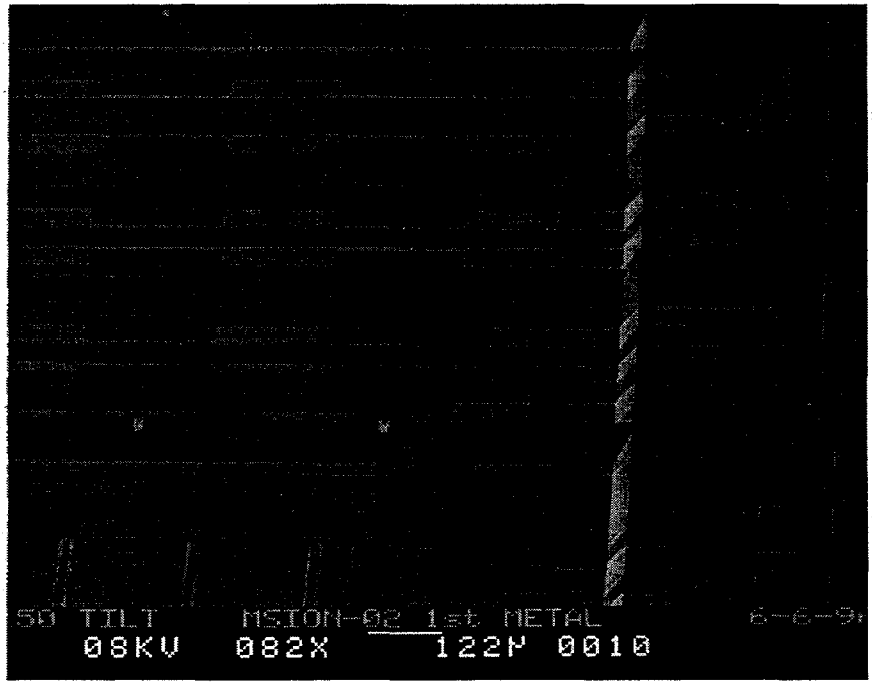

Figure 2.5-8 SEM photograph of ion optics region of mass filter.
The fine lines (spaces) between biased metal regions alter the electric field which focuses the ion beam.

2.5.3 Detector Array and Interface Fabrication

For low charge sensing requirements at the micron scale of the MSOC, MOS (Metal-Oxide Semiconductor) switch arrays are both fast and very sensitive. Mass separated ion charges are directed onto the metal electrode, deposit their charge, become neutral gas species and are removed from the mass filter section via pumps. Charge is then conducted along an isolated metal line to the CMOS switch circuit, located external to the mass filter section, which controls the readout and resetting of each collection capacitor. The readout and signal processing are performed using double correlated sampling.

The detector circuit due to its semiconductor nature possesses a number of noise sources which must be considered in order to determine the correct size of the detector pad. These noise factors come from the charge collection capacitor itself, and shot noises from the current flowing as a leakage through the capacitor dielectric and MOS switch. Our present embodiment has reduced the leakage current to below 10 fA and utilizes double correlated sampling to minimize the shot noises. Therefore, the dominant noise factor is the root mean square noise from the capacitor itself. Uncertainty in the detected charge follows the equation :

[2.5.1] $$\text{rms noise} = \sqrt{\frac{k * T * C}{q}},$$

where k is the Boltzmann constant, T is the temperature in degrees Kelvin, C is the capacitance of the charge collecting electrode and q is the value of an elemental charge (1.6E-19 charges per coulomb). The design capacitance for the collecting electrode is 200 fF, and the rms noise is 183 coulombs at 300 Kelvin. Use of 1 micrometer of silicon oxide as the capacitor dielectric, the size of the collection electrode for 200 fF is roughly 15 micrometers x 250 micrometers. A capacitance between 100 and 1,000 fF can be used with this device to maintain reasonable signal to noise ratios. Larger capacitances require either wider or longer pads.

The ion beam is designed to have a width of approximately 20 micrometers at resolutions which give less than 1 amu resolution on the detector array. A ten micrometer wide aperture is magnified by the ion optic system by a factor of two. Therefore, to maintain adequate resolution in desired areas of the mass range, a pitch of 22 micrometers was chosen for the detector array. For a mass filter width of 1500 micrometers, 64 array elements will be fabricated at the end of the mass filter.

At the small end of the detector size scale, the voltage developed on the capacitor during charging, and the photolithographic design rules for the collection pads over the mass filter regions' well wall and the definition of the readout circuitry dominate. The electrical scheme of the detector array is such that the reset voltage of the collection electrodes is between 6 and 12 volts below system ground. The ion energy is set at 5 volts above system ground, so the collection capacitors potential will not come up to a value which will electrostatically repel the incoming ions. If the potential change of the collection capacitor is significant, then the efficiency of the ion collection would be affected.

An ion from a gas with 100% concentration would deposit 26,870,000 charges onto a single collection capacitor. This would charge the 200 fF collection capacitor to about 50 mV above its original voltage. This is only a fraction of the 11 to 17 volts difference with which the collection electrodes will be relative to the ion energies. Ideally designed collection electrodes would keep the charging voltage to less than 1V to maintain the same efficiency in collecting the charges for low and high intensity ion beams. The smallest capacitor by this criteria is 20 fF, which would be only about 2 micrometers wide for the collection pad. This pitch would require sub-micron design rules to fabricate the readout circuitry connected to the collection capacitor. The performance does not require this for the present application.

With an ionization electron current of 1 microamp in a 10 micrometer diameter beam and a gas pressure of 100 mTorr, a 10 x 26 micrometer opening will draw approximately 4300 pA of positive ion current. Approximately 1% of the extracted ion beam is anticipated to reach the detector array with most of the losses occurring at the ion optic apertures. This results in approximately 43 pA traversing the mass filter region. The calculated space charge limit for this region is 3400 pA for nitrogen at 5 eV, so the current is many orders of magnitude below the space charge limit. Capacitors in the range of 100fF to 1,000fF are preferred to accommodate low sensitivity (ppm) and

high dynamic range (3 orders of magnitude). This capacitance consists primarily of the detector collection pads, and to a lesser extent, the metal interconnect between the pads and external MOS switch. This novel approach enables the bulk of the capacitor to remain a bare metal surface and therefore sensitive to low energy molecular and atomic ions, since environmental issues are not a major concern in the evacuated mass filter cavity.

For an ion with concentration of 100 ppm, the amount of charge which would be detected by the detector array in a 100 millisecond integration time is 2600 charges. This gives a signal to noise ratio of greater than14 for the low current signal from a gas with a concentration of 100 ppm.

To verify the design parameters, a twenty element array has been fabricated and subjected to an ion beam. The response of the detector array is shown in Figure 2.5-9. A broad ion beam with known cross section was directed onto an electrically isolated metal plate which contained a small aperture through which ions were directed onto the detector array's collection electrodes. The current striking the metal plate was measured with an electrometer and the area ratio taken to determine the current striking each collection electrode. The results are presented in Figure 2.5.9. The horizontal axis is the current striking the array collection electrode. The vertical axis is the voltage out of the amplifier interface card for the extreme element on the array. The dotted line is the anticipated response and the line is the fit for the detector data. There is good agreement between the fitted detector response and the system design response.

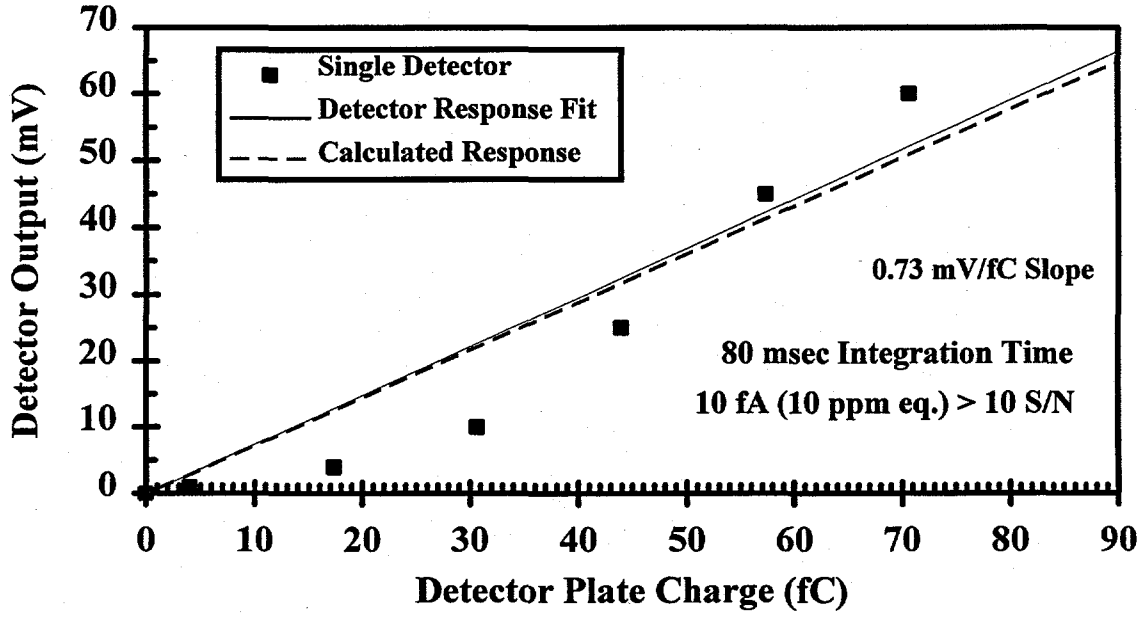

Figure 2.5-9 Response of 20 element detector test circuit to verify design parameters.

Sixty-four element detector arrays were designed and fabricated based on the twenty element array design with on-chip shift registers. Two test devices were fabricated in each cell of the design along with five hybrid devices. The test devices consist of a 20 and 64 element array with the ion collection electrodes on the same substrate. These can be tested in the vacuum test chamber with an ion beam to check device operation without

having to be connected to an integrated gas sensor. Figure 2.5-10 shows a microphotograph of one of the test detector components. Twenty element arrays are fabricated on the same die for process monitoring. On the integrated gas sensor, the digital circuitry and charge to current amplifier will be placed on a separate chip. This chip will be indium flip-chip bonded to the main substrate that contains the charge collecting capacitors. This allows a yield enhancement and removes the digital circuitry from the micromachining steps of the integrated gas sensor.

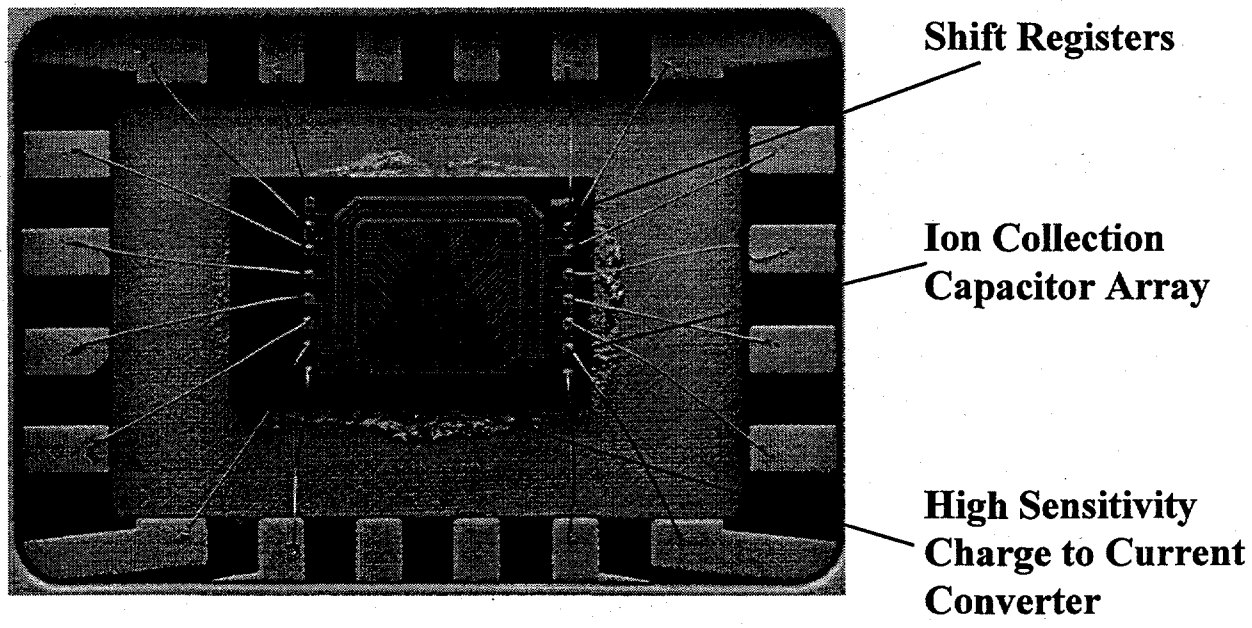

Figure 2.5-10 Photograph of 64-element array on 22 μm pitch.
The charge collecting elements are at the mouth of the c-shaped structure which is the digital shift register.

An improved detector interface has been designed and fabricated. The initial interface had been designed to accommodate a number of different detector designs. Since the on-chip digital shift registers operated with good yield, the design of the interface board focused on this design. Boards were fabricated and tested. Figure 2.5-11 shows the output versus low energy ion current. A linear response to ion current was obtained with a slope of 85.6 mV per femtocouloumb. The noise was less than 0.5 mV for the measurement. This board improved the gain by a factor of 100 over the previous design and utilized one voltage amplifier stage instead of two.

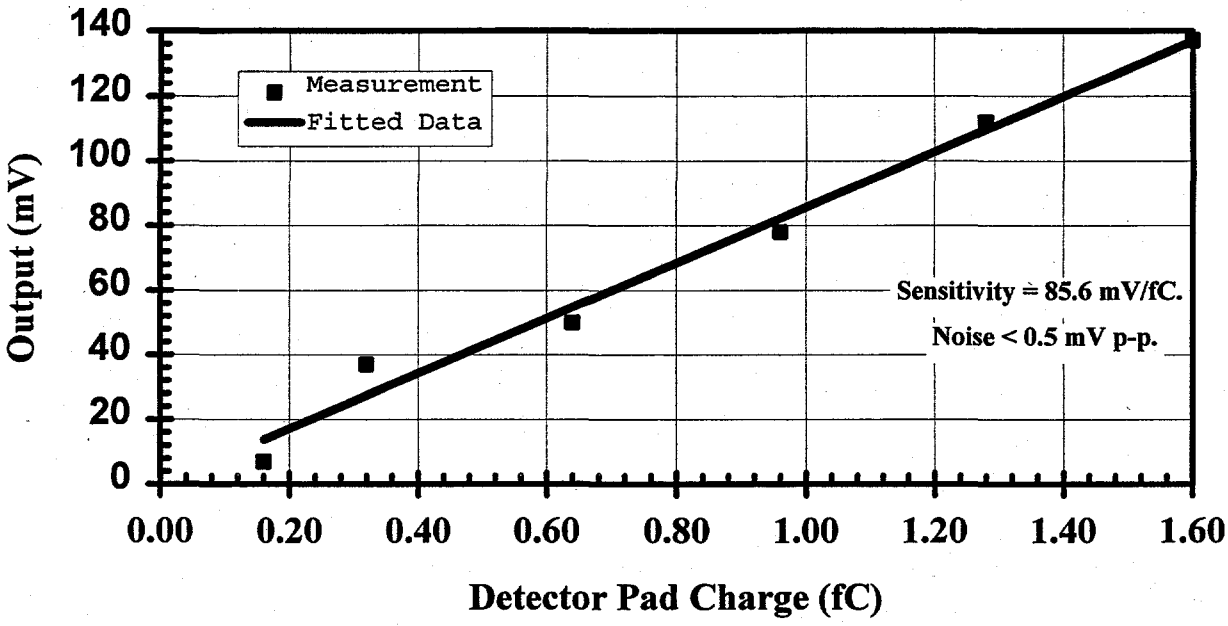

Figure 2.5-11 Response of 64 element detector array to ion beam.

Performance of detector interface electronics demonstrates the gain and linearity required to match with commercially available analog to digital converters for data acquisition.

2.6 Integration Of Components Into Gas Sensor

The chips comprising the integrated gas sensor have been produced through completion of fabrication on the first lot. Figure 2.6-1 shows an integrated gas sensor along with the chips from which it is constructed. These chips contain all of the components that are required to operate a mass spectrograph except the vacuum pumps. The chip on the right side of the photograph contains laser drilled holes for a laboratory vacuum pump to evacuate the device and allow testing of the integrated gas sensor and for mating with the compact vacuum pump assembly.

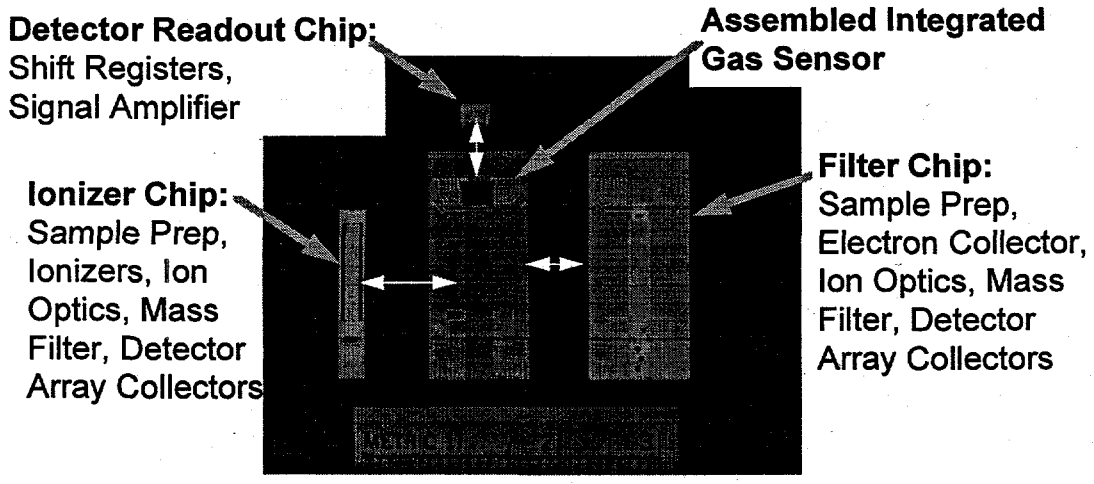

Figure 2.6.-1 Photograph of assembled gas sensor chip showing the three component chips from which it is comprised.

There are two primary substrates for the integrated gas sensor. The lower base substrate contains the electron collector and the electrodes of the mass filter along with the detector chip mounting pads and the electrical wire bonding pads to interface the integrated gas sensor with control electronics. The upper substrate is smaller and contains the solid-state ionizer electron source in place of the electron collector. The detector multiplexer chips for reading out the ion charge collected are fabricated on a third substrate, diced, tested and mounted on the base mass filter chip.

The base chip, or mass filter chip, has served as the primary process development vehicle for the integrated gas sensor. While the diode fabrication process development for electron emitters occurred on planar substrates, the Wein filter and ion collection pad development occurred on substrates containing the 40 μm recessed wells required by the integrated ionizer design. A sprayed photoresist process has been developed to apply an uniform layer of resist on the top planar surface and the lower (bottom of well) surface. The side walls and particularly the top and bottom edges pose the greatest difficulty with the resist being thinner and thicker, respectively, in these areas. This is illustrated in Figure 2.6-2 where the thinning of the resist at the edge of the wall is clearly evident.

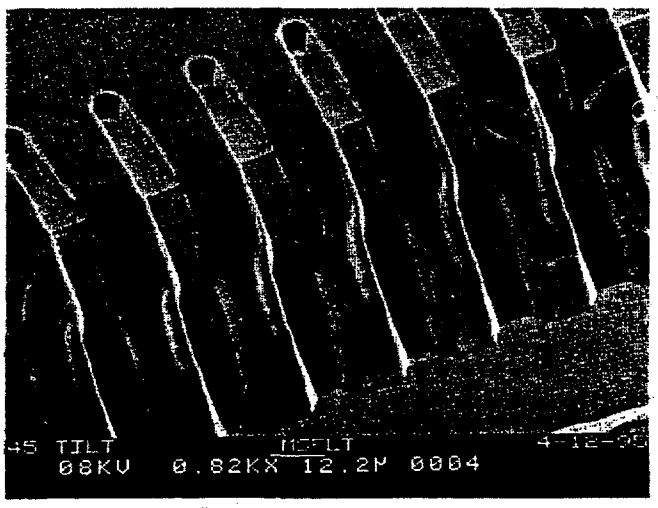

Figure 2.6-2 SEM photograph of ion collection pads patterned in photoresist.
The thinning of resist at the top edge of the wall is evident.

Multiple, thin layers of resist are used to achieve coverage. Contact lithography with minimally diverging illumination has proven successful in exposing patterns on the top surface as well as 40 μm below it. In areas where resist thickness varies significantly, multiple masks to control the exposure in different areas have been used. An example of this is seen in the ion collection pads

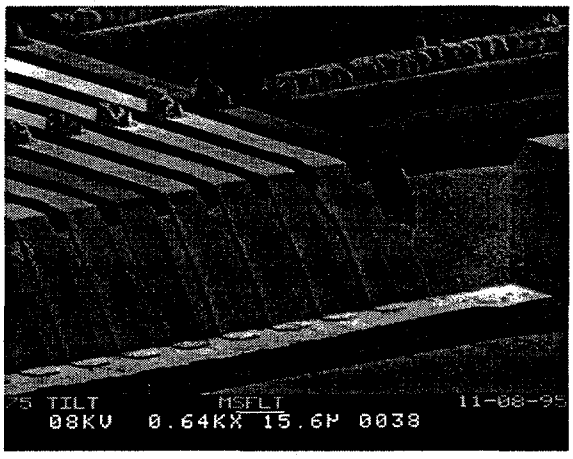

Figure 2.6-3 SEM photograph of ion collection pads used in gas sensor.
Indium bumps for bonding chips together and electrical interconnects are seen at top of picture.

(Figure 2.6-3) where the hourglass shape results from multiple exposures of a given resist layer with separate masks. These techniques have also been applied to the fabrication of the top chip containing the electron emitters. The electron emitters are located 40 μm below the wafer surface and have been successfully fabricated as seen in the SEM of Figure 2.6-4. For these initial units, several selected striped emitter designs were chosen for evaluation.

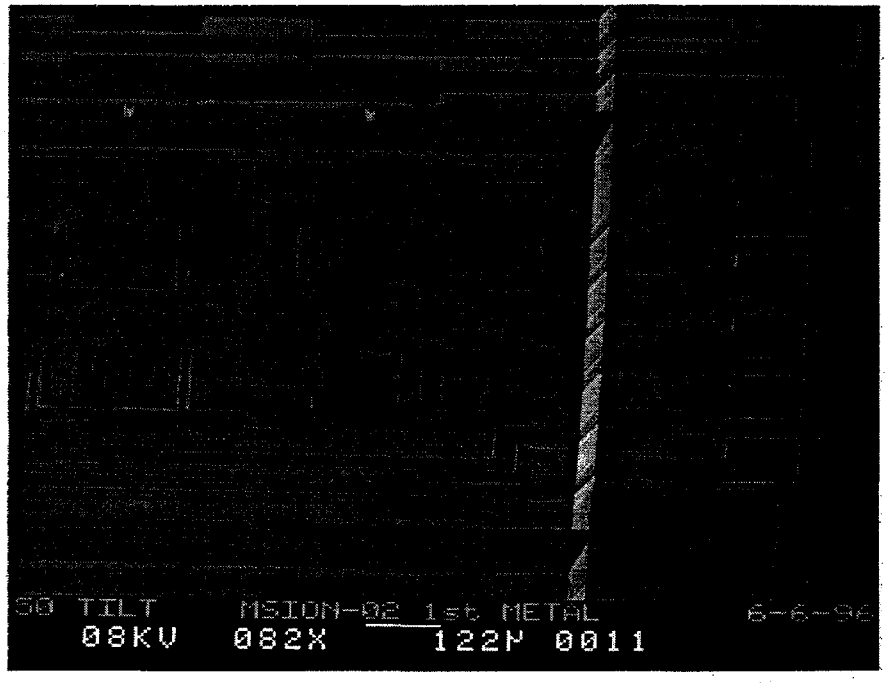

Figure 2.6-4 SEM of ionizer region of gas sensor component.

A photograph of the integrated gas sensor is shown with the electronics control board is shown in Figure 2.6-5. Ten integrated gas sensors were assembled on alumina substrates and wire bonded. Vacuum integrity was achieved on all ten devices using a combination of indium and epoxy seals. Electrical testing was made of the components separately and in combinations. The following paragraphs summarize the results for the first lot of ten sensors which were assembled.

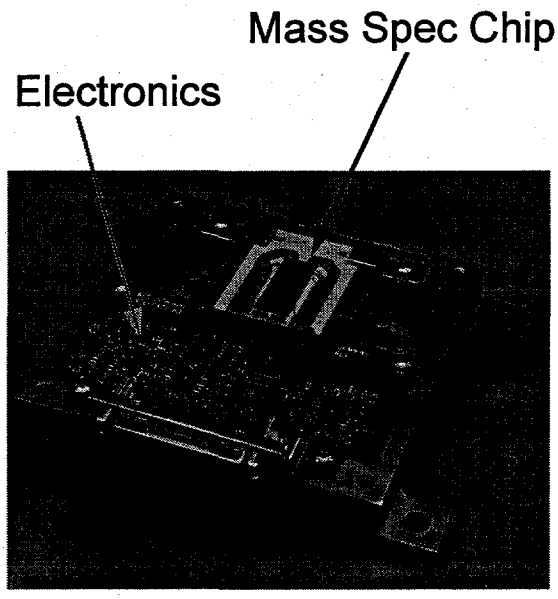

Figure 2.6-5 Photograph of integrated gas sensor in test housing with electronic control board.

For the emitters, 8 of the ten units were found to have operational emitters. That is, the electron emission current could be maintained at 750 nA or greater for periods of time of an hour. No long term testing was attempted. The two that did not show the emission, did show diode characteristics, but there was no evidence of the avalanche breakdown in these diodes.

For the mass filters, 9 of the ten were found to have the expected resistance between the two electrostatic field plates. In addition, electrical continuity was checked between adjacent elements and between the elements and the ionizer substrate. Prior to full electrical biasing of the integrated gas sensor, no element shorts were detected. On the tenth unit, one of the electrostatic field plates was found to be shorted to the ionizer substrate, because of a dielectric stack fault.

For the detectors, 6 of the ten were found to have operational detector chips as evidenced by a electrical pulse coming out the end of the shift registers. The shift registers sequentially open and close the elements of the detector array to the charge to current electrometer amplifier. The four of the ten that did not operate properly were attributed to the present yield of the fabrication process.

The next test was to operate the devices fully. A number of interactions occured that prevented any one integrated gas sensor from fully functioning. The first was an apparent short between the ionizer and detector chips. These are the two chips that are flip-chipped on top of the base filter chip. This occurred on three of the six sensors

with working detectors. Two of the six sensors contained the non-working emitters, and the last of the six sensors developed a short between the ion optic section and the ionizer base chip.

The short between the ionizer and detector chip was potentially linked to the metallization on the alumina mounting substrate going under the base chip. Sealing epoxy prevented short between these elements until the full potential was placed across the elements. In addition, a second epoxy was utilized during the flip-chip process to anchor the chips before the sealing epoxy was applied. This may have provided a conductive path. The base chip was cut longer than necessary for the device and could be trimmed to prevent the metallizations on the alumina substrate from going under it. The second epoxy is not being used for anchoring in places between the ionizer and detector chip.

The emitter operation was checked with individual chips and additional chips were chosen for flip chipping from wafers that indicate proper operation. In terms of the dielectric breakdown, twenty ionizer chips were tested by placing 100 volts potential difference between the substrate and various elements of the ion optics and mass filter. No shorts were found in these twenty chips. Addition checks in optical inspections were included in the procedures for choosing new chips for flip-chip bonding. New chips have been identified and scheduled for assembly as integrated gas sensors.

2.7 Test

2.7.1 Ionizer

A solid-state electron gun of the reverse biased junction, electron emitter design[2-1] was fabricated as a component and operated in a vacuum. The processing steps for the component are compatible with the integrated gas sensor device. The effort for the ionizer component focused on determining the optimum fabrication process steps and device geometry. The planar device fabrications investigated a number of process variables. These variables have included process variations, such as oxide insulator formation, ion implantation dose, use of screen oxides, and others, and geometry of the diode emitting area. Tables 2.7-1 and 2.7-2 shows a summary of the test results of this process variation study.

The effort started with the re-establishment of the initial emitter results that Northrop Grumman obtained earlier with ungated devices. This was successfully done through EMIT 01A using a different ion implantation source that could implant an entire wafer. These wafers were processed with the original lot and not implanted at that time. These confirmed the new ion implantation source as being equivalent to the original one. EMIT 07A was fabricated with a gate structure that was a simple extension of the ungated device process.

Run Num.	Wafer Num.	Amor-phiza-tion	Sb Dose (cm-2) @ 5KeV	Gated Design	Wafer Type	RTA Machine	Peak Anneal Temp.(C)	Metal Sinter	Res. Substr.	Number Tested	Yield >100 nano Amp	Yield >500 nano Amp	Yield >1000 nano Amp	Average Current Large Diodes (nA)
EMIT-1A	1	YES	1.50E+15		VS	P	725	Au 300	0.005	4	0.0%	0.0%	0.0%	0.0
EMIT-1A	2	YES	2.00E+15		VS	P	725	Au 300	0.005	4	100.0%	75.0%	0.0%	755.5
EMIT-07A	3	YES	1.50E+15	YES	VS	P	725	Au 300	0.005	0	-	-	-	-
EMIT-07A	4	YES	2.00E+15	YES	VS	P	725	Au 300	0.005	18	77.8%	72.2%	55.6%	1006.3
EMIT-07A	5	YES	2.50E+15	YES	VS	P	725	Au 300	0.005	3	100.0%	0.0%	0.0%	244.7
EMIT-07A	6	YES	2.00E+15	YES	VS	P	725	Au 300	0.005	7	28.6%	0.0%	0.0%	57.7
EMIT-07A	7	NO	2.00E+15	YES	VS	P	725	Au 300	0.005	6	100.0%	16.7%	16.7%	483.2
EMIT-08	1	NO	1.75E+15	YES	VS	AG	725	Al 450	0.005	17	94.1%	35.3%	0.0%	388.5
EMIT-08	2	NO	1.75E+15	YES	VS	AG	750	Al 450	0.005	11	9.1%	0.0%	0.0%	41.9
EMIT-08	3	NO	2.00E+15	YES	VS	AG	725	Al 450	0.005	10	100.0%	50.0%	30.0%	701.5
EMIT-08	4	NO	2.00E+15	YES	VS	AG	broken	Al 450	0.005	0	-	-	-	-
EMIT-08	5	NO	2.00E+15	YES	VS	AG	850	Al 450	0.005	3	0.0%	0.0%	0.0%	11.7
EMIT-08	6	NO	2.25E+15	YES	VS	AG	725	Al 450	0.005	8	87.5%	12.5%	0.0%	272.2
EMIT-08	7	NO	2.25E+15	YES	VS	AG	800	Al 450	0.005	7	85.7%	0.0%	0.0%	178.0
EMIT-08	8	NO	2.00E+15	YES	VS	AG	850	Al 450	0.005	0	-	-	-	-
EMIT-09	1	YES	1.50E+15	NO	VS	P	725	Al 450	0.005	5	60.0%	0.0%	0.0%	221.8
EMIT-09	2	YES	1.75E+15	NO	VS	P	725	Al 450	0.005	14	0.0%	0.0%	0.0%	2.7
EMIT-09	3	YES	2.25E+15	NO	VS	P	725	Al 450	0.005	11	0.0%	0.0%	0.0%	0.8
EMIT-09	4	YES	2.00E+15	NO	U	P	725	Al 450	0.005	8	87.5%	12.5%	0.0%	224.8
EMIT-09	5	YES	2.00E+15	NO		P	725	Al 450	0.005	15	80.0%	0.0%	0.0%	193.4
EMIT-09	6	NO	2.00E+15	NO	U	P	725	Al 450	0.005	0	-	-	-	-
EMIT-10	7	NO	2.00E+15	NO	U	P	725	Al 450	0.04	4	0.0%	0.0%	0.0%	0.0
EMIT-10	8	YES	1.50E+15	NO	U	P	725	Al 450	0.04	17	0.0%	0.0%	0.0%	0.0
EMIT-10	9	YES	2.00E+15	NO	U	P	725	Al 450	0.04	7	0.0%	0.0%	0.0%	0.0
EMIT-10	10	YES	2.50E+15	NO	U	P	725	Al 450	0.04	9	0.0%	0.0%	0.0%	0.0
EMIT-10	11	YES	3.00E+15	NO	U	P	725	Al 450	0.04	0	-	-	-	-
EMIT-11A	1	NO	1.00E+15	YES	U	AG	725	Au 300	0.01	12	0.0%	0.0%	0.0%	11.0
EMIT-11A	2	NO	1.00E+15	YES	U	AG	800	Au 300	0.01	21	0.0%	0.0%	0.0%	23.4
EMIT-11A	3	NO	1.50E+15	YES	U	AG	725	Au 300	0.01	3	0.0%	0.0%	0.0%	3.0
EMIT-11A	4	NO	1.50E+15	YES	U	AG	800	Au 300	0.01	5	40.0%	0.0%	0.0%	121.4
EMIT-11A	5	NO	2.00E+15	YES	U	AG	725	Au 300	0.01	8	25.0%	0.0%	0.0%	92.1
EMIT-12	1	NO	2.00E+15	YES	U	AG	725	Au 300	0.005	6	100.0%	83.3%	66.7%	1065.2
EMIT-12	2	NO	2.00E+15	YES	U	AG	725	Au 300	0.005	11	90.9%	54.5%	45.5%	1292.0
EMIT-12	3	NO	2.00E+15	YES	U	AG	725	Au 300	0.005	60	100.0%	100.0%	100.0%	3762.5
EMIT-12	4	NO	2.00E+15	YES	U	AG	725		0.005	0	-	-	-	-

Table 2.7-1 The variations in emitter performance was tested using closed loop control on the junction current and determining the peak emitted electron current.

The lifetime of these devices with emitted currents greater than 0.75 microAmps was on the order of minutes.

Run Num.	Wafer Num.	Screen Oxide	Ion	Sb Dose (cm-2) @ 5KeV	Gated Design	Wafer Type	RTA Machine	Anneal Temp. (°C)	Metal Sinter	Res. Substr.	Number Tested of Large Diodes	Yield >100 nA	Yield >500 nA	Yield >1000 nA	Average Current Large Diodes (nA)
EMIT-14	1	NO	Sb	1.00E+14	YES	U	AG	750	Au 300	0.016	6	83.3%	83.3%	50.0%	898.5
EMIT-14	2	NO	Sb	1.50E+14	YES	U	AG	750	Au 300	0.016	0	-	-	-	-
EMIT-14	3	NO	Sb	2.00E+14	YES	U	AG	750	Au 300	0.016	0	-	-	-	-
EMIT-14	4	Yes	Sb	1.00E+14	YES	U	AG	750	Au 300	0.016	0	-	-	-	-
EMIT-14	5	Yes	Sb	1.50E+14	YES	U	AG	750	Au 300	0.016	6	16.7%	0.0%	0.0%	104.0
EMIT-14	6	Yes	Sb	1.50E+14	YES	U	AG	750	Au 300	0.016	0	-	-	-	-
EMIT-14	7	NO	Sb	2.00E+14	YES	U	AG	725	Au 300	0.0066	25	84.0%	68.0%	36.0%	799.2
EMIT-14	8	Yes	Sb	2.00E+14	YES	U	AG	725	Au 300	0.0066	0	-	-	-	-
EMIT-14	9	Yes	As	1.00E+14	YES	U	AG	725	Au 300	0.0066	0	-	-	-	-
EMIT-14	10	Yes	As	1.50E+14	YES	U	AG	725	Au 300	0.0066	0	-	-	-	-
EMIT-14	11	Yes	As	2.00E+14	YES	U	AG	725	Au 300	0.0066	0	-	-	-	-
EMIT-14	1A	NO	Sb	1.00E+14	YES	U	AG	750	Au 300	0.016	32	96.9%	84.4%	71.9%	2811.0
EMIT-14	2A	NO	Sb	1.50E+14	YES	U	AG	750	Au 300	0.016	26	100.0%	76.9%	50.0%	1309.8
EMIT-14	3A	NO	Sb	2.00E+14	YES	U	AG	750	Au 300	0.016	0	-	-	-	-
EMIT-14	4A	Yes	Sb	1.00E+14	YES	U	AG	750	Au 300	0.016	12	100.0%	58.3%	50.0%	4849.0
EMIT-14	5A	Yes	Sb	1.50E+14	YES	U	AG	750	Au 300	0.016	0	-	-	-	-
EMIT-14	6A	Yes	Sb	1.50E+14	YES	U	AG	750	Au 300	0.016	0	-	-	-	-
EMIT-14	7A	NO	Sb	2.00E+14	YES	U	AG	725	Au 300	0.0066	11	100.0%	72.7%	63.6%	832.1
EMIT-14	8A	Yes	Sb	2.00E+14	YES	U	AG	725	Au 300	0.0066	10	60.0%	0.0%	0.0%	192.8
EMIT-14	9A	Yes	As	1.00E+14	YES	U	AG	725	Au 300	0.0066	5	100.0%	20.0%	20.0%	654.4
EMIT-14	10A	Yes	As	1.50E+14	YES	U	AG	725	Au 300	0.0066	7	71.4%	42.9%	14.3%	491.1
EMIT-14	11A	Yes	As	2.00E+14	YES	U	AG	725	Au 300	0.0066	5	60.0%	0.0%	0.0%	133.2

Table 2.7-2 The variations in emitter performance was tested using closed loop control on the junction current and determining the peak emitted electron current.

The lifetime of these devices with emitted currents greater than 0.75 microAmps was on the order of minutes. Note that the striped diodes (indicated with wafer numbers ending in an "A") have a much higher average current than the circular diodes for EMIT 14.

Run	Wafer	Screen oxide	RIE	Sb Dose (cm-2) @5KeV	Gated Design	Wafer Type	RTA Machine	Anneal Temp(°C)	Metal Sinter	Res. Substr.	Number of Diodes Tested	Average Power (mW)	Current Power Ratio
EMIT-14	1A	NO	Sb	1.00E+14	YES	U	AG	750	Au 300	0.016	-	-	-
EMIT-14	2A	NO	Sb	1.50E+14	YES	U	AG	750	Au 300	0.016	-	-	-
EMIT-14	3A	NO	Sb	2.00E+14	YES	U	AG	750	Au 300	0.016	3	1214	0.179
EMIT-14	4A	Yes	Sb	1.00E+14	YES	U	AG	750	Au 300	0.016	2	1362	0.033
EMIT-14	5A	Yes	Sb	1.50E+14	YES	U	AG	750	Au 300	0.016	-	-	-
EMIT-14	6A	Yes	Sb	1.50E+14	YES	U	AG	750	Au 300	0.016	6	961	0.553
EMIT-14	7A	NO	Sb	2.00E+14	YES	U	AG	725	Au 300	0.0066	4	883	0.426
EMIT-15	1	NO	Sb	1.00E+14	YES	U	AG	725	Au 300	0.0164	7	895	0.11
EMIT-15	2	NO	Sb	1.00E+14	YES	U	AG	725	Au 300	0.0164	-	-	-
EMIT-15	3	NO	Sb	1.50E+14	YES	U	AG	725	Au 300	0.0164	4	1148	0.087
EMIT-15	4	NO	Sb	1.50E+14	YES	U	AG	725	Au 300	0.0164	5	373	1.024
EMIT-15	5	NO	Sb	2.00E+14	YES	U	AG	725	Au 300	0.0164	-	-	-
EMIT-15	6	NO	Sb	2.00E+14	YES	U	AG	725	Au 300	0.0164	5	718	0.145

Table 2.7-3 The variations in emitter performance was tested using closed loop control on the emitted electron current and was used to determine the best device design to provide the lifetime of the integrated gas sensor.

The one correlation noted is that the figure of merit (current power ratio) is highest for the devices with a substrate resistivity of 0.016 ohm-cm and an implantation dose of 1.5 x 10^{14} of antimony.

Attempts to fabricate a gated design previous to this utilized a more complicated process to add the gate and produced devices that did not exhibit electron emission. EMIT 07A showed that the simple gate structure was a viable process and design. EMIT 08 was a study of ion implantation dose and anneal temperature of both the ion implantation and the metalization. This run indicated that the ion implantation anneal of 725°C and 2×10^{14} cm^{-2} ion implantation dose was the best process to date. In addition, the run indicated that aluminum metalization could be substituted for gold and the pre-amorphization implant with silicon may not be necessary. EMIT 09 checked the RTA machines. EMIT 09 found a contamination in the liner of the RTA machine that poisoned the emitter surface and reduced the electron emission. To avoid cross-contamination in the future, a liner was purchased with Northrop Grumman funds and dedicated to the MSOC emitters. EMIT 10 was fabricated to determine if a large shift in wafer resistivity was beneficial for the device. From this run, 0.04 ohm-cm resistivity wafers were not appropriate for our present design and process. EMIT 10A had its fabrication aborted, based on the emission results of EMIT 10. EMIT 11 and 11A investigated an intermediate resistivity of approximately 0.01 ohm-cm. The emission results were encouraging in that the devices exhibited a greater ratio of avalanche to tunneling breakdown. Avalanche breakdown gives rise to the emission of electrons, whereas tunneling breakdown does not. The emissions were lower due to the fabricated devices being smaller geometrically from the phosphorus diffusing farther under the same conditions with the 0.01 ohm-cm versus the 0.005 ohm-cm wafers. EMIT 12 was a repeat of the baseline process and exhibited performance of the EMIT 07A wafer 4.

Up to this point, the improvements to the emitter were to be obtained through process optimization. Some data in the literature suggested that a change in geometry would be more beneficial. EMIT 14 was fabricated to check this literature result. EMIT 14 has devices with different geometries. The fabricated emitter die contains both circular and linear device geometries. The circular geometries are fabricated to compare the circular and linear devices performance, as well as check that some other variable was not the cause for differences in performance. Data was desired to show if the geometry change was the factor that leads to a performance change. An additional lot has been fabricated and tested. This lot is EMIT 15. EMIT 15 is a fabrication to test the increase in metallization thickness in reducing the failure seen in EMIT 14. In addition, the EMIT 15 fabrication tests the repeatability of the EMIT 14 successful improvements in lifetime. EMIT 15 devices performed as the EMIT 14 devices with the exception that there were no failures of the devices found in which the device would not pass a junction current. This proved that the metallization was the problem in EMIT 14 and the integrated emitter design was modified to increase the integrity of the metallization.

Early work focused on cylindrically symmetrical emitters of varying diameters and yielded devices that could not maintain emitted currents at the levels required for more than minutes. One interesting note on these devices was the correlation of light and electron emission. Visible light emission was studied under a laboratory microscope in normal atmosphere while power was applied across the device. The visible light emission gave a measurement of the size of the emission area (or periphery). The operation of the reverse bias diode in air did not burn the devices out unless excessive power was applied. After operation in air, emitters operated successfully in vacuum. The use of a 300°C anneal in forming gas for a half hour rejuvenated the devices. Alternatively, devices

unpowered in vacuum for a period of time (three to four weeks) recovered their emission characteristics. After short periods of time of being off, the electron emission returns to the value prior to shutdown and not the initial emission, when the virgin emitter was first operated. These results indicate that the emission changes are due to instability of the surface work function. Long term operation of the device necessitates stabilization of the surface work function by either an increase in emission area or surface treatment.

Devices with larger areas and periphery were investigated. An example of circular devices is given in Figure 2.7-1 and for a striped emitter in Figure 2.7-2. The increase in the lifetime of the striped device is greater than accountable in the change of the geometry. There are two possible mechanisms. The first is that the emission brightness is a function of the width of the device. This phenomenon was also noted by workers at Philip's laboratory.[2-1] A second mechanism is the heating of the emitter surface due to the additional power that these devices are drawing during operation. The power of the larger emitters is between 0.5 and 1.0 Watts as compared to 0.1 to 0.15 Watts for the circular emitters. The heated surface may keep the surface free of absorbed gas surface layers that significantly increase the surface work function.

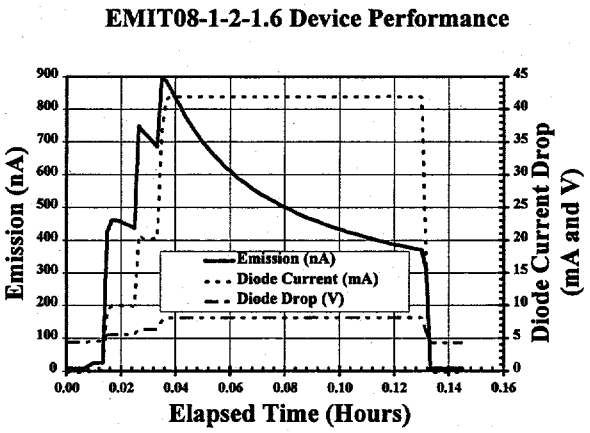

Figure 2.7-1 This circular emitter is very typical of the data acquired for such devices.

The device did not burn out, but was not able to sustain the required current.

EMIT 15-6A-1-7.4 Device Performance

The devices from EMIT 14 and 15 have been tested in both vacuum and at operating pressures with gases. The presence of gases depresses the emission, but the devices still operate for days at the specified currents required. Designs with both the internal and external accelerating gates operated for longer periods of time and with a smaller depression of the electron current. This indicates that the accelerating gate is repelling ions away from the active surface of the emitter and therefore, protecting it from damage. The test setup also incorporates a diverging magnetic field that was suggested through conversations with investigators at Phillips Laboratories.

Lifetime limitations have been found to be due to two areas. The first is the contact line to the phosphorus diffusion. This line in the test emitter components must go over a micrometer dielectric step and thins at this point. During operation, this point opens. The second area is the isolation of the accelerating gate. Some misalignments were encountered during lithography on some of the wafers. Poorly isolated gates lead to poor lifetime performance and conversely, those with good isolation yielded good lifetime.

EMIT 15 was fabricated in order to check the lifetime limitations found with EMIT 14 devices. Thicker contact metallizations and better alignment were done with this lot. No failures due to metallization have been found. In fact, no device has catastrophically failed in testing. The EMIT 15 devices are also confirming the ion implantation doses found in EMIT 14 to be best, and these results are holding. Cesium iodide and cesium oxide have been applied in thin layers (between 100 and 500 Å) to the surface of the emitters. Those coated with cesium oxide displayed reduced emission characteristics as had been noted in the past with oxides of barium, strontium and calcium. Cesium iodide coated devices, on the otherhand, displayed an enhanced emission (slightly) and better lifetime characteristics. These are being quantified. Cesium iodide is the preferred protective coating with bare silicon being second.

The optimized emitter process determined to date is shown in Table 2.7-4.

PROCESS PARAMETER	INVESTIGATION RANGE	EMITTER DEVICE PREFERRED RANGE
Wafer Resistivity	0.005 to 0.040 Ohm-cm	0.005 to 0.020 ohm-cm
Wafer Vendor	Unisil or Virginia Semiconductor	Unisil preferred due to greater resistivity uniformity.
Gate Design	None, internal/external, external.	Internal/external preferred. External only usable.
Rapid Thermal Annealer	Peak and AG Siemens	Both equivalent, cross-contamination between different must be avoided.
Anneal Temperature Maximum	725 to 800 °C	725 °C
Metal Contact	aluminum and gold	aluminum or gold
Silicon Pre-amorphization	With and without pre-amorphization	Without pre-amorphization. (Cost savings)
Implant Ion	Antimony (Sb) and arsenic (As)	Antimony is better understood, arsenic usable.
Implant Ion Dose: 0.005 ohm-cm resistivity.	1.0E14 to 2.3E14 cm^{-2} Sb.	1.8E14 to 2.2E14 cm^{-2} Sb.
Implant Ion Dose: 0.020 ohm-cm resistivity.	1.0E14 to 2.0E14 cm^{-2} Sb.	1.0E14 to 2.0E14 cm^{-2} Sb.

Table 2.7-4. Summary of process variables investigated and tolerances found for desired performance of the reverse bias junctions as electron emitters.

In addition to p-n junctions, metal point emitters were investigated. These emitters have been investigated for flat panel displays and are illustrated in Figure 2.4-2.[2-7] The emitters were obtained from SRC in Menlo Park, CA. Conditioned and unconditioned arrays of emitters were obtained. Chrome metallizations were applied to the tungsten points, since chromium has been tested by Dr. Spindt's laboratory and found to operate in air. The results of the conditioned emitter array is shown in Figure 2.7-4. The emission current was low. The array was 100 x 100 members and were all turned on according to the instructions provided by SRC. The noise of the emitters did not change with time and were considered to noisy for this application. Only a few elements would be usable in the MSOC and so the current would be too low for ppm sensitivity.

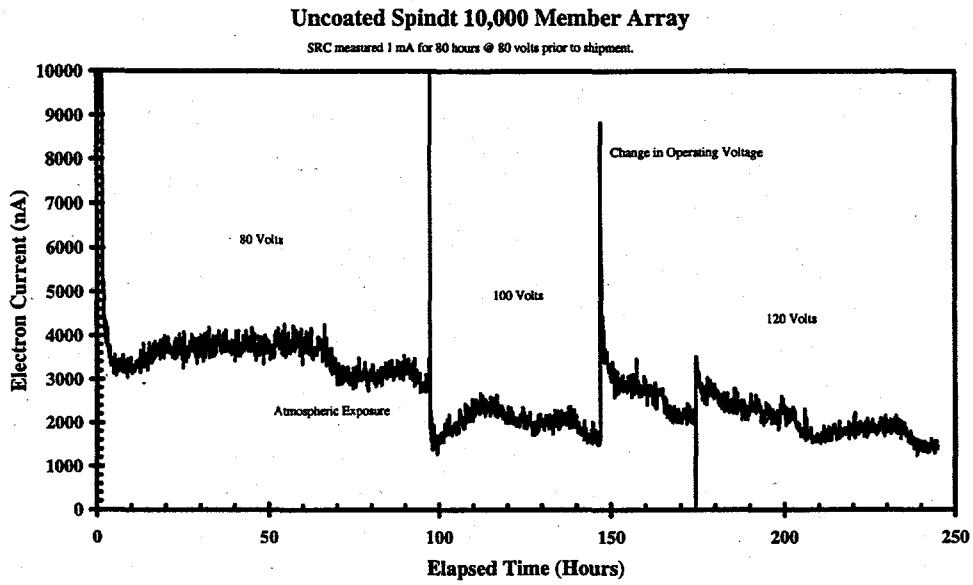

Figure 2.7-4 Cold-cathode point emitters of the Spindt design and fabrication were tested using constant voltage control through a ballast resistor.

The emitted electron current is shown here for the 10,000 member array.

2.7.2 Mass Filter

In the first silicon design, a seven segment, electric field plate was fabricated in the silicon mass filter with voltages determined by a fixed, thin film, resistor bridge. A section of this mass filter The segmented electric field plate was utilized due to the severe aspect ratio of the mass separating cavity. This cavity is approximately 86 micrometers high and 1500 micrometers wide. Both cavity surfaces are parallel to the magnet pole piece (1500 micrometer dimension) and divided into seven gold electrodes defined on top of a thermal oxide dielectric. Upon assembly of the cavity, there are pairs of segments that face each other. One segment is on the upper cavity surface and the other is on the lower. The potential on each member of the electrode pair is nominally the same. Designs were considered that placed a grounded electrode between each powered electrode. Electrostatic modeling shows that a more uniform electrostatic field is generated without interleaving of ground segments between the powered segments. Modeling showed that a twenty-nine segment field generated a significantly more uniform electrostatic

field than a seven segment plate. In addition, a purely resistive film was determined to provide the ideal electrostatic field. The resistivity of the film was calculated for the geometry desired. The resistivity of an appropriate film fell in the range of 100 and 10,000 ohm-cm. Undoped polysilicon of between 0.2 and 0.5 micrometers thickness falls in this resistivity range. Films deposited in our facilities have been measured with resistivities of 1500 to 1900 ohm-cm. Both the seven segment field plate and the resistive film are part of the integrated gas sensor design that have been tested. Undoped polysilicon was found to be suitable for this application and is incorporated into the integrated gas sensor design.

Testing of the silicon mass filter with the seven segment field plate was performed in a two chamber vacuum test station using both pure and mixtures of noble gases. Better resolution was achieved with the silicon mass filter than the previous simple mass filter consisting of the magnet and the electrostatic field plates, as was to be expected due to the more uniform electrostatic field generated with the silicon mass filter. The data were collected using an electron multiplier set up for charge particle counting. An example of the data obtained is shown in Figure 2.7-5. The fields of the permanent and electro- magnets used with the silicon mass filter was measured before assembly. The silicon mass filter scan voltage was converted to mass using the magnetic field and ion energy values and plotted as a function of atomic mass units. An afocal lens and polysilicon resistor film, mass filter prototype have been constructed and inserted into the test stations and evaluated. An example of a mass spectrum taken with the polysilicon mass filter is shown in Figure 2.7-6. Both singly and doubly charged ions of xenon are detected. The xenon isotopes are separated by the silicon mass filter and analysis of the full width at half maximum (FWHM) indicates that the resolution measured is approximately 0.9 to 1.0 amu at 129 amu. Since a mass filter with a constant magnetic field and ion energy is a non-constant resolution device, this resolution at 129 amu is expected for a system having a resolution of 1.0 to 1.1 amu at 150 amu.

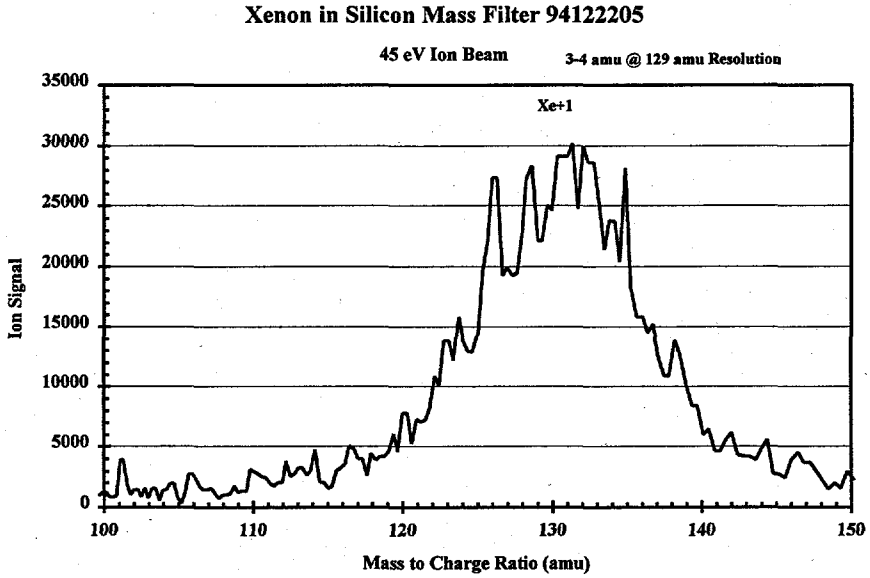

Figure 2.7-5 The seven segment, mass filter separates xenon with the expected resolution of about 1 amu at 50 amu.

This is equivalent to 3-4 amu at 129 amu.

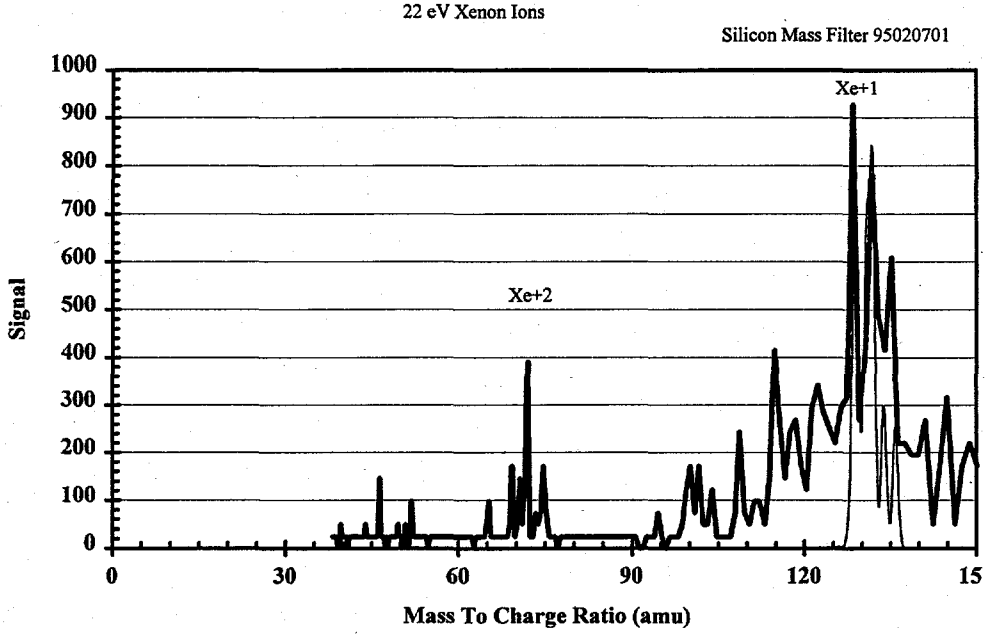

Figure 2.7-6 Mass spectrum obtained from the polysilicon, mass filter component and 3 element ion optics.

The resolution obtained is higher than obtained with either the seven segment or simple mass filter as modeling indicated.

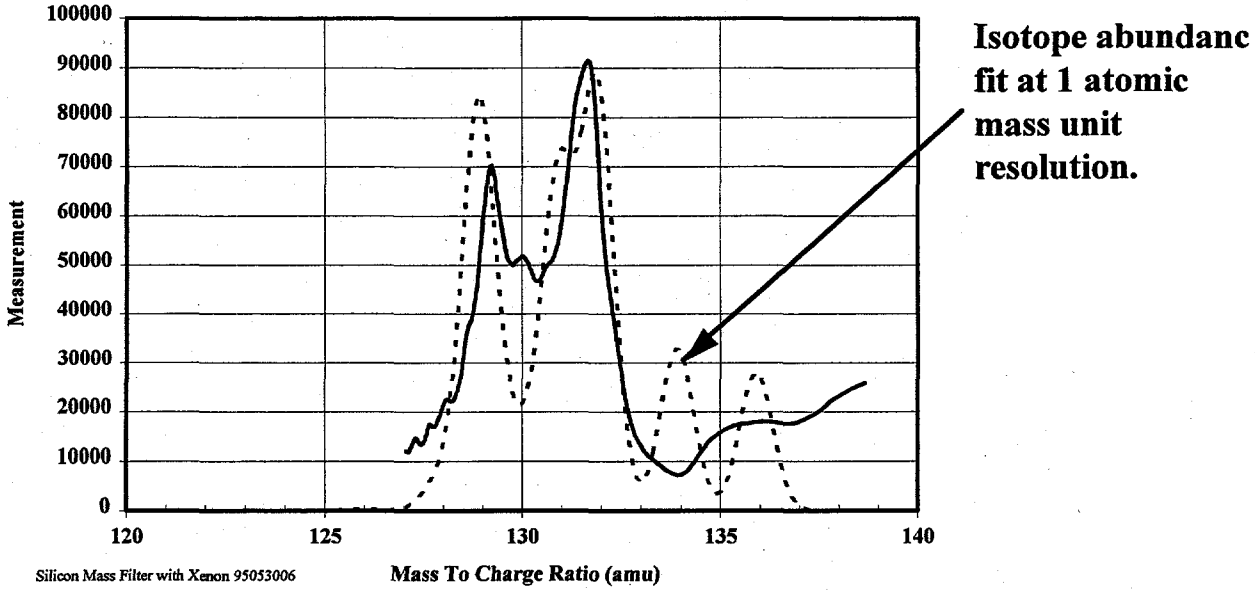

Figure 2.7-7 The isotope pattern for xenon has been resolved at the resolution of 1 amu at 130 amu using a polysilicon mass filter component test piece and 9 element laboratory ion optics.

The polysilicon mass filter has been incorporated into the integrated gas sensor design.

2.7.3 Detector

Both twenty and sixty-four element arrays have been fabricated and subjected to an ion beam. The response of the twenty element detector array is shown in Figure 2.7-8. A broad ion beam with known cross section

was directed onto an electrically isolated metal plate which contained a small aperture through which ions were directed onto the detector array's collection electrodes. The current striking the metal plate was measured with an electrometer and the area ratio taken to determine the current striking each collection electrode. The horizontal axis is the current striking the array collection electrode. The vertical axis is the voltage out of the amplifier interface card for the extreme element on the array. The dotted line is the anticipated response and the line is the fit for the detector data. There is good agreement between the fitted detector response and the system design response.

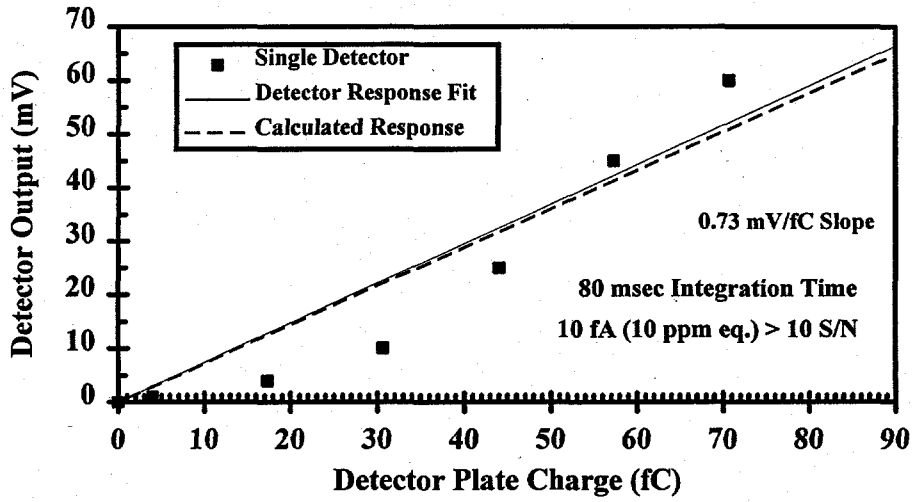

Figure 2.7-8 The response of the twenty element MOS switch linear detector array to an ion beam in a vacuum system shows that the detector and amplifier perform to the design performance.

An improved detector interface has been designed and fabricated. The original interface had been designed to accommodate a number of different detector designs. Since the on-chip digital shift registers operated with good yield, the design of the interface board focused on this design. Boards were fabricated and tested. This board improved the gain by a factor of 100 over the previous design and utilized one voltage amplifier stage instead of two. The new interface is shown in Figure 2.7-9.

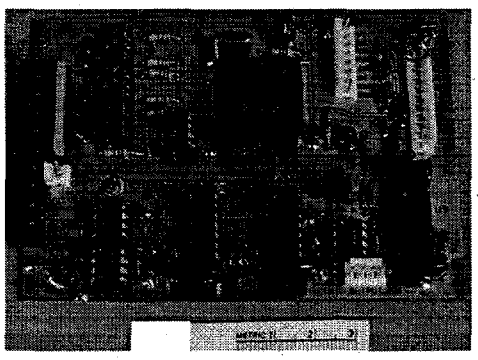

Figure 2.7-9 The new interface electronics for the detector array divides the analog and digital portions of the board in the horizontal direction to reduce noise of the overall section.

This design change allowed the low noise level to be achieved to exceed our program goals.

Sixty-four element detector arrays were designed and fabricated based on the twenty element array design with on-chip shift registers. The digital circuitry and charge to current amplifier are fabricated on this chip. This allows a yield enhancement and removes the digital circuitry from the micromachining steps of the integrated gas sensor. The sixty-four element test component is shown in Figure 2.7-10 and the device for flip chipping to form the integrated gas sensor is shown in Figure 2.7-11.

In both the charge to current amplifier is common to each of the detector pad members of the detector array. This reduces the detector pattern to being simply the variation in the capacitor values. The sixty-four element test component was subjected to both bench and ion beam testing. The results of the ion beam test are shown in Figure 2.7-12. Here again, the response data has been compared to the modeled data and show a good fit for the gain. The noise floor for the new electronics is an order of magnitude lower than required, and so with the proper analog to digital converter, an extra decade of sensitivity can be obtained.

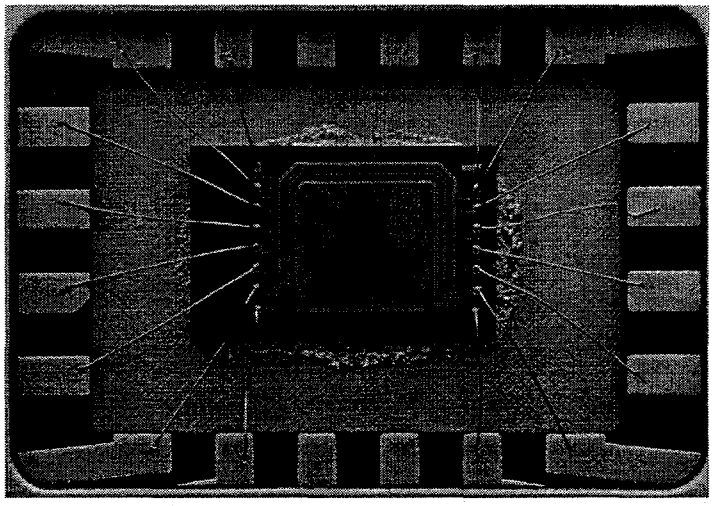

Figure 2.7-10 The sixty-four element detector test component is wire bonded in a dual inline header for testing. *The collection capacitors are located on the lower side of the chip with the common charge to current amplifier on the left, between the wire bond pads and the capacitors.*

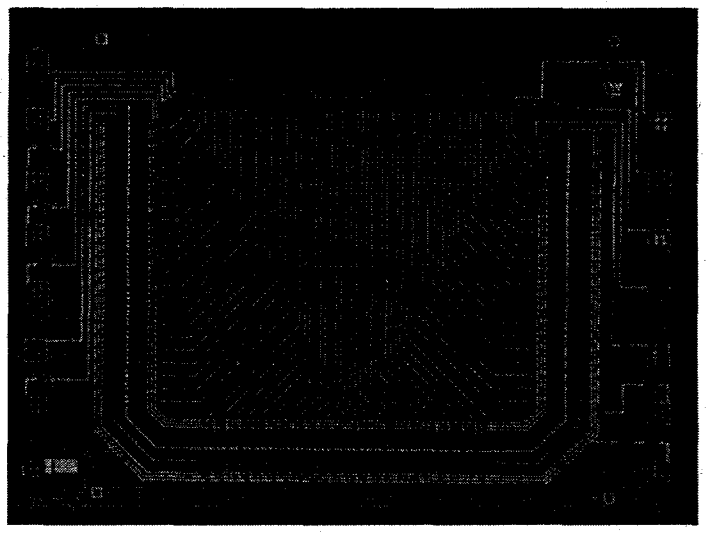

Figure 2.7-11 The sixty-four element device for flip chipping to be a part of the integrated gas sensor is shown with the indium bumps that will provide the electrical connection of the chip to the rest of the sensor.

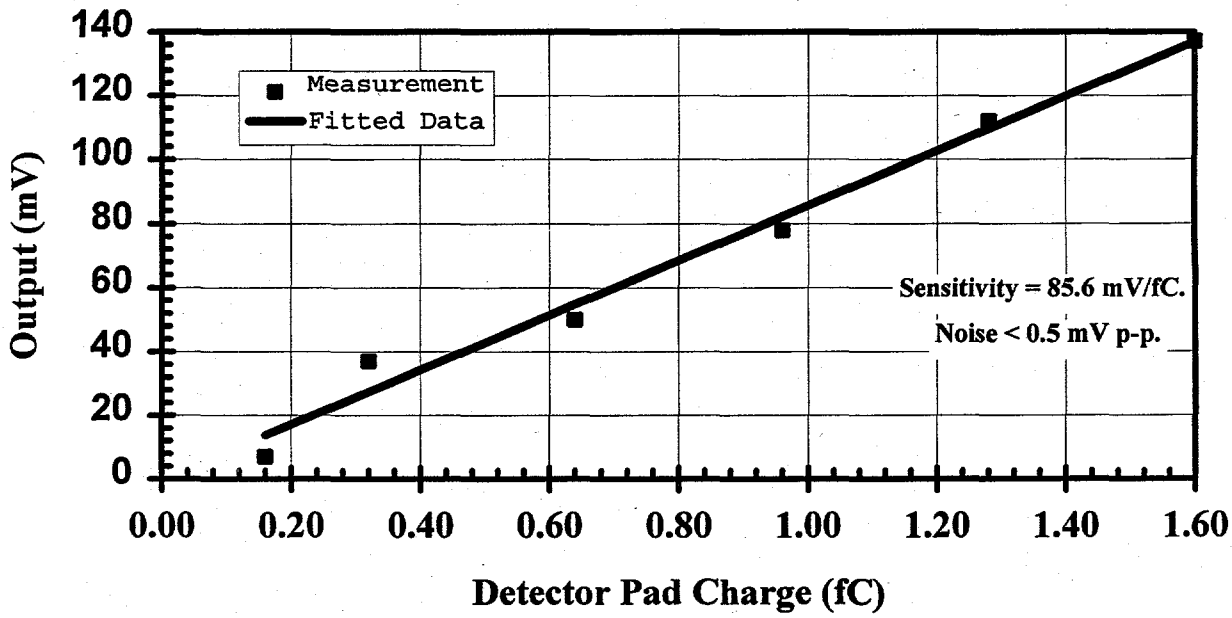

Figure 2.7-12 The sixty-four element test component showed both the sensitivity and lower noise levels than required by the program, allowing the sensitivity of the detector to be 10 ppm rather than 100 ppm.

2.7.4 Integrated Gas Sensor

In order to reduce the risk during the fabrication of the integrated gas sensor, a period of time was utilized to obtain the photolithography parameters needed for some of the critical features in the gas sensor design. This also gave a chance to test mask designs and changes found to be necessary could be done in parallel to the rest of the integrated gas sensor fabrication. The most critical feature in the design is the ion collection array at the end of

the ion separation region. Here, sixty-four collection elements are fabricated along the well edge on a twenty-two micrometer pitch. A ground plane is desired between the individual collection pads to minimize cross-talk and also to minimize the dielectric exposure that can charge up and deflect ions.

A "self-aligned" approach has been taken in the detector array area. One of the problems of using photoresist to define an electrode is that the separation of the electrode on the defining surface leaves a dielectric area exposed. This is illustrated in Figure 2.7-13. This is usually on the order of a few micrometers unless extreme caution and techniques are utilized, such as e-beam lithography. Fabrication of the integrated gas sensor utilizes contact lithography and the deep

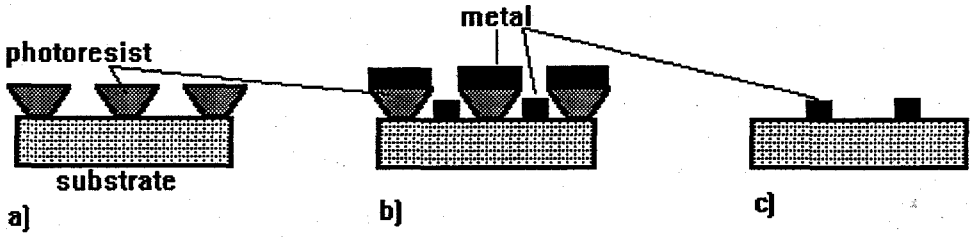

Figure 2.7-13. The process to define a metal line on a dielectric through lift-off resist technique is illustrated. *In a), the photoresist is applied and defined for lift-off, b) the metal is deposited, and c) the photoresist and metal deposited on it are removed.*

depth of focus requirements give a resist line width of about six micrometers or more. On a twenty-two micrometer pitch, this would leave a reasonable amount of dielectric exposed. The self aligned approach uses a multilayer stack of silicon oxide and silicon nitride. This is illustrated in Figure 2.7-14. The top nitride is defined using photoresist and etched. The underlying oxide is etched so that the silicon nitride on top of the silicon oxide overhangs the edge of the etched oxide. The photoresist is then removed and the metal film deposited by evaporation. Evaporated films are line of sight deposits and the source located so that the deposition lines are nearly perpendicular to the surface. Sidewall coverage is minimal in this technique. The ground plane and collector lines are then isolated vertically instead of horizontally. The silicon oxide thickness must be controlled so that bridging does not occur.

The silicon oxide deposition process for this multilayer stack needs to be conformal, or nearly so, that the oxide thickness does not vary greatly in going from the bottom of the well, up the wall and on top of the wafer. Three silicon oxide deposition techniques were tested for the integrated gas sensor geometry. These were an atmospheric pressure chemical vapor deposited oxide referred to as silox, magnetron sputtered quartz, and plasma-enhanced chemical vapor deposited (PECVD) oxide. Deposited films of silox are non-conformal with a thickness variation of over a factor of six over the geometry. Both sputtered quartz and PECVD oxide conformally covered the geometry. Sputtered quartz was chosen, since its etching characteristics were slower and thus would give better control for the undercutting geometry.

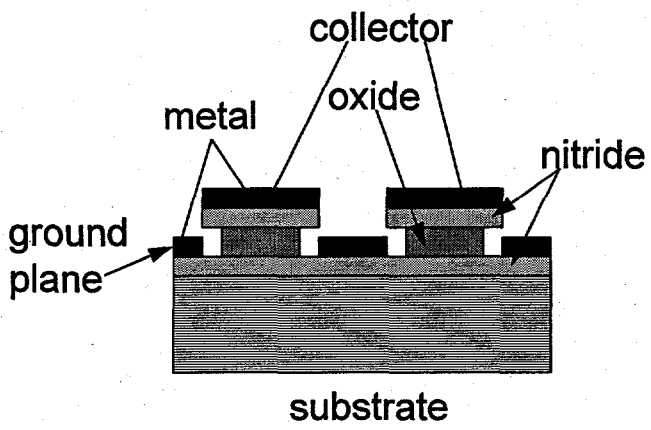

Figure 2.7-14. The deposition of metal on a "self-aligned" geometry is illustrated.

In this technique the insulator separates the electrodes vertically, instead of horizontally, due to the undercut formed in the multilayer dielectric stack that is similar in shape to the photoresist in the lift-off technique.

The results of the lithography and metallization shows a detector collector array that is isolated vertically. Other than a reflection that truncated the detector elements on the ends of the array, the fabrication of the array was achieved. This is shown in Figure 2.7-15.

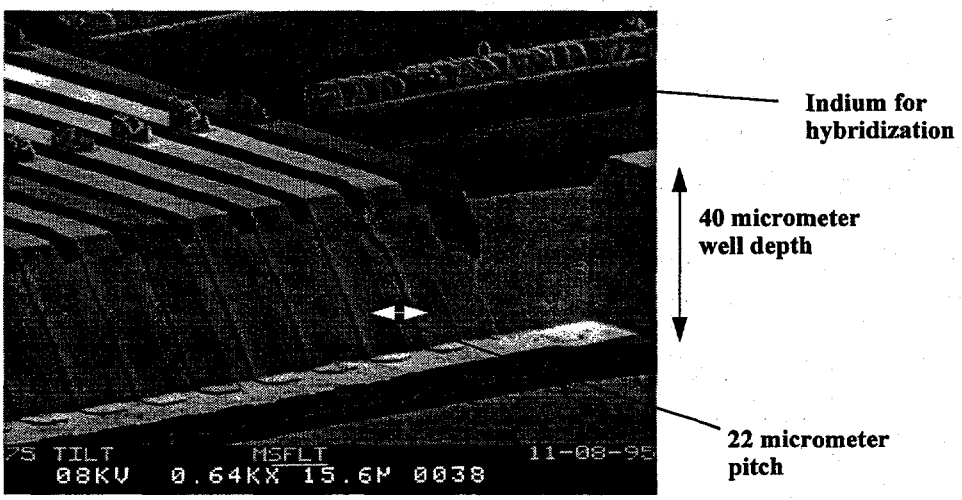

Figure 2.7-15. A scanning electron microphotograph of the detector array end of the integrated gas sensor during a test fabrication over the integrated gas sensor well geometry.

The photoresist defines the collecting electrodes of the capacitor of the detector array. The end element is truncated due to a reflection from the side wall of the well. Widening of the well will eliminate this defect.

The chips comprising the integrated gas sensor have been produced through completion of fabrication on the first lot. Figure 2.7-16 shows a complete flip chip assembly along with the individual chips that are used to form a working integrated gas sensor. These chips contain all of the components that are required to operate a mass

spectrograph except the vacuum pumps. The holes in the chip to the right of the photograph contains laser drilled holes for a laboratory vacuum pump to evacuate the device and allow testing of the integrated gas sensor. Figure 2.7-17 shows the integrated gas sensor with the magnet and base electronics to operate the system.

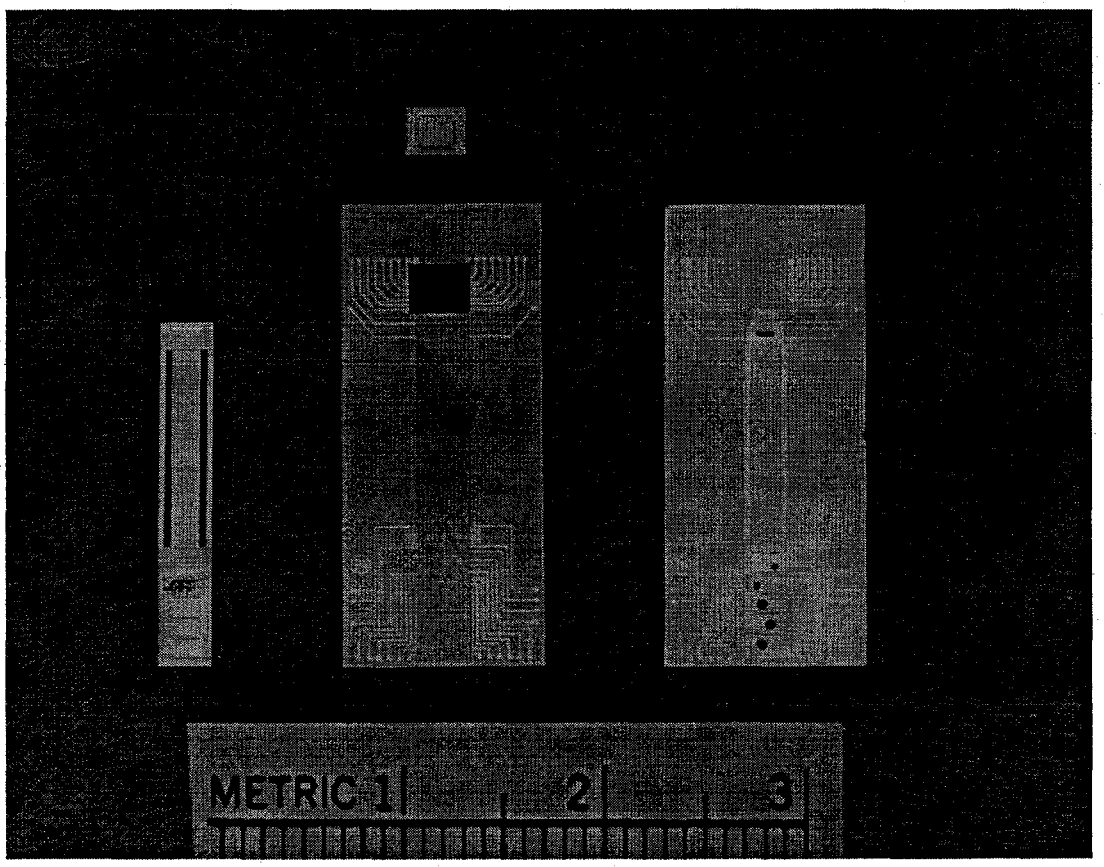

Figure 2.7-16. An assembled integrated gas sensor is shown with a set of individual chips that are being hybridized to form the integrated gas sensor.

The chip to the right of the center has laser drilled holes to allow connection to a laboratory vacuum pump for testing.

Testing of the first assembly of integrated gas sensors showed that the individual components operated within the silicon chamber, when powered separately. Upon attempting to operate the integrated gas sensor as a unit, a short between the ionizer substrate, which operates 90 volts below system ground and ground was found that did not allow the maintenance of the emitter bias without high power dissipation. This was linked to a failure in the multilayer dielectric used to form the collector pads on the end of the analyzer well. The fabrication process was reviewed and another set of ionizer devices were fabricated and tested for dielectric strength. The tests showed that the ground and ionizer substrate were isolated from one another by a dielectric with a breakdown strength of at least 175 volts. The yield on a small sample was determined to be 97%. These ionizer chips have been submitted for integrated gas sensor assembly.

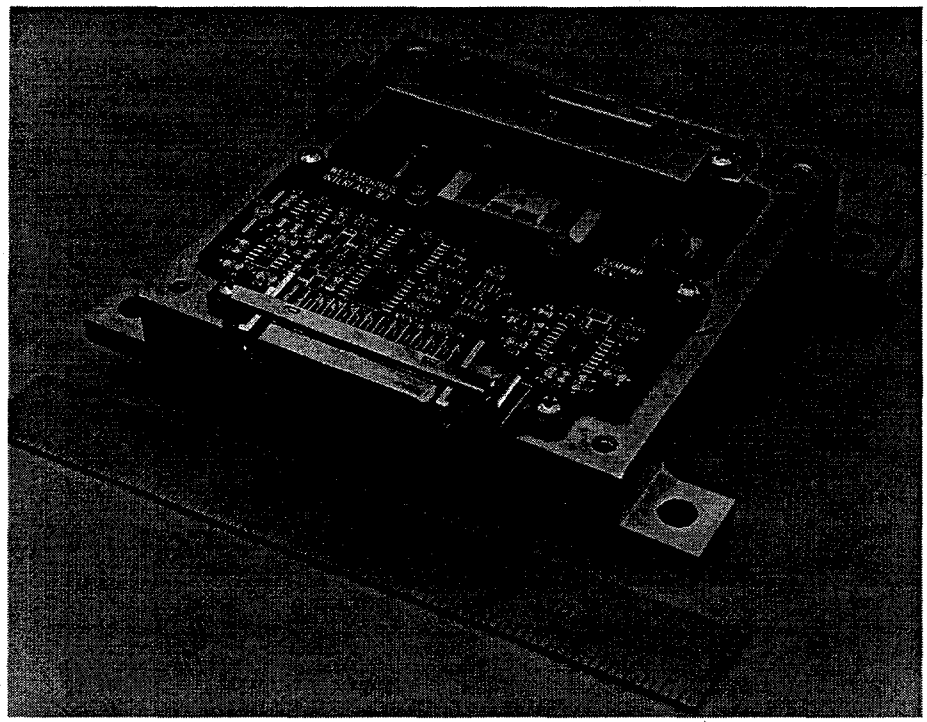

Figure 2.7-17 The integrated gas sensor is pictured with its external permanent magnet and detector electronics. *The aluminum housing supports the vacuum manifold and connects it to the vacuum pump ports. Other than for the display and data acquisition computer board, this unit comprises the MSOC detector unit.*

2.8 *Conclusions*

The MSOC has been proven on the component level and problems with the integration have been identified and solved. The packaging of silicon sensors with external hardware has been achieved in simple ways that allow field replacement of the sensor head practical by skilled workers, but not requiring special training. The fabrication process has been developed so that low cost fabrication is possible at a number of silicon fabrication foundries.

2.9 *References For Section 2*

2-1 G.G.P. van Gorkom, and A.M.E. Hoeberechts, "Back-biased junction cold cathodes: history and state of the art," Proceedings of the 2nd Int. Conf. on Vacuum Microelectronis, (Bath, UK 24-26 July 1989), Inst. Phys. Conf. Ser. No. 99, R.E. Turner, ed. (Institute of Physics, Bristol and New York: 1989) pp.41-52.

2-2 W.L. Fitch and A.D. Sauter, Anal. Chem., Vol. 55, pg. 832-835, 1983.

2-3 L. Patrick and W.J. Choyke, "Electron Emission from Breakdown Regions in SiC p-n Junctions," Physical Review Letters, 2(2) 48-50 (1959).

2-4 R.V. Bellau, R.A. Chanter, and C.L. Dargan, "Activation of a multi- emitter silicon carbide p-n junction cold cathode," J. Phys. D: Appl. Phys. 4, 2022-2030 (1971).

2-5 T.N. Criscimagna and P. Pleshko, "AC Plasma Displays," in: Display Devices, J.I. Pankove, ed. (Springer-Verlag, Berlin: 1980) pp.91-150.

2-6 J. Smith, "Experimental Storage Display Panels Using DC Gas Discharges Without Resistors," IEEE Transactions on Electron Devices, ED-33(9) 642-649 (1975).

2-7 C.A. Spindt, et al., "Field-Emitter Arrays for Vacuum Microelectronics," IEEE Transactions on Electron Devices, 38(10), 2355-2363 (1991).

2-8 C.C. Curtis and K.C. Hsieh, "Spacecraft mass spectrometer ion source employing field emission cathodes," Rev. Sci. Instrum. 57(5) 989 (1986).

2-9 J.J. Hickman, et al., "Surface composition of Si-TaSi2 eutectic cathodes and its effects on vacuum filed emission," Appl. Phys. Lett. 61(21), 2518-2520 (1992).

2-10 J.E. Jaskie and R.C. Kane, "Method of making a field emission electron source employing a diamond coating," US Patent no. 5,141,460, filed August 20, 1991; issued August 25, 1992.

2-11 F. Hochberg, H.K. Seitz, and A.V. Brown, "A Thin-Film Integrated Incandescent Display," IEEE Transactions on Electron Devices, ED-20(11) 1002-1005 (!973).

2-12 C.H. Mastrangelo, J.H.-J. Yeh, and R.S. Muller, "Electrical and Optical Characteristics of Vacuum Sealed Polysilicon Microlamps," IEEE Transactions on Electron Devices, 39(6) 1363-1374 (1992).

2-13 S. Hoshinouchi et al., "Fabrication of a fine heating element for microelectronics," Proceedings of the 2nd Int. Conf. on Vacuum Microelectronis, (Bath, UK 24-26 July 1989), Inst. Phys. Conf. Ser. No. 99, R.E. Turner, ed. (Institute of Physics, Bristol and New York: 1989) pp.13-16.

2-14 D.C. Perno, D.A. Crewe, and A.D. Feinerman, "Micromachined thermionic emitters," J. Micromech. Microeng., 2, 25-30 (1992).

2-15 SIMION is an electrostatic lens analysis and design program revised and developed by the Idaho National Engineering Laboratory. The 2D version used for this analysis is a public domain version. Commercial versions in 3D are to be made available. At the writing of this report, the commercial vendor was unknown.

3 PORTABLE UNIT VACUUM PUMP

3.1 Overview

For an ionic mass spectrograph, a vacuum produces a sufficiently long mean free path for the ions from the ionizer region to travel to the detector array without collisions with other gas molecules. This collisionless condition is required, so that the electrostatic and magnetic fields are the primary determinant for where the ions land on the detector array and the position of the signal on the detector array can then be used to determine the mass to charge ratio of the ion unambiguously.

The mean free path defines the average distance that a gas molecule travels before it collides with another gas molecule. The mean free path is a function of gas density (pressure) and temperature. A collisionless condition is obtained when the mean free path is at least as long as the distance the ion must traverse. The equation for the mean free path in air at 22°C is given in 3-1.1.[3-1]

[3-1.1] $\lambda\,(\text{mm}) = 6.6 / P,$

where λ is the mean free path, and P is the pressure in Pascal. For a 1 centimeter length of mean free path, this pressure is about 0.66 Pa (5 milliTorr). Lower pressures can aid in extending the sensitivity of the gas sensor by removing background deflections that would allow more ions of minor constituents in the sample to reach the detector array. The gas sensor device pressure specification in the mass selection region is 0.66 Pa (5 milliTorr) or less.

Since the inlet pressure is at atmosphere, a vacuum pump reduces the pressure inside the device. The mass spectrograph chip uses differential pumping to obtain the necessary vacuum with a chip-size device. The gas sensor device incorporates four stages of differential pumping. The advantage of differential pumping is that the first stage removes a majority of the gas (approximately 90%) at a high pressure. This allows a staged set of low volume displacement pumps to be used instead of one high volume displacement pump. The gas sensor has a total design gas throughput of 0.2 standard cubic centimeters per minute. Using a single pump, the volume displacement to obtain 0.66 Pa (5 milliTorr) would be 30.4 liters per minute. Two options can be used. The first is to manifold the differential pumping chambers into the mouth of a 30 liter per minute pump and control the conductance of gas from each chamber to the pump. The second is to utilize multiple pumps to individually pump each chamber. The first configuration was done with a pump from Balzers, whereas the second was done with a pump manufactured from Bechdon.

The mean free path is used to advantage in other regions of the mass spectrograph chip, along with the differential pumping approach. The sensitivity of the MSOC gas sensor is directly related to the number of ions that are produced and transported to the detector array. The production of ions is related to two primary factors. These

are the electron current and the gas molecule density in the ionizer chamber. Since the electron emitters that supply the electrons can be located close to the extraction orifices (0.2 mm), a higher pressure (33 Pa or 0.25 Torr) or gas density can be maintained there and still maintain collisionless conditions for the extracted ions. Therefore, the ionizer was designed to be placed in a separate differential pumping chamber and maintained at a higher pressure. Due to its closeness to the extraction orifice, the pressure in the ionizer chamber can be between 13 (100 milliTorr) and 65 Pa (500 milliTorr).

3.2 *Performance Goals*

The goals of the vacuum pump are shown in Figure 3.2-1. Here the gas loads and pressures for each of the differential chambers are indicated.

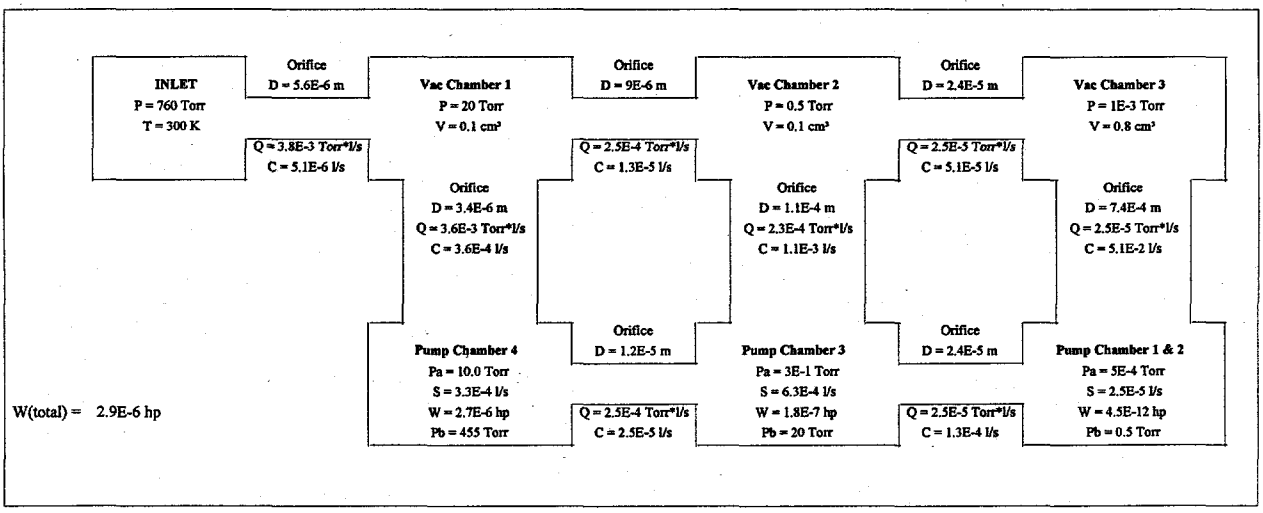

Figure 3.2-1 The schematic of the pumping system for the mass spectrograph on a chip is illustrated above with the size, throughputs (Q) and conductances (C) of the passages.

The pressures (P) and volumes (V) of the chambers are indicated. The input can be from a GC.

As can be seen from the work indication, the vacuum pump, even if configured in multiple stages, id not required to perform a large amount of work to compress the gases from the desired pressures and throughputs to atmospheric pressure. In order to obtain a pump with the lowest power and size, friction produced by the seals of the pumps must be minimized.

The performance goals of the miniature vacuum pump are shown in Table 3.2-1.

Criteria	Value
Total Gas Throughput:	0.2 sccm (20.3 Pa-L/s)
Inlet Pressure:	760 Torr (101,323 Pa)
Pressure in Ionizer Chamber:	100 - 500 milliTorr (13 - 65 Pa)
Pressure in Mass Separation Chamber:	< 5 milliTorr (0.66 Pa)
Volume of Pump:	< 4000 cm^3
Electrical Power Limit:	< 36 Watts

Table 3.2-1 The vacuum pump is required to meet these goals in order to fabricate a miniature GC/MS that is less than 10 kg in mass and 28 liters in volume.

There are two basic designs of vacuum pumps that will handle the gas loads and pressures desired and can be made compact. The first is a multi-stage, rotary vane pump. The second is a molecular drag pump backed by a diaphragm pump. The multi-stage, rotary vane pump was designed by Northrop Grumman STC and manufactured as a prototype by Bechdon. A summary of the design is shown in Table 3.2-2.

The pump design shown in Table 3.2-2 is for an inlet pressure (P0) of 760 Torr. P3 is the ultimate pressure of the pump. Omega is the rotational speed of the pump. The surface tension and viscosity of the gas are used to determine the friction loss and leak rates in the pump. For each chamber, the inlet pressure is designated as the P#a value and the outlet pressure is P#b. The length of the pumping chamber is L#. The gas throughput to the pump is shown in two sets of units as dm# and Q. The leak rate ratio, vane thickness and height, and clearances are shown for each pumping chamber. As would be expected, the pumping chamber (#1) maintaining the lowest pressure is also the largest. The compression ratio of each pumping stage is given.

	P0 [Torr]=	760	P3 [Torr]=	0.001
		Omega [rpm] =	1000	
		Surf Ten [N/m] =	0.025	
		Viscosity [N-s/m²] =	6.70E-05	
Chamber 1	P1a [Torr] =	0.0005	P1b [Torr] =	0.01
	L1[cm] =	2.54		
		dm1 [sccm]=	0.002	
		Throughput [Torr l/s] =	2.53E-05	
		Leak rate ratio =	0.5	
		Vane thickness[cm] =	0.1016	
		Vane Height [cm] =	3.81	
		Reqd max clear[cm]=	2.83E-03	
Chamber 2	P2a [Torr] =	0.008	P2b [Torr] =	0.5
	L2[cm] =	0.635		
		dm2 [sccm]=	0.002	
		Throughput [Torr l/s] =	2.53E-05	
		Leak rate ratio =	0.9	
		Vane thickness[cm] =	0.1016	
		Vane Height [cm] =	1.27	
		Reqd max clear[cm]=	2.37E-03	
Chamber 3	P3a [Torr] =	0.3	P3b [Torr] =	20
	L3[cm] =	0.635		
		dm3 [sccm]=	0.02	
		Throughput [Torr l/s] =	2.53E-04	
		Leak rate ratio =	0.9	
		Vane thickness[cm] =	0.1016	
		Vane Height [cm] =	1.27	
		Reqd max clear[cm]=	1.19E-03	
Chamber 4	P4a [Torr] =	10	P4b [Torr] =	455
	L4[cm] =	0.635		
		dm4 [sccm]=	0.3	
		Throughput [Torr l/s] =	3.80E-03	
		Leak rate ratio =	0.9	
		Vane thickness[cm] =	0.1016	
		Vane Height [cm] =	1.27	
		Reqd max clear[cm]=	9.67E-04	
	Compression			
Chamber	Ratio			
1	20		Total Torque [J] =	0.1007
2	62.5		Total Power [W] =	10.54
3	66.7		Total Vol [cm³] =	17.04
4	45.5		Total Weight [kg] =	0.0767

Table 3.2-2 The multi-stage, rotary vane pump design parameters are summarized for a four stage pump that is roughed by a diaphragm pump to 455 Torr.

This design was given to Bechdon for the purpose of manufacturing and testing of a prototype, miniature, rotary vane pump. The pump is required to used dry lubrication, due to the desire that the orientation of the pump would not be a limitation on its mounting and use, but also to eliminate contamination from organic oils back streaming into the mass spectrometer. The diaphragm pump chosen to back this rotary vane pump was a ASF model 5010.

3.3 Vacuum Pump Operations

The vacuum pump is connected to the mass spectrograph chip through a manifold. This manifold was made to be the same for both the Bechdon and Balzers pump. Schematically, the Bechdon pump is connected to the MSOC as shown in Figure 3.3-1.

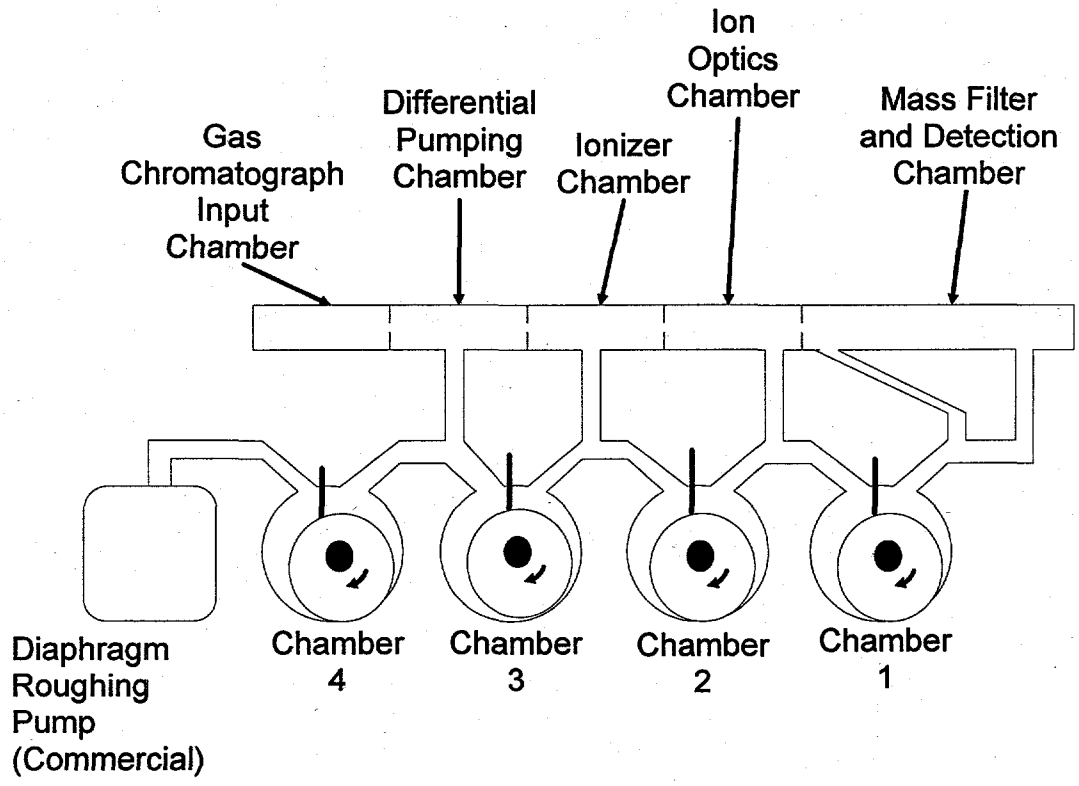

Figure 3.3-1 The multistage, rotary vane pump is connected to the MSOC though a manifold and the compressed gas from each stage is part of the load of the next pumping stage, so that gas flows from chamber 1 to 2, etc. before being discharged back into the atmosphere by the roughing pump.

3.4 Design

The design summary and sizes of the pumping chambers was already shown in Table 3.2-2. The Bechdon layout of the pump was done in circular fashion, so that the movements of each of the rotary chambers was

balanced. The interconnecting passages were cut into a single block of aluminum. The drive motor was connected onto the side and was connected to the rotary feed through via a gearbox. The primary gear contained a hole that activated an optical sensor. This optical sensor opened solenoid valves that were located in the interconnecting passages. These valves were necessary to minimize the back flow between the pumping chambers. The solenoid valves used were Lee model LHDA1211111H. The rotary feed through was a vacuum feed through and the entire pump was operated under reduced atmosphere. This reduced the leaks past seals and moving pieces such as the vanes. The vanes were anodized and impregnated with a coating (Tufram) that reduce the friction of the vane against the rotating drum.

A gearbox was used so that timing adjustments between drum and the solenoid valves could be made. Minor timing adjustments could be made on the control electronics. The control circuit is shown in Figure 3.4-1.

The drum in each chamber was eccentrically located and rotated to minimize the friction between the drum and the chamber wall. Seals were spring loaded to maintain alignment of the vane to the drum. The drums were made to be floating, so that the vane determined the position of the drum and seals. The vane pressure against the drum was maintained by a spring. The design of the spring wells was such that the pressure against the drum was nearly constant, even over relatively large movements of the vane. The spring wells were sealed and evacuated.

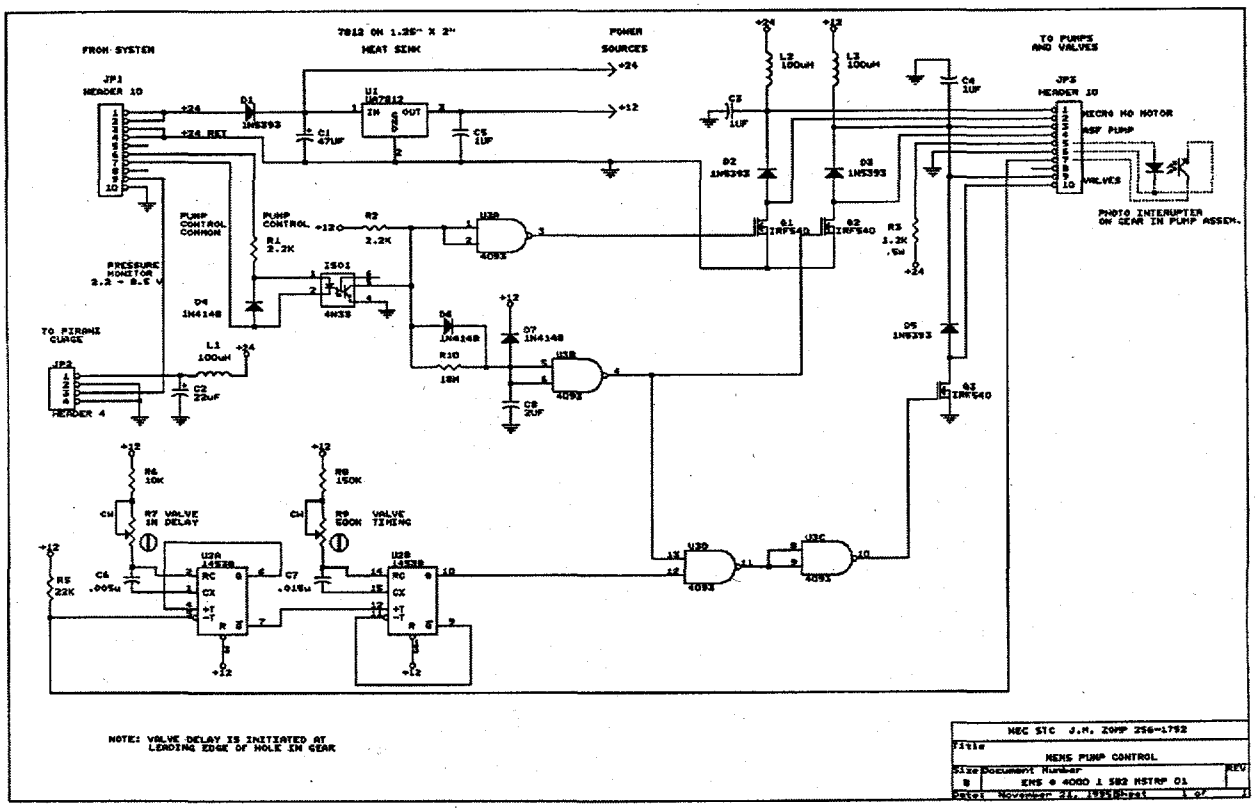

Figure 3.4-1 The electrical control circuit for the Bechdon rotary vane pump shows the photoelectric pickup for the valve control and the valve delay timing adjustment circuit.

The layout of the Bechdon pump is shown in Figure 3.4-2 (a to d) and a picture of the pump is shown in Figure 3.4-3 as a disassembly. An assembled pump is shown in Figure 3.4-4. The pump was assembled and tested for performance. A measured pump down curve is shown in Figure 3.4-5. The pump was performing well in the beginning of operation, but lost speed as the pump ran. The loss of speed was determined to be due to a leak occurring at the vane seal due to excessive wear of the seal material. This area could be modified to make a better seal, but since the Balzer vacuum pump was available, it was agreed by the program team members not to place more resources on the Bechdon pump. These results and conclusions were presented to the Government at a review meeting.

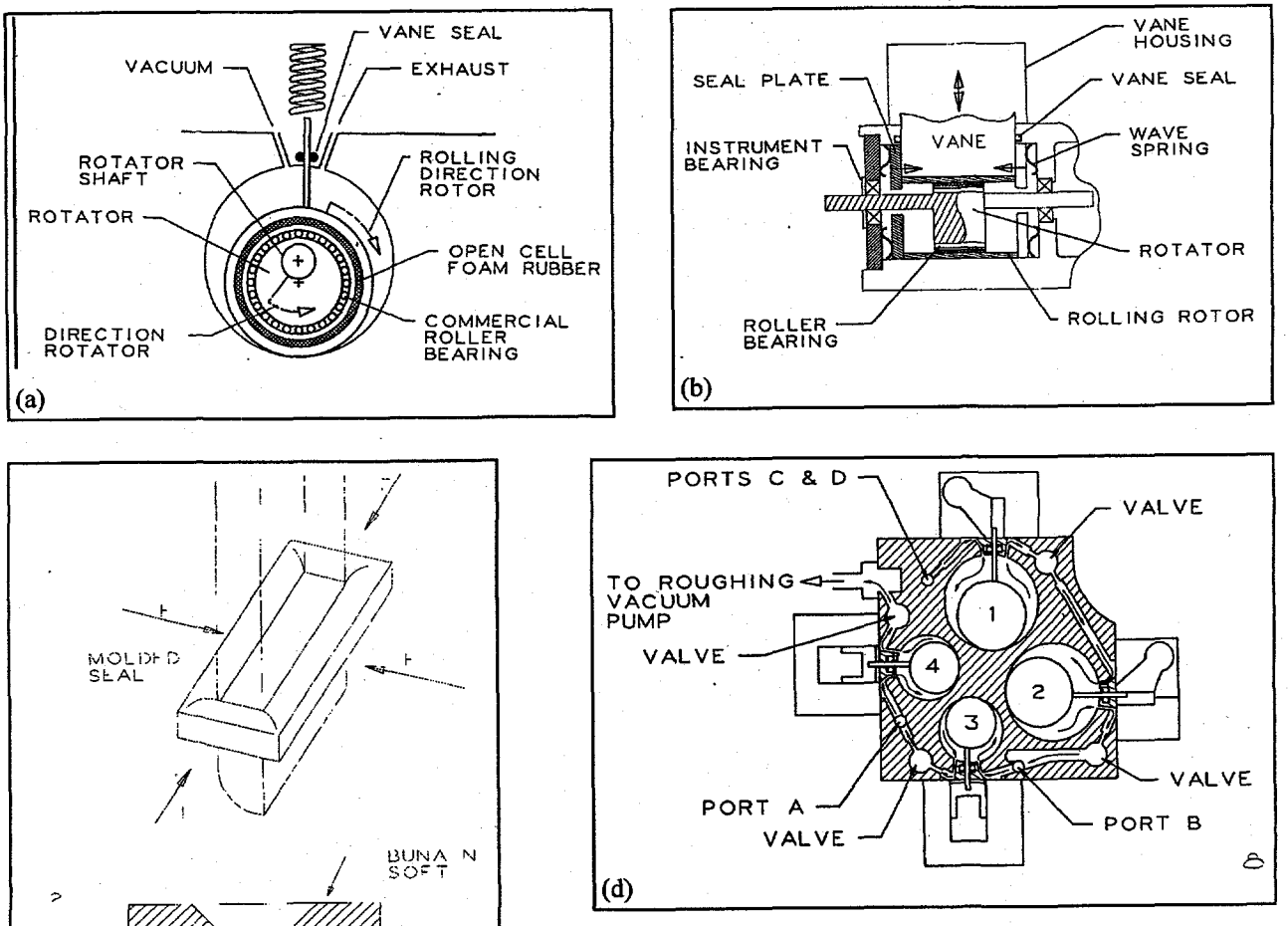

Figure 3.4-2 The details and overall layout is shown in these design drawings.

The implementation of the eccentric roller bearing drum is shown in an end view (a) and side view (b). The design of the vane and seal are shown in (c) and the four chamber assembly in the primary block is shown in (d).

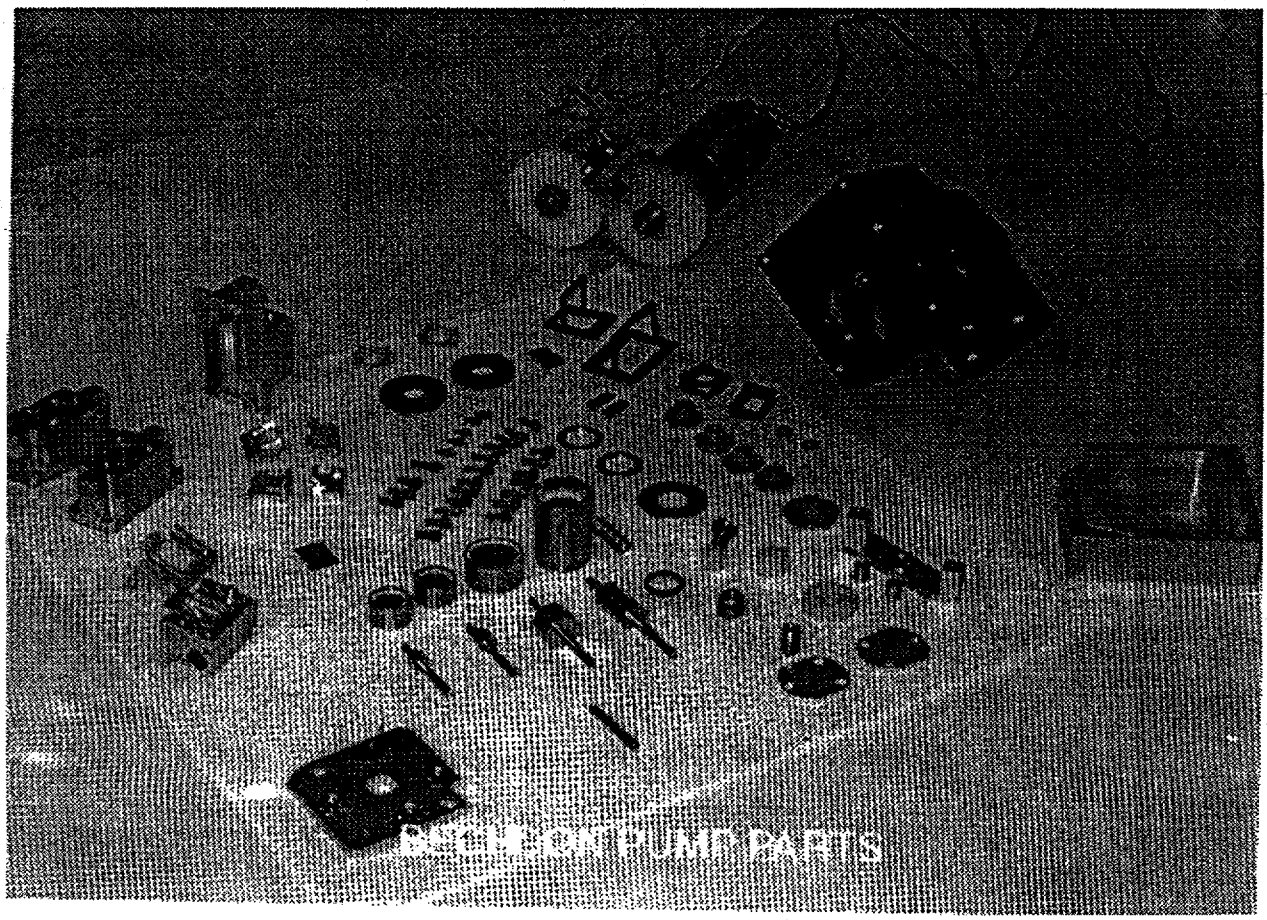

Figure 3.4-3 The complete disassembly of the Bechdon vacuum pump is shown.

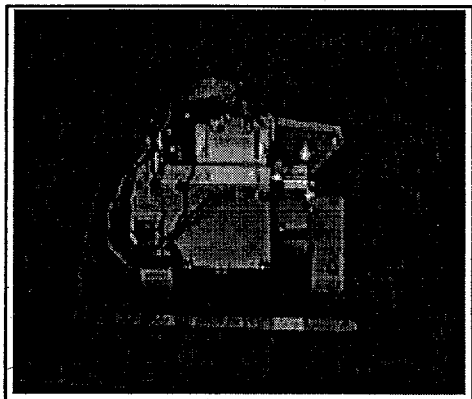

Figure 3.4-4 The assembled Bechdon vacuum pump with a six inch (fifteen centimeter) ruler is shown.

The size of the Bechdon pump met the program requirements.

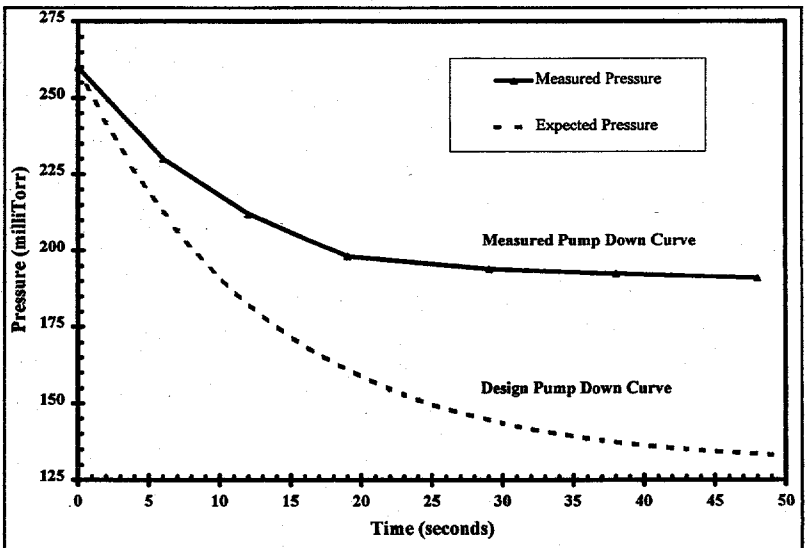

Figure 3.4-5 The measured and expected pump down curves are shown.

The measured curve diverged from the design curve due to leaks at the vane seals due to wear.

3.5 *Balzers PUMP*

A second miniature vacuum pump was provided by Balzer's at no expense to the TRP program. This activity was compatible with Balzer's long-term business objectives. We provided them with the necessary interface specifications to ensure compatibility with the MSOC. A prototype mechanical vacuum pump was initially scheduled for delivery in June, 1995, but actual delivery was in February, 1996. We used this pump for our portable unit integration and test efforts. The Bechdon pump was a more aggressive design (i.e. smaller and lower power) and therefore more compatible with the overall miniaturization objectives. However, the Balzers pump provided a suitable risk mitigation alternative which proved to be necessary in light of the final outcome of the Bechdon pump.

The Balzers drag pump is a Model TPD-020 with 0.6 liter per second pumping speed rating and is shown in Figure 3.5-1 with its diaphrgam backing pump (Balzers model MVP-012) shown in Figure 3.5-2.

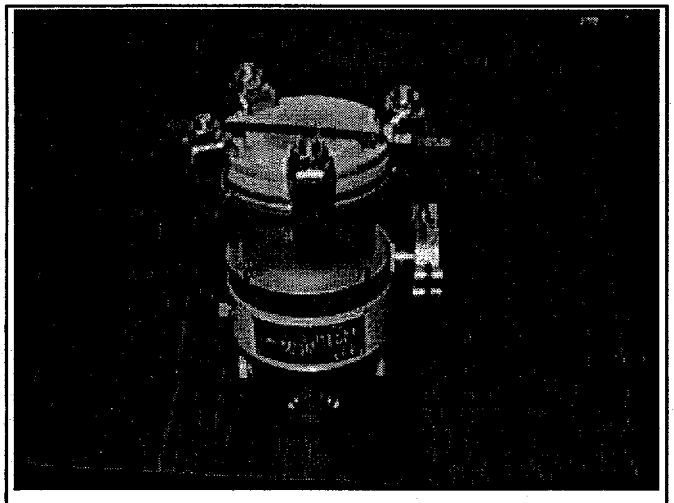

Figure 3.5-1 A small commercially available pump from Balzers has the pumping speed and size for the portable unit.

The ruler on top of the pump is six inches (fifteen centimeters) long.

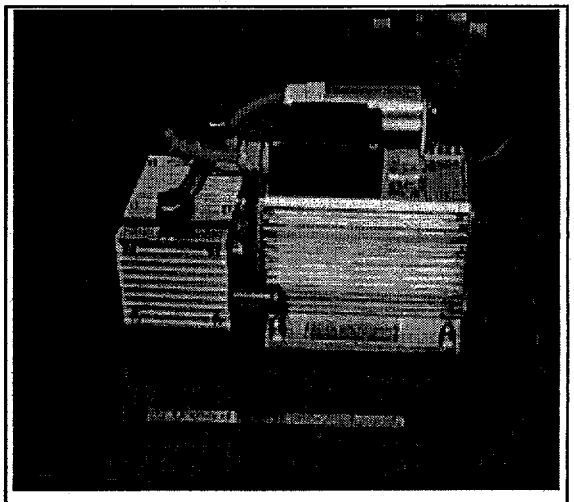

Figure 3.5-2 The backing diaphragm pump for the Balzers drag pump is the smallest commercially available at the time of the program that could maintain the foreline pressure required of the drag pump.

3.6 *References Section 3*

3-1 O'Hanlon, J.F., A User's Guide to Vacuum Technology, Wiley, New York, 1980.

4 PORTABLE UNIT: GAS CHROMATOGRAPH/MASS SPECTROMETER

4.1 Overview

The portable unit chemical detector is a combination of the Microsensor Technology's (MTI) small bore capillary gas chromatograph (GC) with the mass spectrograph on a chip (MSOC). The combination of the GC with the MSOC provides fast identification and quantification of the chemicals within a sample. The GC simplifies the identification of the chemicals by separating the chemical species within a sample into individual chemicals that are presented to the MSOC sequentially. In addition, the GC concentrates the chemicals by presenting a narrower peak time wise and therefore, increasing the individual chemical's concentration by the ratio of the time width of the sample peak to the separated chemical's peak.

The MTI GC was chosen due to its small size and power requirements. In addition, the elution time of the MTI GC is ten times faster than used on larger laboratory based GC units. (The MTI unit elutes in about 2 minutes rather than the 20 minutes of other analytical instruments.) When combined with the MSOC and the miniature vacuum pump, a compact, lightweight GC/MS can be obtained. With this unit, a number of applications are possible that were not pursued due to instrument cost and size. The laboratory procedures can be taken to the field with a unit of this capability and size.

4.2 Performance Goals

The performance goals for the portable unit are shown in Table 4.2-1.

Mass Range:	1 to 400 amu
Mass Resolution:	1 amu at 150 amu
Sensitivity:	100 ppb in 4 minutes
Power:	100 Watts or less
Size:	< 19,000 cm^3
Weight:	< 10 kilograms

Table 4.2-1. The program goals for the GC/MS unit to incorporate the mass spectrograph chip as the detector to a commercially available gas chromatograph column.

4.3 Gas Chromatograph/Mass Spectrometer Operations

The gas chromatograph with a mass spectrograph detector operates in a sequential manner. The gas chromatograph prepares a sample by drawing in a air sample into the injection valve. This is a defined volume between two pneumatically operated valves. The sample is then entrained in the carrier gas and injected onto the chromatograph column as a gas pulse. The constituents in this gas pulse are separated temporally due to their differences in physical interaction with the coating on the column. This interaction is a sorption/desorption process. Constituent chemicals that have a strong interaction take longer to travel down the column than ones with weaker interactions. Examples of the interaction processes include whether the polarity of the molecule, the amount of saturation in an organic molecules, or the presence of halogens. The result is that the gas chromatograph presents separated chemicals to the detector as peaks over an elution time period.

The mass spectrograph detector produces ions from the gases drawn from the gas chromatograph, transports the ions to the detector array and detects the position and quantity of charge collected by the array. This position and quantity information can be used to identify and quantify the vapor species giving rise to the mass spectrum. In the following discussion, the assumption is that there is only the calibrant and single gas species involved in the data set. For multiple vapor species, the ion signals will simply add. Use of mixture software, based on probability based matching and commercially available through Palisades,[4-1] can help deconvolute the components of the spectrum.

Knowledge of the GC column will tell what components are eluted in what order. In general, lighter components (lower molecular weight) are eluted quickly and heavier ones later. Therefore, it is possible to have the MSOC scan change as a function of elution time, taking advantage of quicker scans where the mass range does not have to be as long. This is particularly advantageous, since the earlier eluting GC peaks are narrower in time span than the later GC peaks.

For a GC/MS, the carrier will be used as the calibrant for both mass range and concentration. In fact, the carrier gas will be helium spiked with about 1% argon. The argon will be used for the calibration purposes. If the unit is operating by sampling air directly, then argon in the atmosphere would be used as the calibrant (also present at about 1% by volume in normal atmospheric composition). In both cases the following discussion holds. For any vapor species, the neutral gas must be ionized. There are many methods of accomplishing this. For the MSOC, electron-impact at between 70 and 100 eV ionizes the vapor species into positive ions of the parent molecule and its fragments. Due to the molecular bonding, the fragments are related to the structure of the vapor molecule from which they are formed. Libraries of the fragment ions and there relative intensities can be utilized to identify the vapor species. Even the atomic gases, such as helium, neon and argon, exhibit ions at different masses with varying intensities. Some of this variation is due to isotope abundance and some is due to the formation of multiply charged ions, since the electron impact energy is higher that the thresholds for the ejection of multiple electrons and the atomic gas species can not fragment to dissipate the excess energy imparted by the electron impact.

The MSOC will be operating continuously and can be set for the mass window that contains the main peak of the calibrant gas, argon. The software will maintain this condition until the signal of the calibrant gas goes down. This will indicate that there is something in addition to the carrier gas flowing through the detector. Scanning will begin and continue until the calibrant ion signal returns to its baseline value. The scans gathered during this time will be summed and submitted to the library search routine for analysis. An elution time will be recorded as well as a peak width. These will be required for the determination of the concentration in the original sample. The spectral analysis will return the identity and amount of material in the sample.

There is a difference in the operation of the MSOC as a detector for a GC over directly sampling the air. While directly sampling air, a reasonable assumption can be made for most situations, that the concentration of the chemical species in the air does not change drastically during the scan time. This is true for a point source that is at a stationary location. When a mass spectrometer or spectrograph is sensing the peak of a GC, the chemical concentration is changing dramatically during a single scan. To obtain a library searchable mass spectrum, a number of scans must be taken per peak. The minimum number is three and a more conservative number would be seven or more. The reason for this is illustrated in Figure 4.3-1.

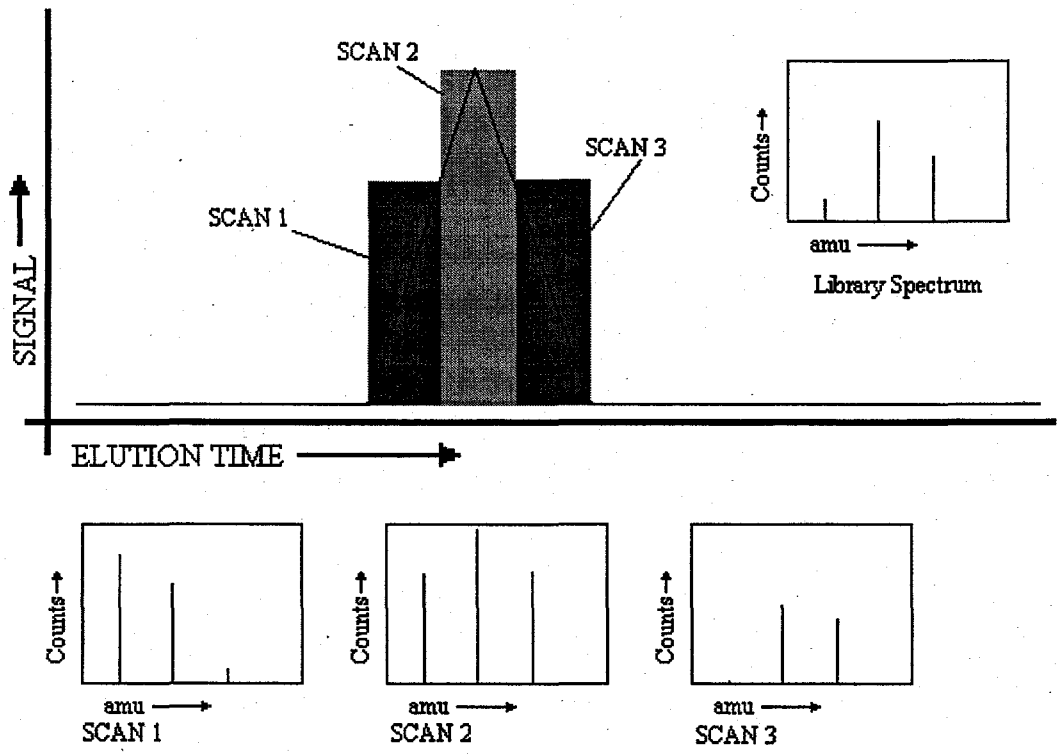

Figure 4.3-1 During the elution of a GC peak, the mass spectrum obtained can be very different due to the changing concentration of the chemical species during the scan.

Due to the scanning of the mass spectrograph, during the rise of the peak, the ions that are scanned later are sensed with a higher intensity. For the MSOC, the scan is assumed to go from higher to lower mass ions. The same is true on the fall of the GC peak, except that the earlier ions will be sensed with a higher relative intensity. In order to obtain a spectrum that is representative of the molecule at a constant concentration, then all of the individual scans must be summed.

In addition to the mass spectral signal as a measure of quantity, the GC peak area would be a way of determining the quantity of a chemical that has been passed through the column. This can be done by measuring the calibrant signal intensity and carrier gas flow rate and determining the reduction in concentration of the calibrant gas.

4.4 Design

A pre-column back flush gas chromatograph (GC) system was determined to be the best match for the intended application of the portable unit, the monitoring of volatile organic compounds (VOCs). The primary difference between a standard gas chromatograph and a pre-column back flush gas chromatograph is the addition of a second column at the front end of the analysis system. Since there are two columns, a valve system can be inserted at the junction of the two columns to effect the back flush of the first column. The benefits of a pre-column back flush gas chromatograph include the prevention of high boiling point ("heavy") sample components from contaminating the GC and mass spectrometer (MS) detector, prevention of "carryover" baseline noise if new samples are injected before elution of the first sample is complete, speeds up the overall GC/MS cycle time therefore increasing sample throughput capacity, and reduces downtime by improving and increasing column/detector life.

MTI is the premier company in high speed GCs by having a unit with an elution time on 2 minutes versus 20 minutes for standard GC manufacturers. With the pre-column back flush, the elution time can be reduced by a factor of at least two, depending on the length of the pre-column in relation to the analytical column. The way a pre-column back flush works is that the sample is injected onto the pre-column. The light sample components pass quickly through the pre-column and are passed to the analytical column. The heavy sample components stick to the pre-column and are back flushed by reversing the carrier gas flow through the pre-column back out the vent. The MTI design of the pre-column back flush GC is shown in Figure 4.4-1.

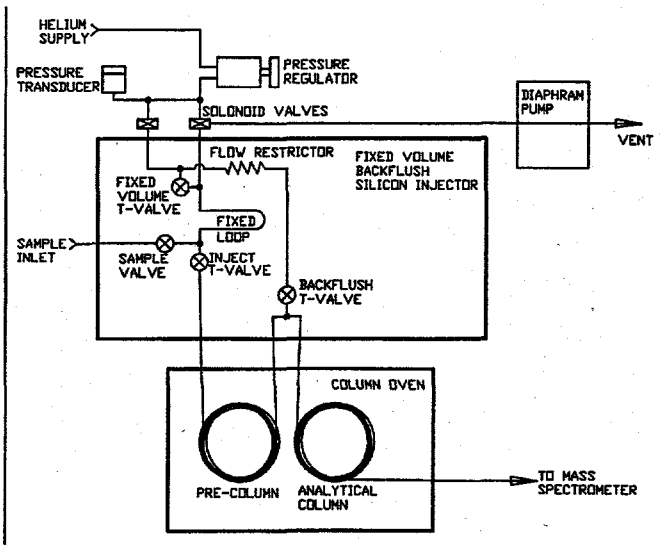

Figure 4.4-1 The pre-column and analytical column are clearly shown in the schematic of the MTI back flush GC.

The architecture chosen allowed the MEMS valve/injection system that MTI had developed for their product line to incorporate the back flush valve system into one chip and reduce the part count and zones where temperature regulation would be required. The new valve/injector/back flush die is shown in Figure 4.4-2.

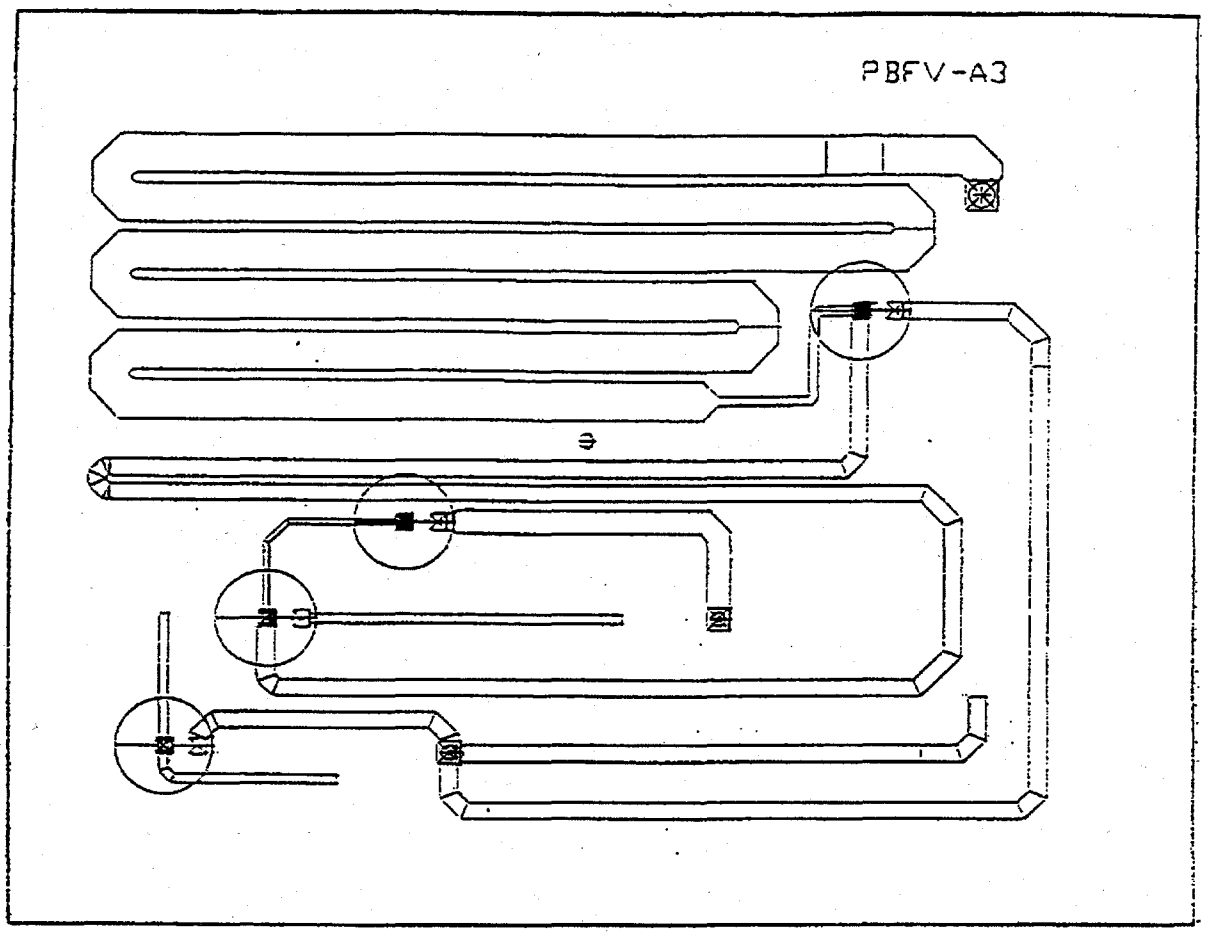

Figure 4.4-2 The fabrication of the back flush valve system used the same processes as the valve/injector system already in use and permitted the integration of the two functions into one die.

4.5 Development

The valve/injector/back flush die was successfully fabricated and incorporated into a pre-column back flush GC brass board laboratory prototype and tested. As can be seen in Figure 4.5-1, the back flush system worked as expected and will be incorporated into the MTI product line, as well as be delivered in a unit for use on this program.

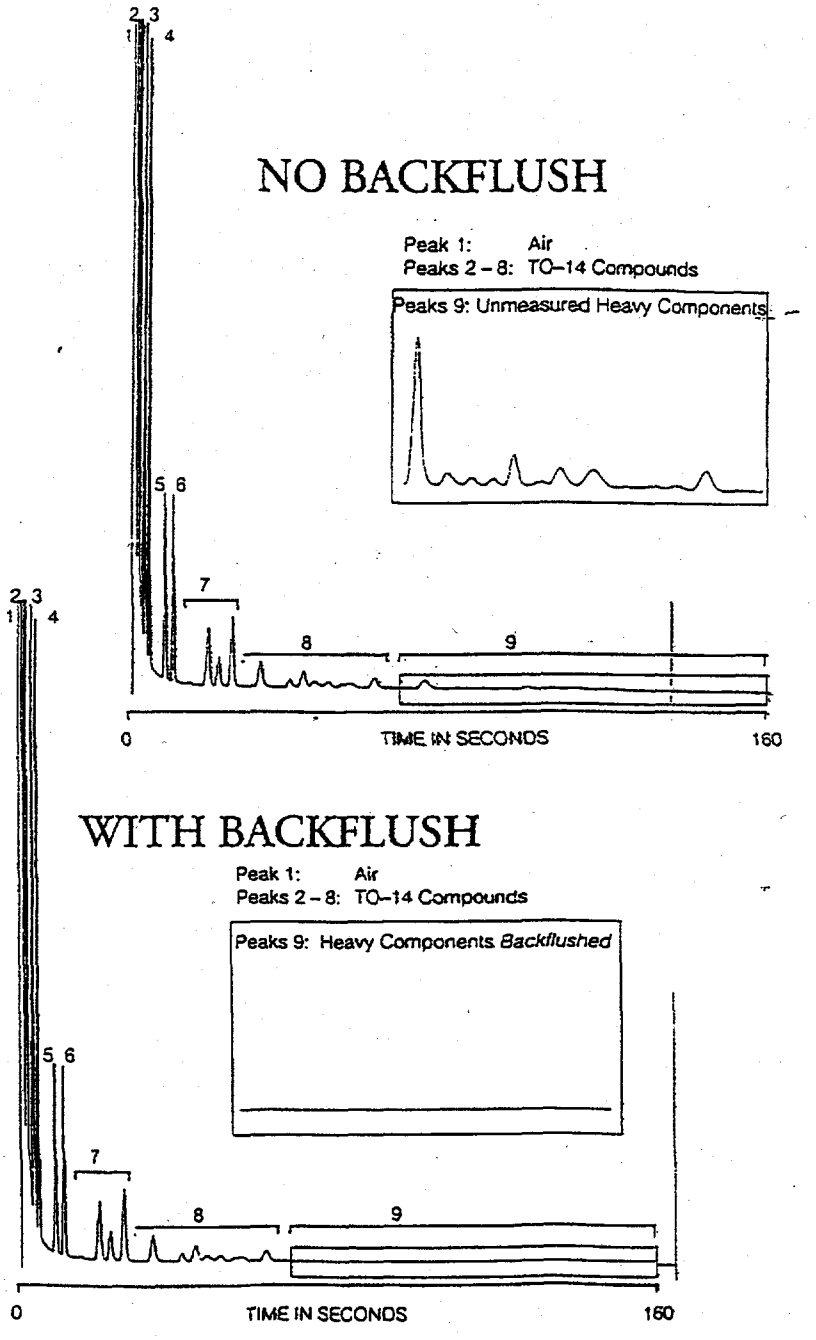

Figure 4.5-1 The pre-column back flush GC performed as expected and eliminated the necessity of waiting for the elution of the heavy organics prior to the injection of a new sample onto the GC.

4.6 References For Section 4

4-1 Palisade Corporation, 31 Decker Road, Newfield, NY 14867. Internet: http://www.palisade.com/mass-spec, Phone 607-277-8000, Fax 607-277-8001.

5 PORTABLE UNIT

5.1 Mechanical

5.1.1 Overview

The mechanical system for the Portable GC/MS unit can be divided into two primary groups including:

1. The MSOC Manifold
2. The Portable Instrument.

These items are described in the following sections.

5.1.2 MSOC Manifold

The MSOC Manifold serves as the mechanical interface between the MSOC and the rest of the Portable Unit. A block diagram of the mass spectrometer interfaces is shown in Figure 5.1-1. As can be seen in the figure, there are three interfaces which includes:

1. Gas Chromatograph to Mass Spectrograph Chip
2. Mass Spectrograph to Vacuum Pump
3. Mass Spectrograph to Processor Electronics

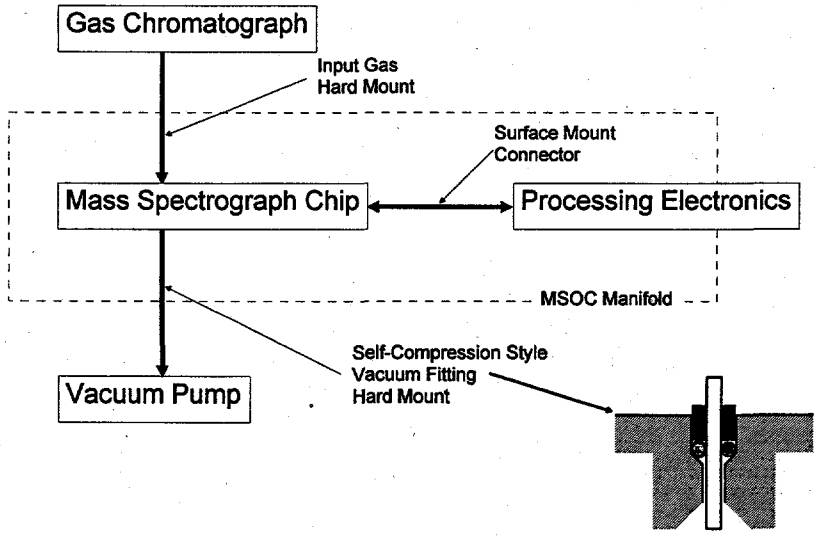

Figure 5.1-1 Mass spectrograph interfaces

Figure 5.1-2 shows several views of the actual MSOC Manifold. Figures 5.1-3 and 5.1-4 show the MSOC mounted on the ceramic interface substrate and the electronics control board, respectively. Figures 5.1-5 through 5.1-6 shows the buildup of the MSOC and manifold.

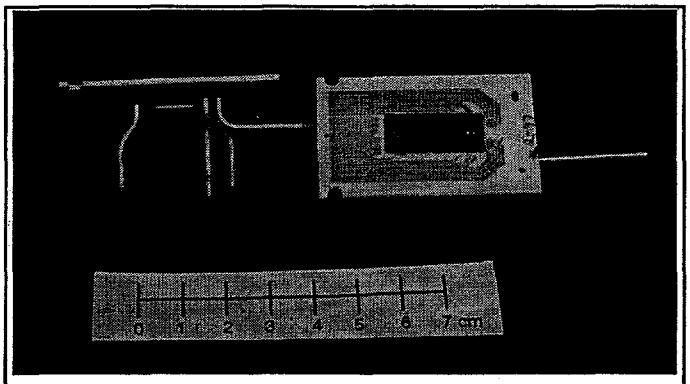

Figure 5.1-2 The MSOC Manifold

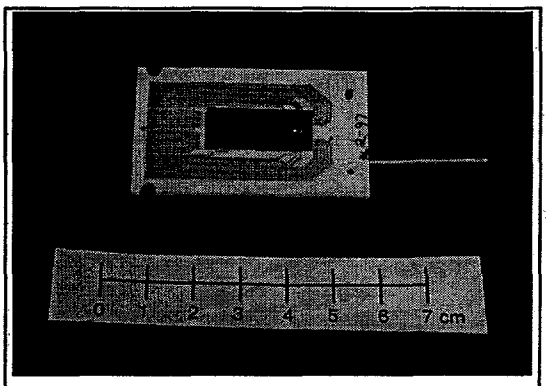

Figure 5.1-3 MSOC and substrate

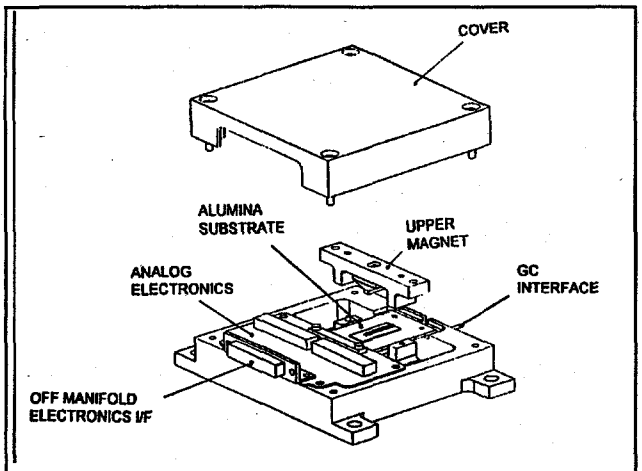

Figure 5.1-4 Drawing of mounted MSOC in sensor housing

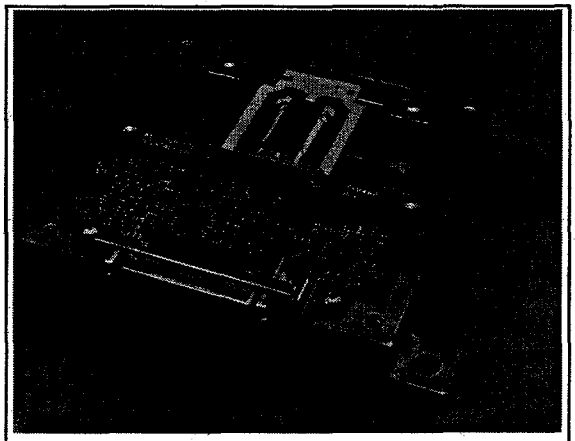

Figure 5.1-5 Substrate, Magnet and Bottom Manifold

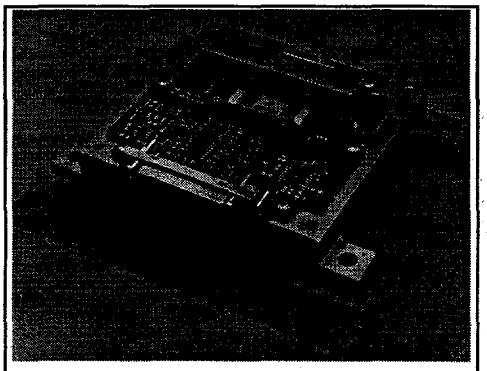

Figure 5.1-6 Buildup Including Upper Magnet

5.1.3 Portable Instrument

The Portable Instrument is a completely self-contained unit that is easily transported by one person and is simple to operate. A block diagram of the Portable Instrument Mechanical Architecture is shown in Figure 5.1-7. The Portable Instrument incorporates modular design in order to facilitate field repair. Figure 5.1-8 shows the actual Portable Instrument. The actual Portable Instrument houses the MSOC/manifold, the GC, vacuum pump, processor, and other support electronics. The Portable Instrument measures about 12 inches high (30 cm), 19 inches wide (48 cm) and 17 inches deep (43 cm) and weighs about 30 pounds (13.6 kg).

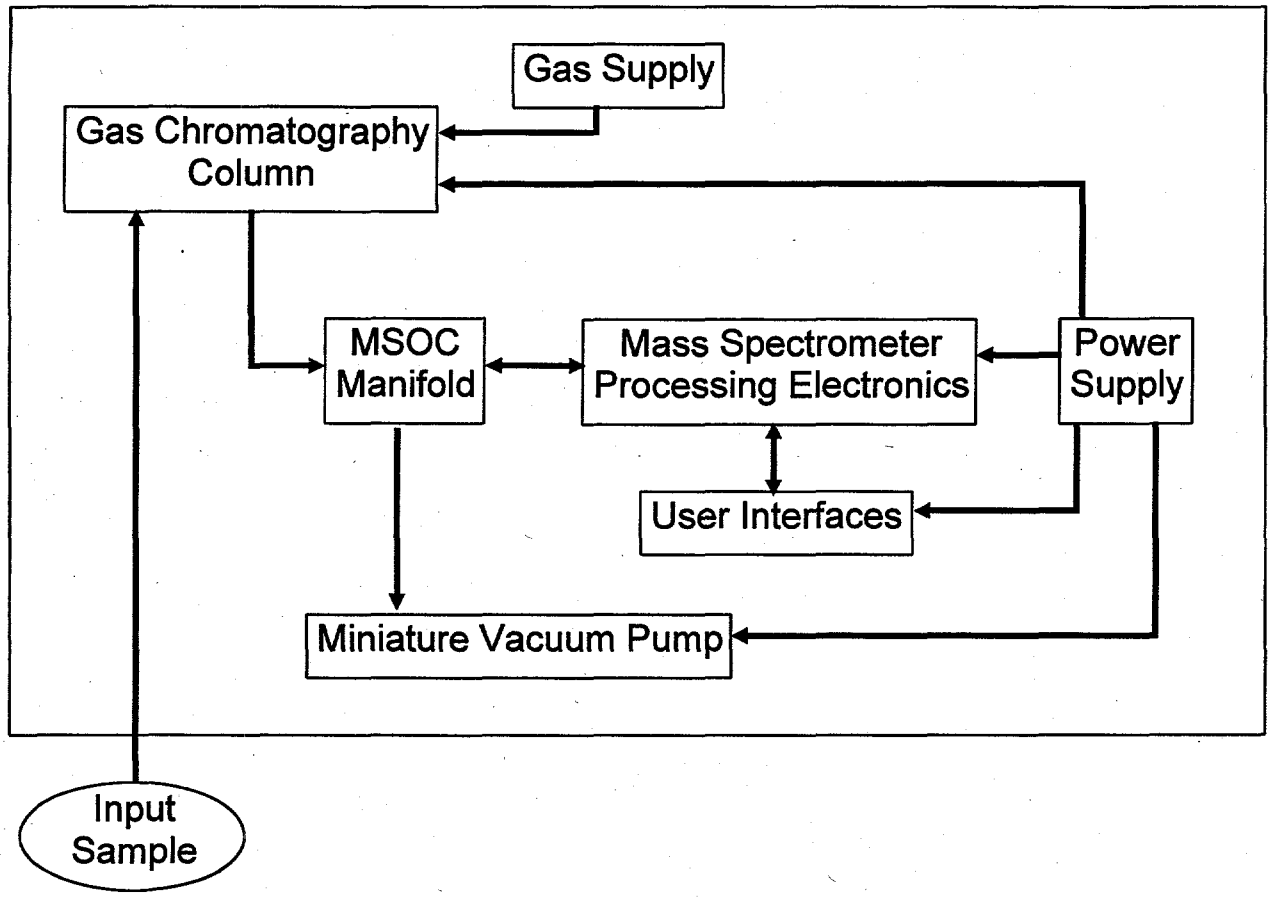

Figure 5.1-7 Portable instrument mechanical architecture is shown in block diagram.

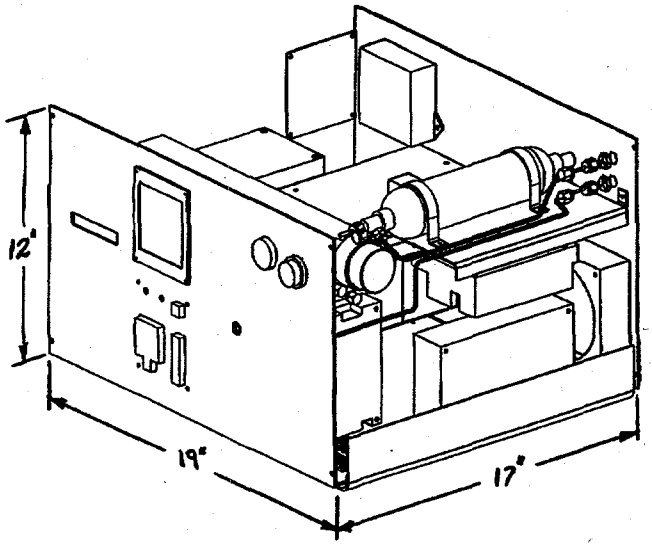

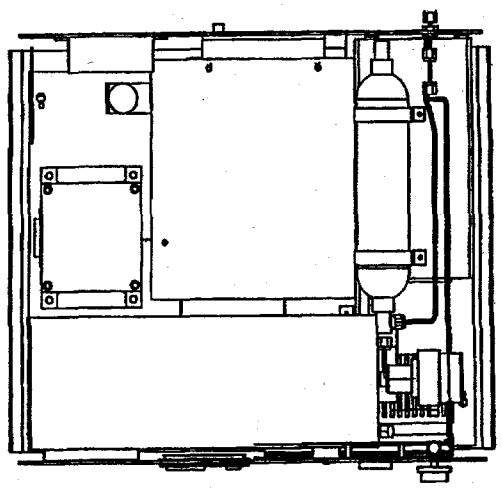

Top View

Figure 5.1-8 A mechanical drawing of the portable unit shows the integration of the parts into a compact casing.

5.2 Electrical

5.2.1. Overview

The electrical system for the Portable GC/MS unit can be divided into several groups of related functions. These groups are described in the following sections.

5.2.2. Functional Block Diagram

The electrical systems that power and control the operation of the Portable GC/MS can be grouped into several functional blocks. These blocks are shown in Figure (FRPTBLOK) and their purpose is described in the following sections.

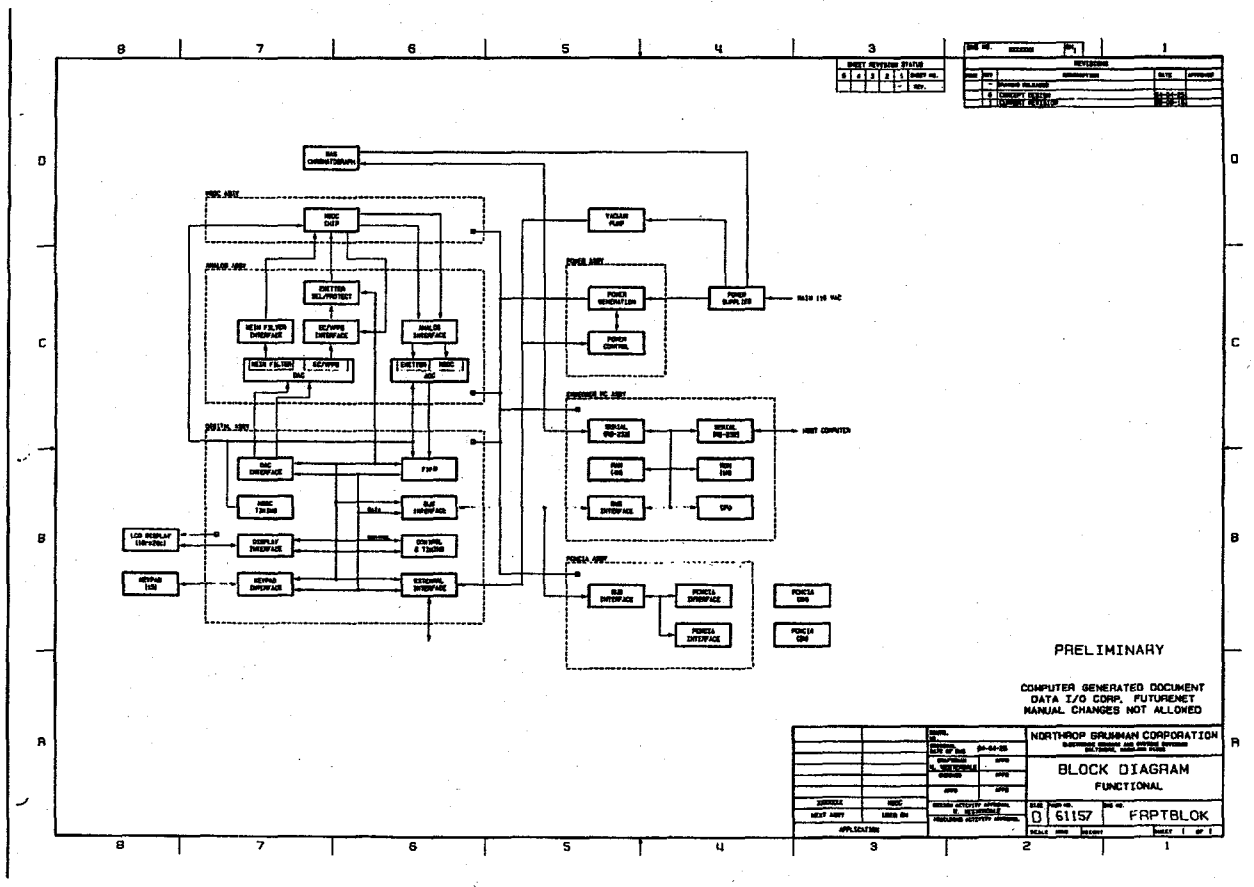

Figure 5.2-1 The functional blocks are schematically shown so that the discussion in the following subsections can be organized.

5.2.3. Vacuum Pump

The Vacuum Pump's purpose is to draw an air sample through the Gas Chromatograph and then through the MSOC Chip, while maintaining a very low pressure within the MSOC Chip. There is also a sensor to monitor the air pressure level.

There were two vacuum pump units considered for use in the Portable GC/MS. The first pump was designed with Bechdon and is described in Section 3.4. The second pump was designed by Balzers and is described in Section 3.5. Although the two pumps are different and have different cabling requirements, the electrical power and control signals are common. This minimized the changes required to accommodate both units.

5.2.4. Gas Chromatograph

The Gas Chromatograph's purpose is to separate the air sample components, in time, into only light weights first, then only medium weights and finally only heavy weights. This improves the operation of the Portable GC/MS.

The Gas Chromatograph used is a commercial unit produced by MTI. The electrical interfaces consist of a single RS-232 serial communication link, some discrete input/output control lines and a power supply input.

5.2.5. MSOC Chip

The MSOC Chip is the heart of the system. It ionizes the air sample, using an internal emitter, and accumulates the amount of component mass-to-charge ratios in the sample, using an internal detector. These ratios are ultimately used to identify the gases in the air sample. The range of ratios to detect is programmable.

The MSOC Chip requires various input control signals. current for the emitter is used to ionize the air sample. The Wein filter voltage is used to select the range of mass-to-charge ratios to acquire. Several digital signals are used to control the reading of the detector's acquired analog mass-to-charge values. Finally, several different power supply voltages are required to properly bias internal points of the chip.

The MSOC Chip outputs one type of signal. The detector's mass-to-charge values are serially output.

The ceramic substrate that the MSOC chip is mounted on, is directly connected to a small circuit board. This board contains circuitry to amplify and buffer the low level analog output signal, before transmission to the Analog circuit board.

5.2.6 Power Distribution

The system requires many different voltages. Some of these are industry standard values, however, those associated with the MSOC chip are specialized. Power distribution is modular and accomplished by several power subsystems. This provides easy testing and reconfiguration during the development phase. All power subsystems have been designed, fabricated and tested.

One power subsystem supplies the vacuum pump and it's controller. This provides +24 volts DC at 2.5 amps. It can be used to power either the original Bechdon pump or the alternative Balzers pump. This is a standard commercial power supply.

Another power subsystem supplies the gas chromatograph unit. This provides +12 volts DC at 5 amps and is a standard commercial power supply.

The final power subsystem supplies the MSOC chip and it's digital and analog control circuitry. This subsystem combines a standard commercial power supply with a Northrop Grumman designed power generation

board. For proper operation, the MSOC chip requires a number of different voltages, which are adjustable for the development phase. The standard supply provides +5 volts DC, +15 volts DC and -15 volts DC. The power generation board provides 15 outputs that can be independently adjusted between +15 volts DC and -15 volts DC. It also provides 2 outputs that are independently adjustable from -1.5 volts DC and -11.5 volts DC. Finally, it provides +15 volts DC and -15 volts DC with respect to a ground that is offset from the primary ground (0 volts) by -91 volts.

5.2.7. Analog Functions

The analog functions provide the primary interface between the real world analog signals and the computer processed digital signals. There are many functions that are performed and these are described below.

The Wien filter voltage is used by the MSOC chip to determine the range of mass-to-charge ratios to be acquired. This voltage is generated by a Digital-to-Analog Converter (DAC) and some amplifiers. Different voltages are set by loading different digital values into the DAC.

The Emitter Current is used by the MSOC chip to ionize the sample gas being tested. This current is generated by a Voltage Programmable Power Supply (VPPS) and a Current Regulator (EC). The VPPS generates a voltage by using a DAC and several amplifiers. Different voltages are set by loading different digital values into the DAC. The voltage is also regulated, by using feedback from the MSOC chip, to maintain a constant voltage to compensate for variations in the emitters. The VPPS voltage is input to the EC, where it is converted to a current, by using several amplifiers. The EC is also regulated by feedback of the emitter current itself.

The MSOC chip contains six individual emitters, only one of which is used at any given time. The Emitter Selection circuitry routes the Emitter Current to the desired individual emitter, leaving the others unpowered. This is accomplished by using digital values to control optically isolated switches.

The emitters may become oxidized and not function properly if the air pressure within the MSOC chip becomes too great and they are powered on. To prevent this from occurring, there is Emitter Protection circuitry to remove power from the emitters before they may be damaged. This circuitry monitors the air pressure and removes the emitter power if the pressure exceeds a certain threshold.

The detected mass-to-charge ratios, from the MSOC chip, are converted to a digital value, using an Analog-to-Digital Converter (ADC) and some amplifiers.

To maintain confidence in the proper operation of the Portable GC/MS unit, several internal analog signals are monitored and converted to digital values. These digital values are processed by the Embedded PC, to verify that they are within proper limits.

5.2.8. Digital Functions

The digital functions provide the primary interface between the Embedded PC, the human operator and the analog functions. There are several functions that are performed and they are described below.

The Embedded PC interface conforms to the PC/104 computer bus standard. As an alternative, connectors and wiring also provided to interface to the IBM PC-AT computer bus. The interface is implemented as a series of 16 bit values, located in the PC's I/O address space. Writing values to these addresses will cause various modes to change and actions to occur. Reading values from these addresses is how conditions are monitored and results returned to the PC.

The human operator interface is a Liquid Crystal Display (LCD) with 16 rows of 20 text characters. The Embedded PC can write any text information to the LCD, for display to the operator. The operator provides information to the Embedded PC through the use of a 15 button keypad. The purpose assigned to each key is always the same.

The MSOC chip requires several special timing waveforms for proper operation. These are generated by a combination of oscillators, counters, flip-flops and discrete logic devices. The mode of operation is set by digital values from the Embedded PC.

The digitized mass-to-charge ratios, output from the analog functions, are temporarily buffered in a First-In-First-Out (FIFO) circuit. This will store and output data in the same order in which it was input. It is used to compensate for the different operating speeds of the MSOC chip and the Embedded PC. The Embedded PC will read data from the FIFO.

The self-test values generated by the analog functions, as well as the digital functions, are also available for output to the Embedded PC.

5.2.9. Operator Interface

The Operator Interface is used by the system to communicate with it's operator. liquid crystal display is used to output information and a keypad is used to input information. The hardware was selected to allow a direct reuse in a hand held GC/MS system, without re-engineering costs.

The liquid crystal display (LCD) is a commercial unit that displays 16 rows of 20 characters. It contains it's own controller and has a parallel interface for passing commands and display information.

The keypad is a custom Northrop Grumman design. It has 15 push buttons and two lights to provide; a numeric entry, some function key inputs and status light outputs.

5.2.10. Embedded PC

The Embedded PC computer provides overall operational control of the Portable GC/MS unit. It also handles the data collection, analysis, display and storage.

The computer is a off the shelf commercial product. It conforms to the IEEE-P996 standard, which is commonly referred to as PC/104. This computer runs standard IBM PC programs and development tools.

To ensure rugged and reliable operation, solid state RAM disks are used instead of the typical rotating hard disks. There are two RAM disks and they conform to the PCMCIA Memory Card standard, commonly used on laptop computers. One RAM disk is used to storage the application program and related files. The other RAM disk is used to store the gas library data files, of the compounds to search for. This disk is easily changed, when it is desired to search for another set of compounds.

The are two basic control interfaces with the Portable GC/MS subsystems. A serial RS-232 interface is used by the Gas Chromatograph. All other subsystems have an interface through the digital functions, as described in Section 5.2.7.

5.2.11. Power

The system requires many different voltages. Some of these are industry standard values, however, those associated with the MSOC chip are specialized. Power distribution is modular and accomplished by several power subsystems. This provides easy testing and reconfiguration during the development phase. All power subsystems have been designed, fabricated and tested.

One power subsystem supplies the vacuum pump and it's controller. This provides +24 volts DC at 2.5 amps. It can be used to power either the original Bechdon pump or the alternative Balzers pump. This is a standard commercial power supply.

Another power subsystem supplies the gas chromatograph unit. This provides +12 volts DC at 5 amps and is a standard commercial power supply.

The final power subsystem supplies the MSOC chip and it's digital and analog control circuitry. This subsystem combines a standard commercial power supply with a Northrop Grumman designed power generation board. For proper operation, the MSOC chip requires a number of different voltages, which are adjustable for the development phase. The standard supply provides +5 volts DC, +15 volts DC and -15 volts DC. The power generation board provides 15 outputs that can be independently adjusted between +15 volts DC and -15 volts DC. It also provides 2 outputs that are independently adjustable from -1.5 volts DC and -11.5 volts DC. Finally, it provides +15 volts DC and -15 volts DC with respect to a ground that is offset from the primary ground (0 volts) by -91 volts.

5.2.12. System Cabling

The electrical devices, subassemblies and cables that makeup the Portable GC/MS are shown in Figure (SYSCAB2). All of these items are mounted within the mechanical enclosure described in Section 5.1.

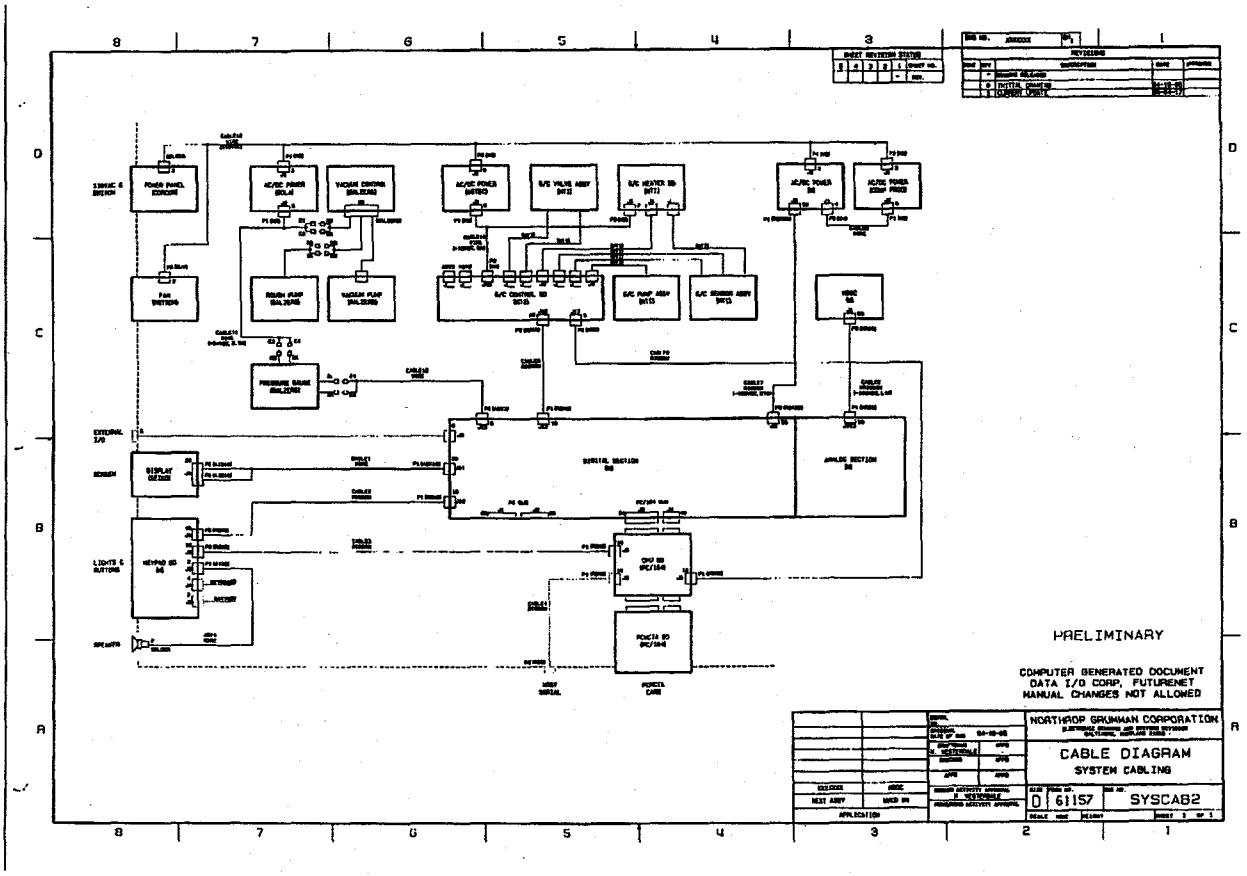

Figure 5.2-2 The system cabling does the power and signal routing in a simple and noise free way.

6 CONCLUSIONS

The mass spectrograph on a chip has been proven on the component level and problems with the integration have been identified and solved. The proven components include

1 A long-life electron emitter and electron optics

2 ion optics zoom lens and its fabrication into a deep etched well,

3 the electrostatic field region for the mass separation section using resistive films, yielding high field uniformity,

4 charge detection system including the fabrication on the side wall of the well,

5 indium compression bonding to seal the silicon pieces that comprise the vacuum chamber and provide electrical connection between the silicon pieces, and

6 assembly techniques to mount the integrated gas sensor onto a ceramic package that provides the vacuum and electrical manifold connections.

The packaging of silicon sensors with external hardware has been achieved in simple ways that allow field replacement of the sensor head by practical skilled workers, but not requiring special training. The fabrication process has been developed so that low cost fabrication is possible at a number of silicon fabrication foundries. A commercially available vacuum pump fits well with the size and power requirements of the portable unit and would supply both the mass spectrograph on a chip as well as the MTI gas chromatograph. Northrop Grumman is aware of a DARPA mesoscopic machines program at SARCOS (Salt Lake City, UT) that is developing a vacuum pump with specifications that would exceed the requirements for the MSOC and be about one-fifth the size and one-sixth as power hungry as the current Balzers drag pump.

The final testing of an integrated gas sensor was not completed due to exhaustion of the funds allocated. Northrop Grumman is interested in pursuing this technology further and would welcome interested Government parties to co-invest in the development.